Prediction of Human Drug Clearance and Anticipation of Clinical Drug-Drug Interaction Potential from In Vitro Drug Transport Studies

Inauguraldissertation

zur

Erlangung der Würde eines Doktors der Philosophie

vorgelegt der

Philosophisch-Naturwissenschaftlichen Fakultät

der Universität Basel

von

Annett Kunze

aus Deutschland

Basel, 2014

Genehmigt von der Philosophisch-Naturwissenschaftlichen Fakultät
auf Antrag von

Prof. Dr. Jörg Huwyler

Dr. Gian Camenisch

Prof. Dr. Henriette E. Meyer zu Schwabedissen

PD. Dr. Albert Neutzner

Basel, den 24. Juni 2014

Prof. Dr. Jörg Schibler
Dekan

This work was performed in collaboration with the University of Basel and the Novartis Institutes for BioMedical Research Basel, Switzerland.

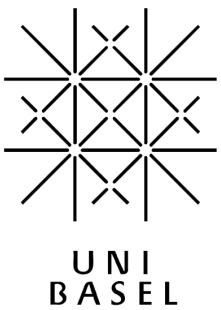

Acknowledgments - Danksagung

In erster Linie möchte ich mich bei Prof. Dr. Jörg Huwyler dafür bedanken, dass er es mir ermöglicht hat diese kollaborative Dissertationsarbeit in seiner Forschungsgruppe zu absolvieren. Für die Zeit, für fachliche Diskussionen, sowie für die Teilnahme an wissenschaftlichen Meetings als auch an Gruppenausflügen möchte ich mich ebenfalls bedanken.

Mein ganz besonderer Dank geht an meine Dissertationsbetreuerin PD Dr. Heike Gutmann. Ihr großes Engagement hat dieses Dissertationsprojekt ermöglicht und Ihre hilfreichen Ideen sowie Ihr stetiger Optimismus waren eine große Unterstützung und Bereicherung für diese Arbeit.

Großer Dank gilt Dr. Gian Camenisch für die Betreuung und Dissertationsleitung. Die fachlichen Gespräche und Beiträge waren eine wertvolle Hilfe für die Durchführung dieses Projektes. Vor allem möchte ich mich auch für das Vertrauen und die Möglichkeit bedanken, dass ich die Novartis Transportergruppe durch interne und externe Pojektpräsentationen vertreten durfte.

Besonderer Dank gilt Dr. Birk Poller für die Mitbetreuung der Dissertationsarbeit. Sein breites fachliches Wissen und die wertvollen Ideen hatten einen großen Anteil am Gelingen dieses Projektes. Für die konsequente Unterstützung dieser Arbeit während der letzten drei Jahre bin ich sehr dankbar.

Bei Prof. Dr. Henriette E. Meyer zu Schwabedissen und PD Dr. Albert Neutzner möchte ich mich herzlich für die Teilnahme am Dissertationskomitee und Übernahme der Koreferate bedanken.

Dr. Olivier Kretz danke ich dafür, dass ich diese Arbeit in der Drug Metabolismus und Pharmakokinetik Abteilung von Novartis, Basel durchführen durfte.

Ganz besonders möchte ich mich bei meinen Laborkollegen Lisa Bijasson, Sylwia Faller, Francis Heitz und Julia Riede für die letzten vier Jahre bedanken. Neben der technischen, war vor allem die persönliche Unterstützung durch Gespräche aber auch durchs "z'Vieri" eine große Hilfe während der Anfertigung dieser Arbeit.

Des weiteren möchte ich mich recht herzlich bei allen Novartis Mitgliedern der DMPK-IDD Gruppe in Basel bedanken, die zum Gelingen dieser Arbeit mitgewirkt haben.

Für die Unterstützung und den Rückhalt während meiner gesamten Ausbildung möchte ich ganz

besonders meinen Eltern und meiner Familie danken.

A very special thank goes to Caroline Piovan who continuously supported and encouraged me during the years of this work. Moreover, I would like to thank Rodrigo De la Garza for his constant support and Pejman Mohammadi, Salvador Carillo, Zhiva Kalinova Skachkova, and Eiko Shepherd for making my stay in Basel a very enjoyable time.

Namensnennung-Keine kommerzielle Nutzung-Keine Bearbeitung 3.0 Schweiz
(CC BY-NC-ND 3.0 CH)

Sie dürfen: **Teilen** — den Inhalt kopieren, verbreiten und zugänglich machen

Unter den folgenden Bedingungen:

Namensnennung — Sie müssen den Namen des Autors/Rechteinhabers in der von ihm festgelegten Weise nennen.

Keine kommerzielle Nutzung — Sie dürfen diesen Inhalt nicht für kommerzielle Zwecke nutzen.

Keine Bearbeitung erlaubt — Sie dürfen diesen Inhalt nicht bearbeiten, abwandeln oder in anderer Weise verändern.

Wobei gilt:

- **Verzichtserklärung —** Jede der vorgenannten Bedingungen kann **aufgehoben** werden, sofern Sie die ausdrückliche Einwilligung des Rechteinhabers dazu erhalten.
- **Public Domain (gemeinfreie oder nicht-schützbare Inhalte) —** Soweit das Werk, der Inhalt oder irgendein Teil davon zur Public Domain der jeweiligen Rechtsordnung gehört, wird dieser Status von der Lizenz in keiner Weise berührt.
- **Sonstige Rechte —** Die Lizenz hat keinerlei Einfluss auf die folgenden Rechte:
    - Die Rechte, die jedermann wegen der Schranken des Urheberrechts oder aufgrund gesetzlicher Erlaubnisse zustehen (in einigen Ländern als grundsätzliche Doktrin des **fair use** bekannt);
    - Die **Persönlichkeitsrechte** des Urhebers;
    - Rechte anderer Personen, entweder am Lizenzgegenstand selber oder bezüglich seiner Verwendung, zum Beispiel für **Werbung** oder Privatsphärenschutz.
- **Hinweis —** Bei jeder Nutzung oder Verbreitung müssen Sie anderen alle Lizenzbedingungen mitteilen, die für diesen Inhalt gelten. Am einfachsten ist es, an entsprechender Stelle einen Link auf diese Seite einzubinden.

Quelle: http://creativecommons.org/licenses/by-nc-nd/3.0/ch/ Datum: 12.11.2013

Contents

List of Figures

List of Tables

Abbreviations

AB	apical to basolateral
ABC	adenosinetriphosphate binding cassette
ADME	absorption distribution metabolism excretion
BA	basolateral to apical
BCRP	breast cancer resistance protein
BCS	Biopharmaceutics Classification System
BDDCS	Biopharmaceutical Drug Disposition Classification System
BSEP	bile salt export pump
CCK8	cholecystokinin octapeptide
DAA	direct acting-antiviral agents
DDI	drug-drug interaction
dpm	disintegrations per minute
E3S	estrone-3-sulfate
ECCCS	extended clearance concept classification system
FBS	fetal bovine serum
FDA	Food and Drug Administration
HEK	human embryonic kidney
IVIVE	*in vitro- in vivo* extrapolation
LC	liquid chromatography
LSC	liquid scintillation counting
MATE	multidrug and toxin extrusion protein
MDR	multidrug-resistant
MRP	multidrug resistance-associated protein
MS	mass spectrometry
NME	new molecular entity
NSB	nonspecific binding
NSAID	nonsteroidal anti-inflammatory drug
NTCP	sodium-taurocholate co-transporting polypeptide
OAT	organic anion transporter
OATP	organic anion transporting polypeptides
OCT	organic cation transporter
OCTN	organic cation and carnitine transporter novel
PEPT	peptide transporter
P-gp	P-glycoprotein
PK	pharmacokinetic
PTC	proximal tubule cell
QTAP	quantitative targeted absolute proteomics
RAF	relative activity factor

REF ..... relative expression factor
SLC ..... solute carrier
SVR ..... sustained virologic response
TEER..... trans-epithelial electrical resistance
UGT ..... uridine diphosphate glucuronosyltransferase

Variables

A	surface area (m)
AUC	area under the concentration-time curve ($kg \cdot h \cdot L^{-1}$)
CL	clearance ($L \cdot h^{-1}$)
CL_{bile}	biliary clearance ($L \cdot h^{-1}$)
CL_{int}	intrinsic clearance ($L \cdot h^{-1}$)
CL_{h}	hepatic clearance ($L \cdot h^{-1}$)
CL_{sec}	secretion clearance ($L \cdot h^{-1}$)
CL_{met}	metabolic clearance ($L \cdot h^{-1}$)
$CL_{r,fil}$	renal filtration clearance ($L \cdot h^{-1}$)
$CL_{r,org}$	renal organ clearance ($L \cdot h^{-1}$)
$CL_{r,sec}$	renal secretion clearance ($L \cdot h^{-1}$)
D	diffusion coefficient ($m^2 \cdot s$)
ER	efflux ratio (-)
$f_{i,inf}$	inhibited fraction of active drug influx (-)
$f_{i,met}$	inhibited fraction of drug metabolism (-)
$f_{i,sec}$	inhibited fraction of biliary drug secretion (-)
fu_{b}	fraction unbound in blood (-)
f_{reab}	fraction reabsorbed (-)
GFR	glomerular filtration rate ($L \cdot h^{-1}$)
I	Inhibitor concentration (mol/m^3)
J_{dif}	diffusive transport rate ($mol \cdot s^{-1}$)
J_{act}	transporter-mediated transport rate ($mol \cdot s^{-1}$)
J_{pas}	passive diffusion rate ($mol \cdot s^{-1}$)
K_{m}	michaelis-menten constant (mol/m^3)
m	mass (kg)
P	permeability coefficient ($m \cdot s^{-1}$)
P_{app}	apparent permeability ($m \cdot s^{-1}$)
PS	surface permeability ($m^3 \cdot s^{-1}$)
PS_{app}	apparent surface permeability ($m^3 \cdot s^{-1}$)
PS_{act}	transporter-mediated surface permeability ($m^3 \cdot s^{-1}$)
$PS_{eff,act}$	active efflux surface permeability ($m^3 \cdot s^{-1}$)
$PS_{inf,act}$	active influx surface permeability ($m^3 \cdot s^{-1}$)
$PS_{inf,pas}$	passive influx surface permeability ($m^3 \cdot s^{-1}$)
$PS_{eff,pas}$	passive efflux surface permeability ($m^3 \cdot s^{-1}$)
PS_{pas}	passive surface permeability ($m^3 \cdot s^{-1}$)
PS_{tot}	total surface permeability ($m^3 \cdot s^{-1}$)
Q_{h}	hepatic blood flow rate ($L \cdot h^{-1}$)
Q_{r}	renal blood flow rate ($L \cdot h^{-1}$)

V . . . . . volume (L)
R_{samp} . . . . . amount of radioactivity associated with cell sample (dpm)
S . . . . . substrate concentration (mol/m^3)
t . . . . . time (h)

Chapter 1

Summary

A major concern in drug development is the characterization of new molecular entities (NMEs) with respect to their safety and efficacy. Both factors are determined by the drugs exposure within the body or its compartments. Thus, to be efficacious a drug needs to reach its target site where a decrease in exposure can result in a loss of efficacy. On the contrary, an increased accumulation of drug in tissues potentially causes adverse drug reactions and toxicity. Alterations in drug exposure, such as observed from drug-drug interactions (DDI) due to co-medication, can therefore significantly impact a drugs safety and efficacy.

A fundamental pharmacokinetic (PK) parameter affecting a drugs exposure is the clearance, which describes the elimination rate of a drug from the body or its compartments. The major clearance organs are the liver and the kidney, where drugs are eliminated by metabolic degradation and/or secretion. In order to enter and leave cellular compartments of eliminating organs, drugs need to cross cellular membranes. However, due to their physiochemical properties, many compounds are unable to cross membranes by passive diffusion. These compounds need to interact with drug transporters which mediate the cellular uptake and efflux of their substrates. Thus, transporters play a pivotal role in drug absorption, distribution, metabolism, and excretion (ADME). Consequently, alterations in transporter activity can significantly impact drug exposure resulting in potentially altered safety and efficacy profiles.

In early drug development, information on the human *in vivo* PK profile of NMEs are lacking. Besides *in vivo* PK studies in preclinical animal species, first investigations of pharmacokinetic parameters are commonly assessed with the help of cell-based *in vitro* systems. In this work, the prediction of human drug clearances and the assessment of the clinical drug-drug interaction (DDI) potential from *in vitro* drug permeation studies was investigated. Within this context, the following aims were defined: (i) The establishment of an *in vitro-in vivo* extrapolation (IVIVE) method to predict the renal clearance of drugs; (ii) The investigation of the transporter protein expression-activity relationship to predict the contribution of transporters involved hepatic drug uptake; (iii) The prediction of the DDI potential of statins based on an extended mechanistic hepatic clearance IVIVE model; (iv) The assessment of the inhibitory potential of telaprevir on renal and hepatic drug transporters.

In the first study, we investigated the prediction of the human renal drug clearance based on *in vitro* drug transport studies. The renal clearance process is composed of glomerular filtration, tubular secretion, and tubular reabsorption. Currently, *in vitro*-based methods to assess the net renal clearance based on its underlying processes are lacking. This study therefore aimed to develop a novel IVIVE method that allows the prediction of the human renal clearance as well as the investigation of the physiological mechanisms driving renal excretion.
For this purpose, 20 marketed drugs covering a wide range of physiochemical properties and all four classes of the Biopharmaceutics Drug Disposition Classification System (BDDCS) were chosen as study compounds. LLC-PK_1 cells were selected as *in vitro* system to measure the bidirectional transmembrane permeation of the study compounds. Subsequently, the generated data were scaled to human organ level using the renal proximal tubule surface as scaling factor. Finally, the upscaled values were applied to a novel mechanistic model and the net human renal clearances were predicted based on renal filtration, secretion, and reabsorption.
For our study compounds, the LLC-PK_1 cells were a feasible *in vitro* tool to investigate the renal secretion of basic and neutral drugs. However, secretion clearance for anionic drugs was underestimated, likely due to a lack of a functional expression of a transport system for organic anions. Nevertheless, including all study compounds our model demonstrated a good predictability of the *in vivo* reported renal clearances. Thus, for 19 out of 20 drugs the net renal clearances were predicted within the three-fold deviation of the clinically observed values. Moreover, we showed that the contribution of the different processes driving the net renal clearances were dependent on the physiochemical drug properties, thereby correlating with their BDDCS assignments. Therefore, our novel IVIVE method allowed the mechanistic assessment of the underlying processes driving renal excretion and the prediction of the human net renal clearance for a diverse set of compounds.

Human cryopreserved suspended hepatocytes express a multitude of drug uptake transporters. Therefore, they represent a widely used *in vitro* system to investigate the *in vivo*-like hepatic drug disposition. However, many drugs including statins exhibit overlapping transporter specificities. Their hepatic drug uptake reflects the sum of all active transporter-mediated processes and passive diffusion. Thus, efforts have been made to assess the quantitative involvement of specific transporters in the net hepatic drug uptake. Recently, quantitative targeted absolute proteomics (QTAP) methods have been established to determine the abundances of drug transporter proteins in tissue and cell samples. First studies applied QTAP analysis to determine the contribution of specific transporters to the net hepatic drug uptake by using absolute transporter protein abundances as surrogates for their activities. However, this method implies that the transporter protein expression directly correlates with the transporter activity.
It was the aim of the second study to further investigate the transporter protein expression-activity relationship to determine the contribution of the organic anion transporting polypeptide (OATP) 1B1 and OATP1B3 to the net hepatic uptake of statins. By that, it was aimed to assess if relative transporter expression factors (REF) could be used to extrapolate the OATP1B1 and OATP1B3 activities determined in single-transporter expressing cell lines into hepatocytes activities.

Absolute OATP1B1 and OATP1B3 expression levels in pooled human cryopreserved hepatocytes and single-transporter-expressing HEK293 cells were determined by QTAP analysis. Moreover, the transporter activities were assessed from drug uptake studies in hepatocytes and HEK293 OATP1B1/1B3 cells. Subsequently, REFs were used to extrapolate the activity data generated in recombinant cell lines to hepatocyte values. Finally, to validate the approach the predictions based on REF-scaling were compared to predictions based on a previously established scaling method using relative transporter activity factors (RAFs).
The obtained transporter protein levels in the cryopreserved hepatocytes were in agreement with literature data. Furthermore, the predicted transporter activities based on either REF or RAF scaling were highly similar. This finding indicates a direct relationship between transporter protein expression and activity. Moreover, we were able to predict the OATP1B1 and OATP1B3 activities in hepatocytes from uptake studies in cell lines over-expressing the specific transporter. Thus, for six out of ten compounds, the predicted transporter activities in hepatocytes were within a two-fold deviation from the determined value, regardless of the scaling method applied. For two transporter-specific compounds as well as for atorvastatin, pravastatin, rosuvastatin, and simvastatin the active hepatic uptake was found to be exclusively mediated by OATP1B1 and/or OATP1B3. In contrast, our results indicated the likely involvement of other hepatic uptake transporters [e.g. OATP2B1 or the sodium-taurocholate cotransporting polypeptide (NTCP)] to the net active uptake of cerivastatin, fluvastatin, pitavastatin, and lovastatin.

As introduced above, drug exposure determines a compounds safety and efficacy. Thereby, drug clearance impacts the exposure of a compound to the body or its compartments. Co-medication can alter the clearance profile of drugs resulting in DDIs that potentially affect the drugs safety or efficacy. Recently, the Extended Clearance Concept Classification System (ECCCS) has been introduced which enables the anticipation of DDI potential of drugs based on their *in vitro* assessed rate-limiting hepatic clearance pathways.The third study of this work aimed to predict the human hepatic clearance of statins by IVIVE to subsequently predict their DDI potential based on the mechanistic extended clearance concept.
In a first step, IVIVE was applied to predict the human hepatic drug clearances. For this purpose the hepatobiliary disposition of eight statins was determined using suspended human cryopreserved, and sandwich-cultured hepatocytes. Moreover, human liver microsomal metabolic data of each statin were obtained from literature. Subsequently, the *in vitro* clearances were scaled to human organ level with the help of reported scaling parameters and the net hepatic clearance of each statin was predicted. In a second step, the mechanistic extended clearance concept was applied to assess the DDI potential of each statin. Therewith, the impact of selected perpetrator drugs on hepatic uptake, metabolism, and biliary secretion of the statins was simulated and the resulting changes in exposure were compared with clinical observations from drug-drug interaction studies.
Our approach resulted in a high predictability of the human hepatic clearance with atorvastatin, fluvastatin, lovastatin acid, pitavastatin, pravastatin, and simvastatin acid projected within the two-fold deviation to the reported values. Cerivastatin was predicted within a three-fold deviation while rosuvastatin was six-fold under-predicted. Moreover, the predicted DDI potentials of each statin were in excellent agreement with the reported values. We showed that for lovastatin

acid and simvastatin acid assigned to ECCCS class 1, as well as for fluvastatin, cerivastatin, and pitavastatin assigned to ECCCS class 2, inhibition of metabolism was projected as major DDI potential. For pravastatin and rosuvastatin (ECCCS class 4) and for atorvastatin (ECCCS class 2) the DDI potential was attributed to all clearance processes driving the hepatic elimination of these statins. Thereby, we showed that a concomitant inhibition of active hepatic uptake, metabolism, and biliary secretion substantially increased the anticipated DDI effects compared to only inhibition of single clearance pathways. In conclusion, we demonstrated that the DDI potential of statins can be assessed *in vitro*, based on the extended clearance concept. Furthermore, we showed that the ECCCS class assignments of statins well predicted their major DDI potential.

As illustrated above NMEs can be the victim of drug-drug interactions. In addition to the assessment of the DDI potential for victim drugs it is also crucial to characterize NMEs with respect to their perpetrator potential. In the last study of this work we therefore investigated the potential of the new antiviral drug telaprevir to inhibit renal and hepatic transporters of the solute carrier family. The inhibitory effect of telaprevir on OATP1B1, OATP1B3, the organic anion transporters (OAT)1, OAT3, the organic cation transporters (OCT) 1, OCT2, and the multidrug and toxin extrusion protein (MATE) 1 was investigated in single-transporter expressing HEK293 cells. For this purpose, the uptake of known transporter reference substrates was assessed in the presence and absence of increasing telaprevir concentrations. Subsequently, the inhibitory effect of telaprevir on the specific transporters was measured by determination of IC_{50} values.
We showed that telaprevir exhibited significant inhibition of the renal transporters, OCT2 and MATE1 with IC_{50} values of 6.4 µM and 23.0 µM, respectively. In contrast no effect of telaprevir on the renal transporters OAT1 and OAT3 was observed. Furthermore, telaprevir inhibited all investigated hepatic transporters with IC_{50} values of 2.2 µM for OATP1B1, 6.8 µM for OATP1B3, and 20.7 µM for OCT1. Telaprevir has a reported maximal plasma concentration of 5.2 µM. Therefore, telaprevir is anticipated to be a potent *in vivo* inhibitor of OATP1B1, OATP1B3 and OCT2. Consequently, clinically relevant DDI might result upon co-administration of telaprevir with a substrate of these transporter.

Chapter 2

Introduction

2.1 Drug Transporters

Drug transporters are membrane-bound proteins. They are expressed in tissues throughout the body and localized at the blood-tissue or tissue-lumen boundary epithelial in various organs (Klaassen and Aleksunes, 2010). There, they mediate the cellular influx or efflux of endogenous compounds such as hormones, nucleotides, vitamins or metabolites as well as of xenobiotics including various drugs. Due to their physiochemical properties many of these compounds cannot cross cellular membranes passively and hence need to interact with drug transporters to penetrate into tissues. Consequently, drug transporters play a pivotal role in absorptive, distributive, and secretive processes within the body.
With respect to their molecular characteristics, drug transporters are grouped into two superfamilies: solute carriers (SLCs) and adenosinetriphosphate binding cassettes (ABCs) (Klaassen and Aleksunes, 2010). Figure 2.1 illustrates drug transporters from the SLC and ABC families expressed in liver, kidney, intestine, and brain that are known to play a key role in the disposition of drugs. In the following sections, major SLC and ABC transporters are introduced.

2.1.1 SLC transporters

The solute carrier family is grouped into 52 subfamilies containing 386 proteins in human (Schlessinger A and KM, 2013). Most members of the SLC family function as cellular uptake transporters that facilitate the membrane permeation of a variety of compounds. Therefore, transport by SLC transporters can be a requirement for the tissue penetration of drugs. In the following, SLC transporters that are recognized to play a significant role in drug disposition are introduced.

SLC22 transporters

The *SLC22* subfamily includes members of organic anion transporters (OATs) and organic cation transporters (OCTs) that mediate the cellular uptake of anionic, cationic, and zwitterionic compounds (Russel, 2010).

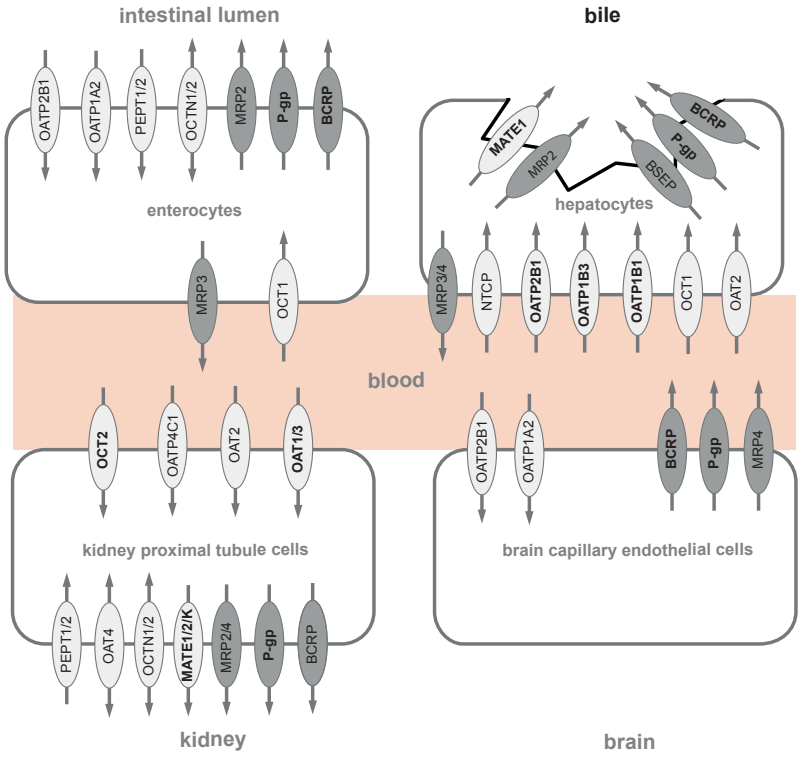

Figure 2.1: Localization of drug transporters in enterocytes, hepatocytes, kidney proximal tubule cells, and brain capillary endothelial cell. Transporters of the adenosinetriphosphat binding cassette (ABC) family are shown in dark gray and members of the solute carrier (SLC) are light gray. Arrows indicate the direction of drug transport. For hepatocytes, the canicular membrane that separates the bile pockets is indicated in black. According to the international transporter consortium (ITC), transporters that should be primarily considered in drug development are indicated in bold letters (Hillgren et al., 2013). The following abbreviations are used: BCRP, breast cancer resistance protein; BSEP, bile salt export pump; MATE, multidrug and toxin extrusion protein; MRP, multidrug resistantance-accociated protein; NTCP, sodium-taurocholate co-transporting polypeptide; OAT, organic anion transporter; OATP, organic anion transporting polypeptide; OCT, organic cation transporter: OCTN, organic cation transporter novel; PEPT, peptide transporter.

Substrates of OATs are generally hydrophilic with a molecular weight below 500 Da (Russel, 2010). OATs interact with various endogenous compounds e.g. bile salts and steroid hormones, as well as drugs including diuretics, nonsteroidal anti-inflammatory drugs (NSAIDs) (e.g. methotrexate), antivirals (e.g. adefovir, tenofovir), and statins (e.g. pravastatin, rosuvastatin) (Riedmaier et al., 2012).

As illustrated in Figure 2.1 OAT1 (*SLC22A6*) , OAT2 (*SLC22A7*) , and OAT3 (*SLC22A8*) are co-expressed at the basolateral membranes of kidney proximal tubule cells (PTCs) (Hosoyamada et al., 1999; Sun et al., 2001). In contrast to OAT1 and OAT3, which are predominately expressed in the kidney, OAT2 is mainly localized in hepatocytes (Sun et al., 2001; Sekine et al., 1998). In the kidney, OAT4 (*SLC22A11*) is expressed at the apical membrane of PTC (Ekaratanawong et al., 2004). There it is involved in secretive and reabsorptive processes of organic anions and is shown to mediate the exchange of urate (Hagos et al., 2007).

Major organic cation transporters are OCT1 (*SLC22A1*), OCT2 (*SLC22A2*), and OCT3 (*SLC22A3*) which mediate the cellular uptake of cationic compounds (MW < 400 Da) including hormones,

metabolites, and neurotransmitters, as well as of drugs such as antihistamines (e.g. cimetidine), anti-arrhytmics (e.g. quinidine), or anti-diabetics (e.g. metformin) (Roth et al., 2012; Nies et al., 2011).
Expressed at basolateral membranes, OCT1 and OCT2 are generally considered to be liver and kidney specific transporters, respectively, while OCT3 expression has been shown in various tissues throughout the body (Nies et al., 2011). The organic cation and carnitine transporter novel (OCTN)1 (*SLC22A4*) and OCTN2 (*SLC22A5*) are expressed in various tissues and localized at the apical membranes of PTC and enterocytes (Russel, 2010). OCTNs expressed at PTC are involved in the reuptake of cations and carnitine from the tubular fluid (Roth et al., 2012).

SLCO transporters

The *SLCO* family consists of organic anion transporting polypeptides (OATP). These transporters mainly mediate the cellular uptake of more bulky (MW > 450 Da), hydrophobic organic anions including bile acids, thyroid hormones, or hormone conjugates (Russel, 2010). Besides endogenous substrates, OATPs transport various drugs including statins (e.g. atorvastatin, pravastatin) , sartans (e.g. telmisartan, valsartan), or antihistamines (e.g. fexofenadine) (ITC, 2010).
As summarized by Hagenbuch et al. among OATPs, OATP1B1 (*SLCO1B1*) and OATP1B3 (*SLCO1B3*) are exclusively expressed in the liver while other members of the family such as OATP1A2 (*SLCO1A2*) and OATP2B1 (*SLCO2B1*), show broad tissue localizations (Hagenbuch and Gui, 2008). OATP4C1 (*SLCO4C1*) is a kidney-specific transporter expressed at the apical membrane of PTC (Hagenbuch and Gui, 2008).

SLC47 transporters

Solute carriers mainly consist of cellular uptake transporters. An exception is described by the group of *SLC47* transporters, including the multidrug and toxin extrusion protein (MATE)1 (*SLC47A1*), MATE2 (*SLC47A2*) and the splice variant MATE2-K (Hillgren et al., 2013). MATEs exhibit overlapping substrate specificity with OCTs and mediate the cellular efflux of cationic compounds (Tanihara et al., 2007). Apically expressed, MATE1 is localized in hepatocytes and PTC while MATE2-K is almost exclusively expressed in the kidney (Otsuka et al., 2005; Tanihara et al., 2007).

SLC10 transporters

The sodium-taurocholate co-transporting polypeptide (NTCP) (*SL10A1*) is a member of the *SLC10* subfamily that contains sodium-dependent bile acid transporters. Among them, NTCP is a liver specific uptake transporter expressed at the basolateral membrane of hepatocytes (Petzinger, 2006). Besides the transport of conjugated bile acids, NTCP is involved in the hepatic uptake of statins (Bi et al., 2013).

SLC15 transporters

The *SLC15* subfamily contains proton-coupled oligopeptide transporters that mainly mediate the transport of di- and tripeptides as well as peptide-like drugs including β-lactam antibiotics

(Brandsch, 2009). At the apical membrane of PTCs, the peptide transporters (PEPT)1 (*SLC15A1*) and PEPT2 (*SLC15A2*) mediate the active cellular reabsorption of di- and tripeptides from the tubular fluid (Brandsch, 2009; Smith et al., 2013). Moreover, PEPT1 is apically expressed in enterocytes where it is involved in the absorption of its substrates from the intestine into the blood circulation.

2.1.2 ABC transporters

The ABC superfamily contains seven subfamilies, denoted A to G, which currently include 52 human transporters (Sair, 2014). Human ABC transporters that play a key role in drug disposition are exclusively efflux transporters. Physiologically, these transporters exhibit protective functions. Expressed at the interface to sensitive tissues e.g. at the blood-brain or blood-placenta barrier, they prevent potential toxic compounds to accumulate into cells (König et al., 2013). However, in pharmacotherapy this protective function also has its downside. In fact, the impact of drug efflux transporters on drug disposition became first recognized by their role in multidrug resistance (MDR) and treatment failure due to the transporter-mediated efflux of anticancer-agents from the target tissue (Fletcher et al., 2010). In the following, major members of the ABC family that are involved in drug distribution are introduced.

ABCB transporters

The ABCB subfamily includes the most well studied efflux transporter, the P-glycoprotein (P-gp) (*ABCB1*). Also denoted MDR1, P-gp was first identified in tumor cells where it was studied in the context of MDR (Juliono and Ling, 1976). As illustrated in Figure 2.1, P-gp is localized in various tissues and apically expressed in liver, kidney, and intestine and basolaterally expressed in the brain (Klaassen and Aleksunes, 2010). It exhibits a broad substrate variety but generally mediates the cellular efflux of bulky (> 500 Da), cationic compounds including protease inhibitors (e.g. indinavir, ritonavir), anti-arrhytmics (e.g.digoxin) or anticancer drugs (e.g. vinblastine, imatinib) (Russel, 2010; ITC, 2010).

Besides P-gp, the bile salt export pump (BSEP) (*ABCB11*) is another member of the *ABCB* subfamily that has been shown to be of importance in drug disposition. BSEP is predominately expressed at the apical membrane of hepatocytes where it mediates the cellular efflux of conjugated and unconjugated bile salts into the bile (Gerloff et al., 1998). Furthermore, BSEP is reported to be involved in the hepatic secretion of the statin pravastatin (Hirano et al., 2005).

ABCC transporters

The *ABCC* subfamily contains multidrug resistance-associated proteins (MRPs). Among MRPs, MRP2 (*ABCC2*), MRP3 (*ABCC3*), and MRP4 (*ABCC4*) are involved in the cellular efflux of organic anionic compounds. MRPs mediate the disposition of endogenous compounds such as bilirubin-diglucuronide, bile acids, or urate as well as various drugs including antivirals (e.g. adefovir, tenofovir), NSAIDs (e.g. methotrexate), or anticancer agents (e.g. vinblastine) (Russel, 2010; ITC,

2010).
MRPs are localized in multiple tissues, including brain, liver, kidney, intestine or placenta (Klaassen and Aleksunes, 2010). In hepatocytes MRP4 is expressed at the basolateral membrane, mediating the transport of substrates from hepatocytes into the blood circulation.

ABCG transporters

The breast cancer resistance protein (BCRP) (*ABCG2*) is the predominant member of the ABCG subfamily that is involved in active cellular efflux of drugs. BCRP was first discovered in a resistant breast cancer cell line (Doyle and Yang, 1998). It shows a diverse expression pattern and is apically expressed in hepatocytes, PTCs, and enterocytes and basolaterally localized in brain endothelial cells (Klaassen and Aleksunes, 2010). Substrates of BCRP are hydrophobic compounds including conjugated steroid hormones, folates or uric acid, as well as anticancer agents (e.g. imatinib, erlotinib), statins (e.g. pravastatin, rosuvastatin) or the antineoplastic agent mitoxantrone (Russel, 2010).

2.2 Mechanism of Drug Permeation over Cellular Membranes

As described in the previous section, drugs have to cross cellular barriers to distribute within the body. This can occur by paracellular or transcellular movements while the latter one is more common for drugs (Rowland and Tozer, 2011c). Most drugs are small molecules (100 - 1000 Da) that cross cellular membranes (transcellular) by passive diffusion and/or active drug transporter-mediated transport (Rang et al., 2012). In the following, these mechanism are introduced and the impact of physiochemical drug properties on passive permeation is described.

2.2.1 Passive permeation and active transport

Diffusion is a passive process which is mathematically described by Fick's first law of diffusion (Silbernagel and Despopoulos, 2009):

$$J_{dif} = D \cdot A \cdot \frac{\Delta S}{\Delta X} \tag{2.1}$$

where J_{dif} states the diffusive transport rate (mol/s), D is the diffusion coefficient (m^2/s), A is the surface area (m^2), ΔS is the difference in substrate concentration (mol/m^3), and ΔX states the membrane thickness (m). For passive permeation over cellular membranes (J_{pas}) Eq.2.1 is adapted to account for the lipid solubility of the substrate:

$$J_{pas} = \underbrace{k \cdot \frac{D}{\Delta x}}_{P} \cdot A \cdot \Delta S = P \cdot A \cdot \Delta S \tag{2.2}$$

where permeability [P; (m/s)] is a function of the the oil-and-water partition coefficient, k (-), D, and ΔX (Silbernagel and Despopoulos, 2009). In pharmacokinetics, permeation over the cellular

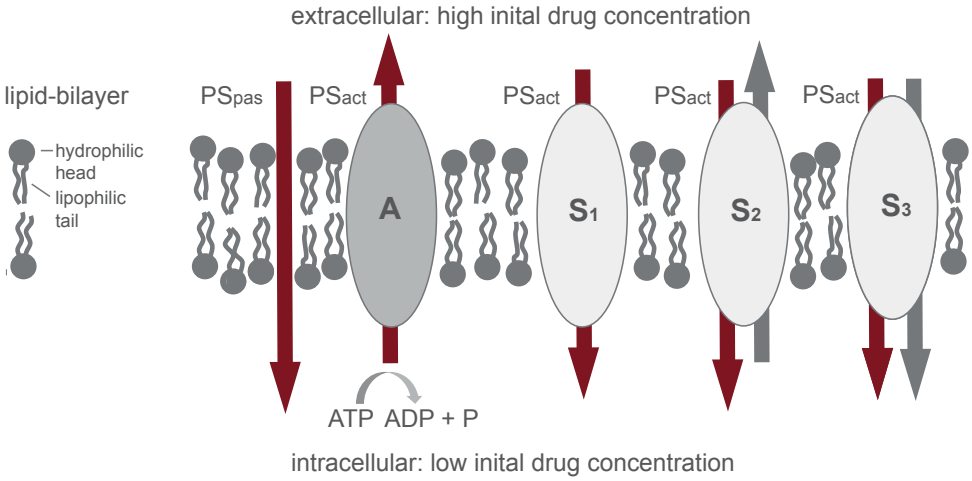

Figure 2.2: Mechanism of drug permeation over cellular membranes. Biological membranes are lipid-bilayers containing a hydrophilic head and lipophilic tail. Transcellular movements of drugs over the lipid-bilayer occurs by passive diffusion (PS_{pas}) and/or transporter-mediated permeation (PS_{act}) by ABC (A) or SLC ($S_{1\text{-}3}$) transporters. ABC transporters use the hydrolyis of ATP as source of energy to transport drugs against their electrochemical gradient. SLC transporters work as channels (S_1) or co-transporters which either mediate the antiport (S_2) or symport (S_3) of drugs and co-substances. Red and gray arrows indicate the direction of drug permeation and co-substances, respectively.

membrane is generally normalized to the initial substrate concentration (S_0) and the resulting permeability is referred as surface permeability [PS, ($m^3 \cdot s^{-1}$)]. Consequently, with respect to equation 2.2 passive surface permeation (PS_{pas}) is described as followed (Tavelin et al., 2002):

$$PS_{pas} = \frac{J_{pas}}{S_0} \tag{2.3}$$

Drug transporter mediated permeation is distinguished in primary and secondary active transport or facilitated diffusion. Members of the ABC family are primary active transporters, that use energy obtained from hydrolysis of ATP to move substrates against their electrochemical potential (Klaassen and Aleksunes, 2010). In contrast, most SLC transporters act as channels and uniporters by facilitating diffusion across membranes (Klaassen and Aleksunes, 2010). Other SLC members are co-transporters that act as secondary active transporters which use established electrochemical gradients as driving force to move substrates in the same direction (symport) or opposite direction (antiport). Figure 2.2 summarizes the mechanism of membrane permeation.
The drug permeation mediated by drug transporters is an active process characterized by saturability. Mathematically its transport rate (J_{act}) can be expressed by the Michaelis-Menten equation (Silbernagel and Despopoulos, 2009):

$$J_{act} = \frac{J_{act,max} \cdot S_0}{Km + S_0} \tag{2.4}$$

where $J_{act,max}$ (mol/s) is the maximum transporter mediated transport rate, and K_m is the michaelis-menten constant (mol/m^3).

Analogue to PS_{pas}, the transporter-mediated surface permeability (PS_{act}) is derived by dividing equation 2.4 by S_0:

$$PS_{act} = \frac{J_{act,max}}{Km + S_0} \tag{2.5}$$

Finally, the total surface permeation PS_{tot} of a drug over cellular membranes is a function of PS_{act} and PS_{pas}:

$$PS_{tot} = PS_{act} + PS_{pas} \tag{2.6}$$

2.2.2 The impact of physiochemical drug properties on passive diffusion

As shown in Figure 2.2, biological membranes are bilayers of amphiphatic phospholipids that contain a hydrophilic head oriented the outside of the bilayer and inwardly oriented lipophilic tails (Brunton et al., 2011). Lipophilic compounds can dissolve in the lipid-bilayers and the degree of lipophilicity correlates with the membrane permeability of a compound. Thereby, the partition coefficient between an aqueous and octanol solution ($logD_{pH}$), determined at a specific pH, is a measure of the degree of lipophilicity (Khojasteh et al., 2011a). Thus, the higher $logD_{pH}$, the more lipophilic and the less hydrophilic is a drug.
Generally, diffusion through the lipid-bilayer is favored for small, lipophilic, and unionized compounds and decreases with the size of the molecule (Rowland and Tozer, 2011c). The pH partition hypothesis states, that only unionized, lipophilic drug penetrates the membrane by passive diffusion (Rowland and Tozer, 2011c). However, most drugs are weak acids or bases whose degree of ionization is pH dependent (Rowland and Tozer, 2011c). Thereby, the pKa of a drug reflects the degree of ionization which is defined as followed (Khojasteh et al., 2011a):

$$pKa = -pH + log\left(\frac{[A^-]}{[HA]}\right) \tag{2.7}$$

$$pKa = -pH + log\left(\frac{[B]}{[BH^+]}\right) \tag{2.8}$$

where variables in brackets refer to concentrations, A states acids, B states bases, and H refers to protons. Consequently, HA and B are the neutral form of acids and bases while A^- and BH^+ are the ionized forms, respectively. Thus, equation 2.7 and 2.8 refer to the pKa for acidic and basic compounds, respectively.

Figure 2.3 illustrates the influence of the pH on the degree of ionization for acids and bases. Given the impact of the pH on a drugs ionization state, the rate of passive diffusion is influenced by physiological pH differences within the body. An example is described by the passive permeation of weak bases through kidney PTC. Proximal tubule cells separate the blood (pH 7.4) from the tubular fluid (pH 6.8) (Silbernagel and Despopoulos, 2009). Since the degree of ionization of weak bases is less on the blood site, their passive permeation is favored from blood to the tubular fluid than the other way around.
Another example of the influence of charge on drug distribution is given by trapping of drugs in

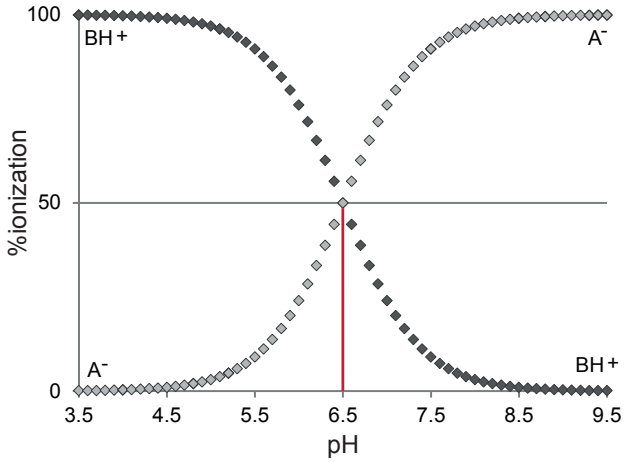

Figure 2.3: The influence of pH on drug ionization. A^- and BH^+ refer to the ionized state of acidic and basic compounds, respectively, according to equations 2.7 and 2.8. The pka defines the pH at 50% ionization which is indicated with a red line.

intracellular organelles. Thus, lipophilic basic drugs that are neutral at physiological pH (7.4) are shown to accumulate in lysosomes (pH 4-5), a process also known as lysosomal trapping (Kazmi et al., 2013; Funk and Krise, 2012). Those drugs permeate into lysosomes by passive diffusion and get protonated inside the organelle. With respect to the pH partition theory, only unionized compounds can penetrate cellular membranes passively, and consequently lipophilic basic drugs literally get trapped into lysosomes due to their charged state.

2.3 Human *In Vivo* Drug Elimination

After drugs reach the system circulation they are distributed and subsequently eliminated from the body. In pharmacokinetics, drug elimination is described by the term clearance that refers to the rate of elimination of a drug from the body or its compartments [CL; ($L \cdot h^{-1}$)] (Rowland and Tozer, 2011a). *In vivo* , the systemic drug clearance can be assessed as the ratio of the drug dose (mg) applied intravenously and the area under the drug concentration-time curve (AUC, $mg \cdot h \cdot L^{-1}$) (Rowland and Tozer, 2011b). The AUC is a measure of a drugs exposure, and thus directly impacted by drug clearances.

The major clearance organs are the the liver and the kidney. There, an interplay between metabolic enzymes and drug transporters mediate the elimination of drugs either by metabolism and/or by direct secretion. In the following sections these elimination pathways are described. Moreover, a drug classification system that allows the prediction of elimination pathways based on *in vivo* drug metabolism data is briefly introduced.

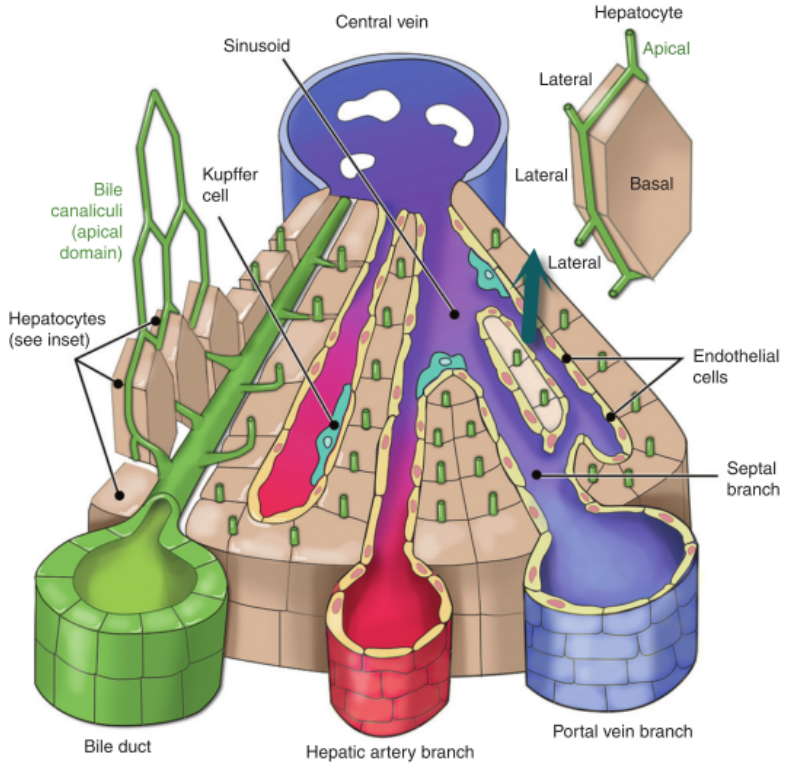

Figure 2.4: Microanatomy of the liver. Blood enters the liver mainly through branches of the hepatic artery and portal veins and flows through sinusoids into the central vein. Hepatocytes are the predominant cells within the liver and mediate the secretion of compounds from the blood into the bile canaliculi. *The figure was taken from Chu et al. (Chu et al., 2013).*

2.3.1 Hepatic clearance

The hepatic clearance of drugs from the blood invovles hepatic metabolism and hepatobiliary secretion. After a brief introduction of the functional anatomy of the liver, these hepatic drug elimination mechanism are introduced.

Liver anatomy

Figure 2.4 illustrates the microanatomy of the liver. Blood enters the liver through branches of the portal vein and the hepatic artery, the main vascular blood supply systems (Malarkey et al., 2005). Then, the blood flows into capillaries, called sinusoids, before it collects into the central veins. The functional unit of the liver is the hepatic acinus containing branches of the hepatic artery, the portal vein, the bile duct and the surrounding mass of liver cells (Kuntz and Kuntz, 2006). Hepatocytes are the most abundant hepatic cells (60%) and are the place of hepatic drug elimination (Malarkey et al., 2005; Rowland and Tozer, 2011a). They face sinusoids with their basolateral (sinusoidal) and bile canaliculi with their apical (canicular) membranes.

Drug elimination

Before drugs can be eliminated from the blood they need to enter the hepatocytes. As illustrated in Figure 2.1 hepatocytes express various drug transporters including OATPs, OAT2, OCT1, and NTCP at their sinusoidal membrane that mediate the active hepatic uptake of drugs from the blood

(Christoph, 2008). Elimination by biliary secretion is mediated by drug transporters expressed at the canicular membrane including BCRP, MRP2, MATE1, P-gp, and BSEP (Christoph, 2008).

Hepatocytes are enriched with metabolic enzymes and metabolism is considered as the major hepatic clearance pathway of drugs. Metabolism is categorized into phase I and phase II reactions (Liddle and Stedman, 2007). Phase I reactions involve oxidation, reduction, and hydrolysis thereby introducing reactive groups to the drug molecule (named functionalization). The majority of metabolic phase I drug reactions is attributed to the the cytochrome P450 family (Williams et al., 2004; Rowland and Tozer, 2011a). Within this family, CYP3A4 is the most abundant member of CYP450 in the liver. Phase II reactions are described by conjugation processes including glucuronidation, acetylation, or sulfation that mainly result in an increased hydrophilicity of the drug metabolite that facilitates its subsequent secretion (Liddle and Stedman, 2007). For most drugs the predominant enzymes mediating phase II reactions are uridine diphosphate glucuronosyltransferases (UGTs) (Williams et al., 2004).

2.3.2 Renal clearance

Glomerular filtration, renal metabolism, tubular secretion, and tubular reabsorption concomitantly contribute to the net renal blood clearance (Masereeuw and Russel, 2001). These processes take place in the nephron, the functional unit of the kidney. In the following, the anatomy of the nephron is briefly summarized and the renal clearance steps are illustrated.

Nephron anatomy

Figure 2.5 illustrates the nephron. It consists of the glomerulus and the renal tubules in which the urinary filtrate is formed. The tubules are segmented into the proximal convoluted tubule, the loop of henle, and the distal tubule which joints the collecting duct (Lote, 2012). Blood enters the kidney through the renal artery which branches into final afferant arterioles that supply the glomerular capillaries with blood. The glomerular capillaries form a knot called the Bowman's capsule. The blood leaves the glomerulus through efferent arterioles that from a net of peritubular capillaries enclosing the tubular segments and subsequently leaves the kidney through the renal vein (Lote, 2012).

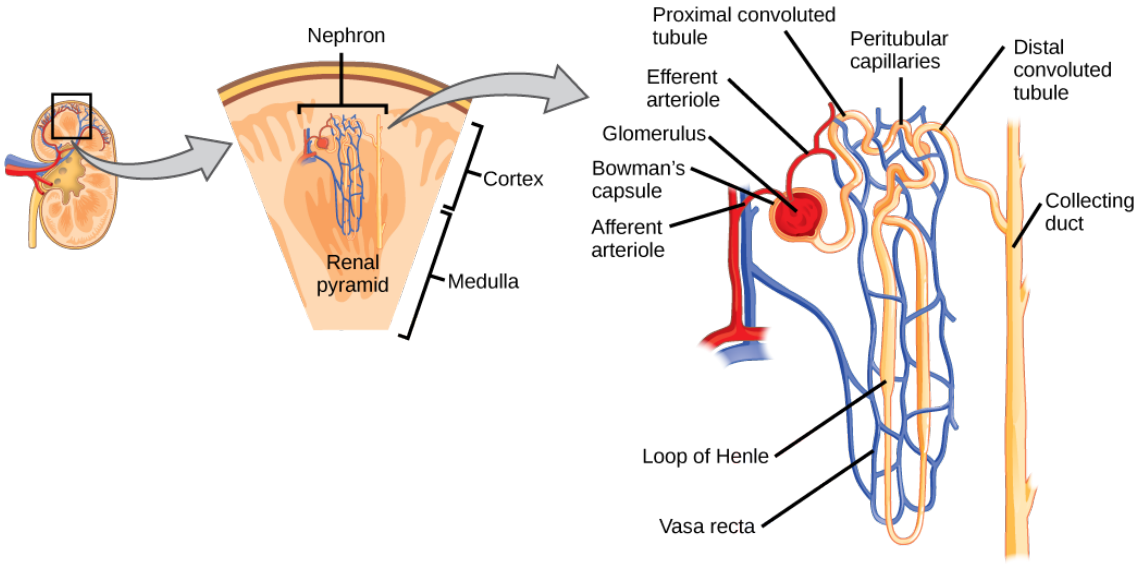

Figure 2.5: The nephron as functional unit of the kidney. The nephron is localized in the cortex and medulla of the kidney. It contains the Bowman's capsule and tubules which are surrounded by a net of capillaries. The tubules are segmented into proximal tubule, the loop of Henle, and the distal tubule. *The figure was taken from http://cnx.org.*

Drug elimination

Drugs enter the kidney with the blood flow thereby reaching the nephron at the glomerulus. Within the glomerulus, drugs can be subjected to filtration into the proximal tubule. Glomerular filtration is a passive, size-selective process and only unbound drug with a molecular weight below 2000 g/mol are filtered (Fagerholm, 2007). The rate at which the blood is filtered is called glomerular filtration rate (GFR) that has an average value of 1.71 mL/(min·kg) in human (Rowland and Tozer, 2011a). Drugs that don not undergo glomerular filtration leave the Bowman's capsule through efferent arterioles.

Tubular epithelial cells exhibit a boundary function between the blood to their basolateral and the tubular fluid to their apical side, thereby mediating the transport of compounds from one compartment into the other. Proximal tubule cells express a variety of drug transporters and are the main side of active transport within the tubule (Masereeuw and Russel, 2001). Thus, drugs moving within the blood flow along efferent arterioles can be actively taken up into PTCs by basolateraly expressed transporters including OATs and OCTs and subsequently secreted into the tubular fluid by apically transporters including MRPs, P-pg, MATEs, and BCRP (see Fig. 2.1).

Drugs in the tubular fluid can be subject to tubular reabsorption into efferent arterioles. For most compounds, reabsorption mainly occurs by passive diffusion which is influenced by the physiochemical properties of the drug (see section 2.2.2). However, drug uptake transporters expressed at the apical membrane of PTCs including OCTNs, OAT4, or PEPTs are involved it the active reuptake of drugs from the tubular fluid.

Drug clearance by metabolism mainly occurs in the liver, and metabolism in the kidney often is expected to be a minor elimination pathway (Rowland and Tozer, 2011a). However, the proximal tubule cells contain phase I and II metabolizing enzymes including members of the CYP450 family

and UGTs (Lohr et al., 1998).

2.3.3 The Biopharmaceutical Drug Disposition Classification System (BDDCS)

In 1995 Amidon and co-workers established a Biopharmaceutics Classification System (BCS) to predict the rate and extend of oral drug absorption (Amidon et al., 1995). The BCS categorizes drugs into four classes according to their aqueous solubility and intestinal permeability. According to the Food and Drug Administration (FDA) the classification criteria are as follows: Drugs are classified as highly soluble when the highest marketed dose strength is soluble in 250 mL of aqueous media over a pH range of 1-7.5 and highly permeable when the extent of oral absorbed drug is at least 90% of the administered dose in human (FDA, 2005). In 2005, Wu and Benet applied the BCS to over 100 drugs (Wu and Benet, 2005). They recognized that the BCS class assignment of drugs correlates with their main route of elimination. Thus, drugs assigned to class 1 (highly soluble; highly permeable) and class 2 (low soluble; highly permeable) are primarily eliminated by metabolism while drugs assigned to class 3 (highly soluble; low permeable) and 4 (low soluble; low permeable) are primarily eliminated by renal and/or biliary secretion.
Following their analysis, Wu and Benet observed that a classification into high vs. low permeability reflected the accessibility of drugs to metabolizing enzymes, thereby correlating with the main route of drug elimination. Thus they proposed the Biopharmaceutical Drug Disposition Classification System (BDDCS) which exchanged the permeability criterion from the BCS with the extent of metabolism. Another rational behind the use of metabolism data rather than permeability data is the easier access to human *in vivo* metabolism data (Wu and Benet, 2005).
Within the BDDCS drugs are classified as extensively metabolized when 70% or more of orally administered drug undergoes metabolism. The purpose of the BDDCS is the prediction of drug disposition, elimination pathways and drug-drug interaction, thereby assessing the involvement of drug transporters (Wu and Benet, 2005; Benet, 2013). Table 2.1 lists BDDCS class-specific characteristics. Drugs categorized in classes 1 and 2 are extensively metabolized and consequently their major elimination organ is the liver while for classes 3 and 4 renal and/or biliary secretion of unchanged drug is predicted as the main route of elimination.

Table 2.1: Characteristics of the BDDCS.

BDDCS	solubility	metabolism	predicted transporter effects
Class 1	high	extensive	minimal effects in gut and liver
Class 2	low	extensive	efflux transporter effects predominate in gut; both uptake and efflux transporters can affect liver
Class 3	high	poor	absorptive transporter effects predominate
Class 4	low	poor	absorptive and efflux transporter effects could be important

BDDCS refers to the Biopharmaceutics Drug Disposition Classification System. *The table was adapted according to Wu and Benet (2005).*

2.4 Cell-Based *In Vitro* Methods to Study Drug Membrane Permeation in Liver and Kidney

The following sections introduce cell-based *in vitro* systems that are commonly used to investigate the hepatic and renal drug membrane permeation. Furthermore, the methodology of frequently used assays is summarized and the derivation of permeability values from these experiments is explained.

2.4.1 Cell systems

Cell-based *in vitro* systems can be categorized in either primary systems or cell lines. Primary systems are derived directly from intact tissues and exhibit a limited life-span (Masters, 2000). In contrast, cell lines are subcultured systems from primary tissues and can be subjected to immortalization. Therefore, immortalized cell lines or cell lines derived from cancerous tissue, have the ability of unlimited reproduction making them a valuable *in vitro* tool (Masters, 2000).

Primary hepatocytes

As introduced in section 2.1, hepatocytes express a multitude of drug transporters at their basolateral and canicular membranes. On a functional level, well-established hepatocyte models are commonly used *in vitro* systems to study the hepatic drug uptake and hepatobiliary secretion (Yabe et al., 2011; De Bruyn et al., 2011; Shitara et al., 2003). To overcome the shortage of freshly-isolated cells, cryopreservation methods have been established and cryopreserved hepatocytes are now commercially available. Thereby, functional expression of drug uptake transporters in cryopreserved hepatocytes was shown in various experiments (Shitara et al., 2003; Lu et al., 2006). A well-established assay to investigate the hepatic drug uptake is performed with either freshly-isolated or cryopreserved suspended hepatocytes. The suspended cells are incubated with the compound of interest and subsequently the uptake is terminated by the so-called oil-spin-method, by separating the cells from the incubation solution. The methodology of this assay is summarized in Figure 2.6.

During the isolation procedure, hepatocytes loose their cell polarization and hepatic architecture, including the formation of bile pockets (Groothuis et al., 1981; Maurice et al., 1988). Besides, it has been shown that after isolation apically expressed efflux transporters are rapidly internalized (Bow et al., 2008; Hoffmaster et al., 2004). This can be overcome when using the so-called hepatocyte sandwich-culture technique where freshly-isolated cells are cultured between two layers of gelled collagen. First shown by Dunn et al., sandwich-cultured hepatocytes retain their *in vivo*-like physiology including polarized growth properties and formation of bile pockets, pre-requirements for hepatobiliary secretion studies (Dunn et al., 1989, 1991). Thus, sandwich-cultured hepatocytes provide a functional *in vitro* system to study active biliary drug excretion (Swift et al., 2010). Figure 2.6 illustrates the methodology of the sandwich-cultured based hepatocyte assay.

Hepatic drug uptake can also be assessed in sandwich-cultured hepatocytes. However, uptake transporter expression on mRNA level is shown to be lower in sandwich-cultured hepatocytes

A Hepatocyte oil-spin assay

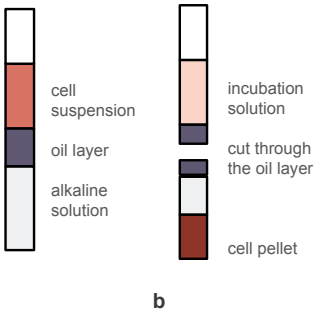

Methodology

Following incubation of suspended hepatocytes with the compound of interest, the cell suspension is placed on top of an oil layer in a microcentrifugation tube (**a**). By centifugation the cells move through the oil layer into the alkaline solution while the incubation solution stays on top of the oil layer. Following an overnight freezing peroid, the tube is cut through the oil layer, allowing a separate analysis of the amount of compound in the cell pellet and in the incubation solution (**b**).

Advantages

Feasible for studies with freshly-isolated or cryopreserved hepatocytes, thus allowing flexibility. Hepatocytes functionally express physiological uptake transporters and the net hepatic uptake can be assessed.

Disadvantages

Identification of transporter-specific compound interaction is limited. The assay throughput is low.

B Sandwich-cultured hepatocyte assay

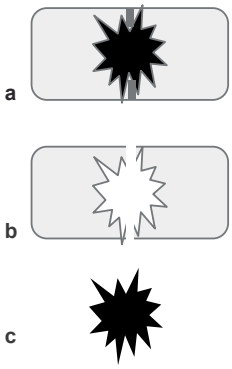

Methodology

Incubation of the test compound in a calcium containing buffer preserves tight junctions. Consequently, secreted compound accumulates in the bile pockets (**a**).

Incubations performed in calcium-free buffer disrupts the tight junctions (**b**). Subsequent washing steps remove compound which is accumulated in the bile pockets. Thus, accumulation of compound within the cells can be measured.

The accumulated amount of compound in the bile pockets (**c**) is determined by substracting the values obtained from incubations in the presence and abscence of calcium.

Advantages

Sandwich-cultured hepatocytes maintain the hepatocyte architecture and cell polarity. Canicular efflux transporters are functionally expressed and hepatobiliary drug secretion can be measured.

Disadvantages

The identification of transporter-specific compound interaction is limited. The assay is costly and throughput is low.

C Uptake and efflux transporter assay

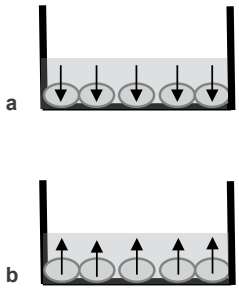

Methodology

Incubation of a test compound solution with plated transporter-transfected cells and untransfected control cells in the presence and abscence of specific transporter inhibitors. Subsequently, the solution is aspirated and the compound accumulation within the cell samples is analysed.

Uptake-transporter interaction (**a**) with a compound is indicated if compound accumulation in transfected cells is significantly higher (i) compared to untransfected control cells and (ii) in the abscence of control inhibitors. For efIflux-transporter studies (**b**) the oppsite indicates a transporter-compound interaction.

Advantages

Allows characterization of transporter-specific substrates and inhibitors. Throughput is high and the assay is cost-effective.

Disadvantages

These artificial cell systems do not represent physiological conditions in terms of transporter activity and protein expression levels.

D Transwell assay

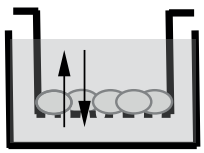

Methodology

Cells are seeded on a porous filter-membrane in transwell inserts. The system contains two chambers and bidirectional transmembrane transport can be assessed following incubation with a compound solution.

Advantages

Allows characterization of transporter-specific substrates and inhibitors. Cellular compound uptake and transmembrane permeability can be assessed.

Disadvantages

Cell systems require polarized thight growth properties. The assay throughput is low.

Figure 2.6: Overview of cell-based *in vitro* assays. *Content is partially taken from Jin and Di (2008); Xia et al. (2007).*

compared to suspended hepatocytes and variations in cultivation conditions can significantly alter the transporter expression (Luttringer et al., 2002). Moreover, the sandwich-culture assay is cost-intensive, cell cultivation is work-intensive, and throughput is low. Therefore, suspended hepatocytes are commonly chosen as *in vitro* tool to assess the hepatic uptake of drugs.

Primary kidney cells

In contrast to hepatocytes, renal primary *in vitro* systems to study drug transport are less well-established. As illustrated in section 2.1 human proximal tubule cells express a variety of drug transporters that mediate renal drug secretion. Efforts have been made to establish PTC models from various species (Lash et al., 2006; Terada and Inui, 2007; Brown et al., 2008; Gowder and McMartin, 2010; Schlatter et al., 2006). Thereby, expression of major renal drug transporters in freshly-isolated cells was demonstrated on mRNA, protein, and functional level. However, the isolation procedure is very work-intensive and today no primary kidney model has been established that provides an *in vitro* system applicable for reproducible transepithelial renal drug transport studies.

Cell lines

Two heptocarcinoma cell lines evaluated for drug transporter expression and functional activity are HepG2 and HepGR cells. In contrast to HepG2 cells which do not exhibit mRNA expression of OATP1B1, NTCP, and OCT1, HepGR cells showed expression levels of major hepatic uptake and efflux transporters on mRNA and functional level (Lee et al., 2006). However, in both cell lines transporter expression was significantly down-regulated when compared to expression levels in primary hepatocytes (Lee et al., 2006).
The porcine proximal tubule cell line LLC-PK_1 and the American opossum kidney cell line OK have been used to investigate *in vitro* renal drug permeation. Studies with LLC-PK_1 cells indicated that the cells contain a functional organic cation system, while OK cells are reported to exhibit a functional organic anion system (Saito et al., 1992; Urakami et al., 2005; Takano et al., 1994; Habu et al., 2000). Besides, studies showed that LLC-PK_1 cells exhibit tight growth properties required for transmembrane permeation studies, while this characteristic is lacking in OK cells (Liang et al., 1999).

Although drug transporter expressions on mRNA level are shown for cell lines of hepatic and renal origin, transporter expression mostly is significantly down-regulated compared to expression in primary systems (Hilgendorf et al., 2007; Lee et al., 2006; Ahlin et al., 2009). Furthermore, cell lines often do not exhibit both, a functional organic anion and cation transport system. That is why primary cells are generally the *in vitro* system of choice to investigate the net permeation of drugs. However, since primary cell systems express a multitude of drug transporters they are not suitable in order to characterize transporter-specific drug interactions.
In contrast, transporter-overexpressing cell lines generated by stable or transient transfection are a frequently used *in vitro* tool to assess transporters-specific drug transport. The human embryonic kidney (HEK) cell line HEK293, LLC-PK_1 and the Madin-Darby canine kidney cell line MDCK

are widely used host cell lines to generate single, or multiple-transporter over-expressing systems used for uptake, efflux or transmembrane permeability studies (Barton et al., 2013; Xia et al., 2007). The methodology of these assays is illustrated in Figure 2.6.

2.4.2 Assessment of membrane permeation from cell-based *in vitro* studies

Incubation studies with radio-labeled compounds are a frequently used method to quantify substance accumulation within cells, or in the incubation media. Samples containing radioactivity can be analyzed by liquid scintillation counting (LSC), a process referred to the conversion of the energy of a radioactive decay event into photons of light. Thereby, the absolute sample activity is determined in disintegrations per minute (dpm).
With the help of the *in vitro* systems introduced above, apparent surface permeabilities (PS_{app}) and apparent transmembrane permeabilites (P_{app}) can be derived. As described in section 2.2.1, PS_{app} and P_{app} reflect net values that can involve active, transporter-mediated, and passive permeation processes. The derivation of PS_{app} and P_{app} values from *in vitro* assays and the assessment of the contribution of active processes is described in the following.

Uptake and Efflux assays

Following cellular uptake or efflux experiments using radio-labeled compounds, the apparent surface permeability (PS_{app}; $\mu L \cdot min^{-1} \cdot mg^{-1}$) is calculated as the amount of radioactivity associated with the cells (R_{samp}; dpm) divided by the concentration in the incubation medium (S_0; $dpm \cdot \mu L^{-1}$) and normalized to the incubation time (t;min) and the amount of protein (m; mg) within the sample:

$$PS_{app} = \frac{R_{samp}}{S_0 \cdot t \cdot m_{prot}} \tag{2.9}$$

When incubation studies are performed with transporter-transfected cell system, the contribution of active transport can be assessed by control experiments performed in mock-transfected cells. Thereby, active transport is determined from the PS_{app} difference between studies performed in transporter-expressing cells and mock-transfected cells (Webborn et al., 2007). However, for studies in primary systems, including suspended and sandwich-cultured hepatocytes, no such control systems are available.
A method to assess active uptake in these systems is to perform parallel incubations at 37°C and 4°C, assuming that active transport is not functional at 4°C. A drawback of this method is that membrane fluidity and consequently passive permeation can be affected by this temperature change, thus limiting this method for qualitative rather than quantitative investigations (Frezard and Garner-Suillerot, 1998).
Another commonly used approach are control incubations performed in the presence of transporter inhibitors. Thereby, a difference of permeability values obtained in the presence and absence of the inhibitors indicate the involvement of active transport. Limitations are the availability of

specific transporter inhibitors and the underlying assumption that the inhibitor totally inhibits the respective transporter activity. Moreover, since active transport is a saturable process, incubation studies performed with an increasing substrate concentration can be used to assess the involvement of transporter-mediated processes. By that, a decrease in surface permeabilities by an increasing substrate concentration indicates transporter saturation.

Transmembrane transport assays

Transport assays are a useful tool to directly investigate the permeability of a drug across cellular monolayers. To perform transwell experiments, a polarized growth property and monolayer integrity of the cells system are required. Following experiments using transwell inserts (see Figure 2.6), the apparent permeability (P_{app}; cm·min^{-1}) is determined as follows:

$$P_{app} = \frac{V_R \cdot S_R}{A \cdot t \cdot S_{D,0}} \tag{2.10}$$

where V_R is the incubation volume in the receiver chamber (µL); S_R is the substrate concentration in the receiver chamber at the end of the incubation (dpm·µL^{-1}); t is the incubation time (min), A is the transwell surface area (cm^2); and $S_{D,0}$ is the initial substrate concentration in the donor chamber (dpm·µL^{-1}).

Since cell polarization is a requirement, the permeability of a drug can be assessed from basolateral to apical direction (BA) and vice versa (AB). The performance of bidirectional transwell studies allows the determination of efflux ratios (ERs) that are defined as the ratio of $P_{app,BA}$ to $P_{app,AB}$. ERs that significantly differ from 1.0 indicate the involvement of active transport. Similar to uptake and efflux studies, the contribution of active transport can also be assessed following compound concentration-dependent experiments (transporter saturation) or permeation studies in the presence of transporter inhibitors. Control experiments performed at 4°C cannot be used to assess active transport in transwell studies, since the membrane fluidity is affected by the change in temperature impacting passive transcellular and paracellular drug permeation.

2.5 *In Vitro in Vivo* Extrapolation Methods to Predict the Human Drug Clearance

Generally, *in vitro- in vivo* extrapolation (IVIVE) methods to determine human drug clearances contain three major steps (Lave et al., 2009): **(i)** the *in vitro* determination of the underlying processes driving the intrinsic organ clearance (CL_{int}) ; **(ii)** the scaling of these *in vitro* parameters to human *in vivo* values to determine CL_{int}; **(iii)** the incorporation of CL_{int} into whole organ models. Thereby, CL_{int} describes the ability of an organ to eliminate drugs by metabolic (CL_{met}) or secretive (CL_{sec}) processes, regardless of other impacting factors such as blood flow or drug binding to blood or plasma proteins (Khojasteh et al., 2011b). These so-called "external" factors are taken into account when applying whole organ models (Khojasteh et al., 2011b). In the following, IVIVE methods to assess hepatic and renal drug clearances are introduced.

2.5.1 Hepatic IVIVE methods

The first hepatic IVIVE was performed by Rane et al. (1977) who predicted the *in vivo* hepatic clearance in rat from studies with liver microsomes. Generally, for the following 30 years human hepatic IVIVE methods were mainly focused on metabolism studies in hepatocytes or liver microsomes by approximating the hepatic intrinsic clearance ($CL_{h,int}$) with metabolic clearance only ($CL_{h,int} \approx CL_{met}$). Although an overall good predictability was achieved a tendency to rather underpredict the *in vivo* observed clearance became recognized and partially attributed to neglecting the involvement of hepatic drug transport processes in this approach (Chaturvedi et al., 2001; Obach, 1999; Chiba et al., 2009).
With the establishment of hepatocyte *in vitro* assays to determine active hepatic uptake and biliary secretion, studies were performed evaluating the predictability of the hepatic organ clearance from hepatic uptake ($CL_{h,int} \approx PS_{inf}$) or biliary secretion ($CL_{h,int} \approx CL_{bile}$) (Abe et al., 2009; Webborn et al., 2007). Results showed that the predictability of these methods was highly compound-dependent and usually successful if the examined clearance pathway was the overall rate-limiting step in the net hepatic clearance.
More recently, based on the extended hepatic clearance concept, mechanism-based hepatic IVIVE methods were developed taking active transport and metabolic clearances into account (Shitara et al., 2006; Kusuhara and Sugiyama, 2009; Umehara and Camenisch, 2012; Jones et al., 2012). Thereby, Umehara and Camenisch (2012) demonstrated a significant improvement in predictability when the model accounts for all processes driving the hepatic clearance (sinusoidal transport, metabolism, canicular transport). In the following, this mechanism-based hepatic IVIVE approach is described.

Step 1: *In vitro* determination of hepatic clearance processes.

As introduced in section 2.3.1 the *in vivo* hepatic clearance involves the hepatic drug uptake followed by metabolism and/or biliary secretion. These three processes define the intrinsic hepatic clearance. Mathematically, $CL_{h,int}$ can be expressed as follows (Kusuhara and Sugiyama, 2009):

$$CL_{h,int} = \frac{PS_{inf,act} + PS_{inf,pas}}{PS_{eff,act} + PS_{eff,pas} + CL_{bile} + CL_{met}} \cdot (CL_{bile} + CL_{met}) \qquad (2.11)$$

where $PS_{inf,act}$ and $PS_{inf,pas}$ are the active and passive hepatic drug uptake permeabilites over the sinusoidal membrane, respectively; $PS_{eff,act}$ and $PS_{eff,pas}$ refers to the active and passive efflux from the hepatocytes back into the blood (sinusoidal efflux); CL_{bile} is the biliary secretion clearance and CL_{met} refers to the metabolic clearance.
As introduced in section 2.4.1, *in vitro* cell systems based on primary hepatocytes provide useful tools to study hepatic drug permeation. *In vitro* tools for assessing hepatic metabolism are isolated hepatocytes and liver microsomes (Houston and Carlili, 1997; Obach, 1999). Thus, all processes driving the intrinsic hepatic clearance can be assessed by established *in vitro* tools.

Step 2: Upscaling of *in vitro* to human *in vivo* values and determination of the intrinsic hepatic clearance.

The *in vitro* determined PS and CL values are normalized to either the protein amount or the number of cells used in the respective *in vitro* systems. In order to extrapolate the *in vitro* data to organ levels, species,-and *in vitro* system-specific scaling factors are applied : $99 \cdot 10^6$cells/(g liver) for suspended hepatocytes; 53 (mg protein)/(g liver) for liver microsomes; 116 (mg protein)/(g liver) for sandwich-cultured hepatocytes; and 25.7 (g liver)/(kg body weight) (Carlile et al., 1997; Swift et al., 2010). Subsequently, using the upsclaled values equation 2.11 can be used to calculate the human hepatic intrinsic clearance.

Step 3: Hepatic organ models.

Three liver models are mainly used for hepatic IVIVE: the well-stirred liver model, the dispersion model, and the parallel-tube model. Among those, the well-stirred liver model is most frequently applied (Lave et al., 2009; Ito and Houston, 2004). The approach is based on the assumption that instantaneous and complete mixing occurs within the liver and only unbound drug is subject to elimination. Mathematically, based on the well-stirred model the hepatic organ clearance is assessed as follows (Pang and Rowland, 1977; Rowland and Tozer, 2011a):

$$CL_h = \frac{Q_h \cdot f_{u,b} \cdot CL_{h,int}}{Q_h + f_{u,b} \cdot CL_{h,int}} \tag{2.12}$$

where Q_h is the hepatic blood flow rate ($L \cdot h^{-1}$) and fu_b is the fraction unbound of drug in blood (-). Thus, if fu_b is available, the hepatic clearance can be calculated with the help of the upscaled $CL_{h,int}$ values from equation 2.11 .

2.5.2 Renal IVIVE methods

As described in section 2.3.2, the net renal clearance involves glomerular filtration, tubular secretion, renal metabolism, and tubular reabsorption. In contrast to IVIVE methods to predict human hepatic clearances, renal IVIVE methods are less well established for multiple reasons including mainly the lack of suitable *in vitro* systems to study secretive and reabsorptive processes and the complexity of the underlying renal physiology. Thus, in contrast to hepatocytes where all hepatic clearance processes occur, renal clearance involves multiple cell and tissue structures (glomerulus, proximal tubule, distal, tubule; see section 2.3.2).

Nevertheless, renal organ models were establish taking glomerular filtration, tubular secretion, and tubular reabsorption into account (Kusuhara and Sugiyama, 2009; Watanabe et al., 2011):

$$CL_r = \left(\underbrace{f_{u,b} \cdot GFR}_{filtration} + \underbrace{\frac{Q_r \cdot f_{u,b} \cdot CL_{r,int}}{Q_r + f_{u,b} \cdot CL_{r,int}}}_{secretion} \right) \cdot \underbrace{(1 - f_{reab})}_{reabsorption} \tag{2.13}$$

where GFR is the glomerular filtration rate ($L \cdot h^{-1}$), Q_r is the renal blood flow rate ($L \cdot h^{-1}$), $CL_{r,int}$ is the renal intrinsic clearance ($L \cdot h^{-1}$), and f_{reab} is the fraction of drug reabsorbed (-). In equation 2.13 the well-stirred liver model is adapted to describe the tubular secretion clearance. Following this approach, the filtration clearance can be determined when fu_b of a drug is known while $CL_{r,int}$ and f_{reab} require input data from *in vitro* studies. However, *in vitro*-based methods that allow the determination of these values are lacking, thus limiting the application of equation 2.13 on renal IVIVE.

2.5.3 Quantitative absolute targeted proteomics to assess transporter protein abundance

Recently, novel technology based on liquid chromatography-linked tandem mass spectrometry (LC-MS/MS) with multiple reaction monitoring has been established that allows the quantitative assessments of drug transport proteins in cell samples (Ohtsuki et al., 2011). This method has been shown to be a useful tool to characterize cell samples with respect to their absolute transporter protein expression (Ohtsuki et al., 2012; Kamiie et al., 2008; Sakamoto et al., 2011; Uchida et al., 2011). Moreover, protein abundance data have been used to investigate the quantitative contribution of specific drug transporters to the net hepatic uptake of drugs by assuming a direct transporter protein expression-activity relationship (Bi et al., 2013; Kimoto et al., 2012; Karlgren et al., 2012). As illustrated above, active transport processes are determinants of the hepatic and renal clearances. Thus, quantitative targeted absolute proteomics (QTAP) to determine transporter protein abundances is expected to be a promising tool in the investigation of underlying clearance processes. In the following, the methodology of QTAP for the assessment of drug transporter protein levels is illustrated.

Quantitative assessment of transporter protein levels

Sensitive analysis of whole proteins by LC-MS/MS is limited by the size and solubility of the protein (Steen and Mann, 2004; Ohtsuki et al., 2011). Therefore, QTAP is performed with selected target peptides as surrogates for the respective proteins. Target peptides need to fulfill certain requirements including a unique amino acid sequence, efficient tryptic digestions and good MS sensitivity (Steen and Mann, 2004; Ohtsuki et al., 2011). Based on *in silico* investigations, Uchida et al. published a list of suitable target peptides of most commonly investigated drug transporters (Uchida et al., 2011). Once, target peptides are identified, stably isotope-labeled and unlabeled peptides of the same amino acid sequence are synthesized, serving as internal standards. Consequently, the internal standards are eluted at the same retention time as the target peptides but can be

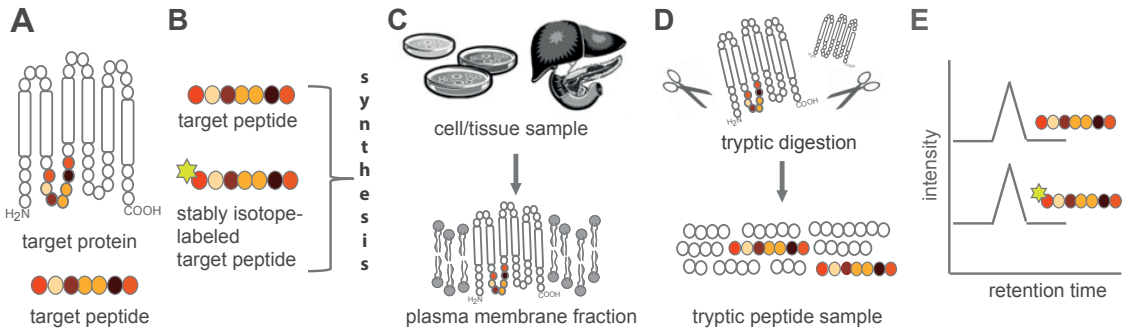

Figure 2.7: Methodology of quantitative targeted absolute proteomics (QTAP) analysis. A) Selection of target peptides from the target protein. B) Synthesis of stably isotope-labeled and unlabeled target peptide serving as internal standards. C) Extraction of the plasma membrane fractions of the cell or tissue samples. D) Tryptic digestion of the plasma membrane fractions causes cleavage of the target proteins into peptides including the target peptides. E) Addition of a fixed amount of labeled peptide (internal standard) to the tryptic peptide sample followed by LC-MS/MS analysis. The absolute amount of the target peptide is determined from the peak ratio obtained from the target peptide and internal standard. *The figure was adapted from Ohtsuki et al. (2011).*

distinguished by MS due to the difference in mass (Ohtsuki et al., 2011).
The first step in the sample preparation is the isolation of the plasma membrane fractions from the respective cell or tissue samples. Thereby, subcellular fragmentation is achieved following multiple centrifugation and homogenization steps according to established protocols (Sakamoto et al., 2011; Ohtsuki et al., 2012). Once the plasma membrane fractions are obtained they are subjected to tryptic digestion thereby cleaving the transporter proteins into respective peptides, including the selected target peptides. After adding a fixed amount of synthesized labeled target peptide (internal standard) the solution is analyzed by LC-MS/MS with multiple reactions monitoring, thus allowing simultaneous quantification of up to 37 proteins per assay. The absolute amount of target peptide is quantified by calculating the peak ratios of the target peptides to those of the internal standards (Steen and Mann, 2004; Ohtsuki et al., 2011). Figure 2.7 summarized the main steps of the QTAP analysis.

2.6 Assessment of the Transporter-Mediated Drug-Drug Interaction Potential from Cell-Based *In Vitro* Studies

As illustrated in the previous sections drug transporters exhibit a pivotal role in the human drug elimination. Therefore, inhibition of renal and hepatic transporters due to co-medication can result in a reduced drug clearance, potentially causing an increase in drug plasma concentrations and/or systemic drug exposure of the victim drug.
During the last decade, several examples for transporter-mediated DDIs were described in literature. In 2001 the lipid-lowering drug cerivastatin was withdrawn from the market after causing severe cases of myopathy and fatal rhabdomylysis. Thereby, an increased risk of side-effects

was recognized following co-administration with gemfibrozil (Staffa et al., 2002). Cerivastatin is primarily eliminated by the liver and retrospective analysis based on *in vitro* pharmacokinetic data linked the clinically observed DDIs to the concomitant inhibition of OATP1B1 and metabolic enzymes (Shitara et al., 2004). Furthermore, clinical studies reported severe adverse effects including toxicity upon co-administration of methotrexate and non-steroidal anti-inflammatory drugs (NSAIDs) (Liegler et al., 1969; Thyss et al., 1986). It was observed that NSAIDs lowered the renal clearance of methotrexate. Based on *in vitro* studies it was shown that methotrexate is actively renally secreted by OATs and MRPs and the clinically observed DDI are likely caused by inhibition of these transporters due to co-medication (Uwai et al., 2000, 2004; El-Sheigk et al., 2007).
The examples above illustrate that drug transporter-mediated DDIs can have a significant impact on a drugs safety and efficacy. Therefore, the assessment of the DDI potential of new molecular entities is an important step in the drug development process. Static, *in vitro* based methods have been established to predict the impact of transporter inhibition due to co-medication (pertrator drug) on NMEs (victim drug). In the following, these methods are introduced.

2.6.1 Transporter inhibition and IC_{50} values

A measure of the inhibitory potential of a perpetrator substance on a drug transporter is given by the IC_{50} value, representing the drug concentration that causes 50% inhibition of the maximal observed transporter activity. The IC_{50} value can be assessed with the help of cell-based *in vitro* systems introduced in 2.4.1. A commonly used approach is based on co-incubation of transporter-transfected cells with a transporter-specific substrate and an increasing concentration of the perpetrator drug. Following, the IC_{50} can be determined based on curve fitting using sigmoidal Hill kinetics:

$$\%of\ control = \frac{\%_{max} \cdot I^n}{IC_{50}^n + I^n} \tag{2.14}$$

where % of control is the observed transporter inhibition in the presence of a potent transporter inhibitor, $\%_{max}$ is the maximal observed transporter inhibition caused by a perpetrator, I is the concentration of the perpetrator drug and n is the Hill coefficient which is a measure of the cooperativity of the inhibition affinity to the active binding sites (n = 1, no cooperativity; n < 1, negative coorperativity; n > 1 indicates positive cooperativity). The lower the IC_{50} value the higher is the *in vitro* inhibitory potential of a perpetrator on the respective transporter.

2.6.2 R-value approach

Based on *in vitro* data, The R-value approach is used to assess the *in vivo* impact of transporter inhibition on a drugs exposure. By that, estimates of the AUC ratio in the presence and absence of a perpetrator drug (i) (AUC_i/AUC) can be calculated as follows (Shitara et al., 2005; Barton et al., 2013):

$$R = \frac{AUC_i}{AUC} = 1 + \frac{I \cdot (1 + S/K_m)}{IC_{50}} \tag{2.15}$$

where I is the *in vivo* concentration of the perpetrator drug. The variables S and K_m refer to the transporter-specific probe substrate which was applied in the *in vitro* inhibition assay to determine the IC_{50}. If the substrate concentration is sufficiently below the K_m (S « K_m), the R-value can be approximated as follows:

$$R = 1 + \frac{I}{IC_{50}} \tag{2.16}$$

In contrast to the IC_{50} value which is only a measure of the inhibitory potential of a perpetrator on a transporter the R-value approach predicts the clinical relevance of this inhibitory potential, as given by the change in exposure. Thus, the higher the inhibitor concentration and the inhibitory potential on drug transporters (indicated by a low IC_{50}) the higher is the anticipated DDI potential. However, due to its simplification the R-value approach rather provides a qualitative estimation if transporter-effects are anticipated to be of clinical relevance than a quantitative prediction of the DDI potential.

2.6.3 DDI assessment based on the mechanistic hepatic clearance model: Introduction of the Extended Clearance Concept Classification System (ECCCS)

For the liver, the hepatic clearance can be described with the well-stirred approach. Following oral administration of a drug and its perpetrator and assuming that the liver is the only clearance organ and that the fraction of drug absorbed, the hepatic blood flow rate, and the fraction of drug unbound in blood does not change in the presence of the perpetrator, the AUC ratio can be determined as follows (Einolf, 2007):

$$\frac{AUC_i}{AUC} = \frac{CL_{h,int}}{CL_{h,int,i}} \tag{2.17}$$

Based on the mechanistic extended clearance concept, the intrinsic hepatic clearance is described as a function of all governing processes, as stated in equation 2.11. A perpetrator can exhibit inhibitory potential (f_i) on all active processes driving the hepatic intrinsic clearance (Camenisch and Umehara, 2012):

$$\begin{aligned} CL_{h,int} = & \frac{[(1-f_{i,inf})\cdot PS_{inf,act} + PS_{inf,pas}]}{[(1-f_{i,eff})\cdot PS_{eff,act} + PS_{eff,pas}] + [(1-f_{i,sec})\cdot CL_{bile}] + [(1-f_{i,met})\cdot CL_{met}]} \\ & \cdot [(1-f_{i,sec})\cdot CL_{bile} + (1-f_{i,met})\cdot CL_{met})] \end{aligned} \tag{2.18}$$

Table 2.2: Characteristics of the ECCCS.

ECCCS	rate-limiting clearance pathway	anticipated DDI potential
Class 1	$PS_{inf,pas}$	metabolic enzymes
Class 2	CL_{bile}, CL_{met}	canicular efflux transporters and metabolic enzymes; only metabolic enzymes (if $CL_{sec} \ll CL_{met}$)
Class 3	$PS_{inf,act}$, $PS_{inf,pas}$	sinusoidal uptake transporters
Class 4	all governing processes	sinusoidal and canicular transporters, metabolic enzymes

ECCCS refers to the Extended Clearance Concept Classification System. $PS_{inf,act}$ and $PS_{inf,pas}$ refer to the active and passive hepatic influx over the sinusoidal membrane; $PS_{eff,act}$ and $PS_{eff,pas}$ are to the active and passive hepatic efflux over the sinusoidal membrane; CL_{bile} is the biliary clearance, and CL_{met} refers to the metabolic clearance. *The table was adapted according to Camenisch and Umehara (2012).*

Camenisch and Umehara recently reported an extended clearance concept classification system (ECCCS) which allows the prediction of the DDI potential of drugs based on their rate-limiting hepatic clearance pathway (Camenisch and Umehara, 2012). In contrast to the BDDCS, introduced in section 2.3.3, the ECCCS does not require human *in vivo* data but is based on the incorporation of *in vitro* parameters, driving the hepatic clearance as described by equation 2.18. According to the ECCCS drugs are categorized into four classes whose characteristics are summarized in Table 2.2. Metabolism is projected as the major hepatic DDI potential of highly permeable class 1 and 2 compounds. While passive hepatic uptake is the rate-limiting step for class 1 compounds, the interplay between metabolism and transporter-mediated biliary secretion is predicted to be rate-limiting for class 2 compounds. Hepatic uptake is predicted to be the rate-limiting step for class 3 compounds and major DDI effects are anticipated upon inhibition of hepatic uptake transporters. For class 4 compounds, all processes driving the hepatic elimination (metabolism, uptake and efflux) can be rate-limiting. Therefore, inhibition of metabolic enzymes as well as sinusoidal and canicular drug transporters is anticipated as DDI potential of class 4 compounds. Thus, application of the ECCCS allows for a compound-class dependent assessment of the DDI potential of drugs based on the extended mechanistic clearance concept.

Chapter 3

Objectives

The development of new molecular entities is a step-wise process involving preclinical and clinical phases. In this context, the early characterization of NMEs with respect to their safety and efficacy is of major concern. Both components are influenced by the exposure of the drug within the body which itself is affected by drug clearance processes. As introduced in chapter 2, drug transporters play a pivotal role in the pharmacokinetics of absorption, distribution, metabolism, and excretion (ADME). Thereby, transporters are now well recognized as major determinants of drug clearances. Besides their involvement in the hepatobiliary and renally secretion of drugs they impact the access of drugs to clearance organs and hence metabolic enzymes. Alterations in transporter activities can therefore affect a drugs exposure and consequently its safety and/or efficacy (see section 2.6). That is why the early characterization of the PK profile, including drug-transporter interactions, is a key step in the development of NMEs. However, in preclinical drug development information of human *in vivo* PK data are lacking. Therefore, as described in sections 2.4 and 2.5, *in vitro*-based methods are commonly used to first assess PK properties of NMEs. Consequently, the development, validation, and characterization of these methods is of major importance in drug development.

It was the aim of this work to investigate the prediction of human renal and hepatic drug clearances by IVIVE models that account for active drug transport processes. In a second step, the applicability of *in vitro*-based methods to predict the DDI potential of drugs was assessed. Within this context, the following objectives were defined:

- **The establishment of a mechanistic IVIVE method to predict the human renal clearance of drugs**.
  As introduced in sections 2.3, the renal clearance is a major elimination pathway of drugs and thus an important parameter in the PK profile of NMEs. Current *in vitro*-based methods for the early assessment of the human renal clearance are lacking (see 2.4 and 2.5). To overcome this drawback, this study aimed to develop a novel physiologically based IVIVE method that enables the prediction of the human renal drug clearance based on filtration, secretion, and reabsorption. To gain mechanistic understanding of the renal excretion, the method should allow the assessment of the contribution of the underlying clearance pathways to the net organ clearance. This study further aimed to investigate, if the major renal drug clearance pathways correlate with their assignment to the Biopharmaceutical Drug Disposition Classification System.

- **The investigation of the transporter protein expression- activity relationship to predict the contribution of transporters involved in hepatic drug uptake.**
  Section 2.5.3 introduced the application of quantitative targeted absolute proteomics to investigate the drug transporter protein abundance. This method proved to be a promising tool to characterize cell systems with respect to their quantitative transporter protein expression. Moreover, QTAP was applied to investigate the contribution of transporter-specific drug uptake into hepatocytes based on a transporter protein expression-activity correlation. An objective of this study was to further investigate the transporter protein expression-activity relationship. For this purpose the following hypothesis was questioned: If transporter protein abundance directly translates into transporter activity, activities determined in cell lines could be extrapolated into other tissues by using relative protein expression values as scaling factors. This study aimed to investigate this hypothesis by assessing the predictability of the contribution of OATP1B1- and OATP1B3-mediated transport in hepatocytes from activity measurements in single-transporter expressing cell lines.

- **The prediction of the DDI potential of statins based on an extended mechanistic hepatic clearance model.**
  Statins are lipid-lowering drugs that are widely prescribed for the prevention of cardiovascular diseases. Therefore, patients treated with statins are likely under co-medication and a multitude of clinical studies investigated the impact of co-medication on statin exposure. As described above the characterization of NMEs in terms of their safety is crucial in early

drug development. Section 2.6, introduced a recently established method that allows the prediction of the DDI potential of compounds based on their rate-limiting hepatic clearance pathways. In order to further validate this method, a direct comparison between the predicted DDI potentials and clinically observed DDIs would be benificial. Moreover, a novel hepatic IVIVE method has been recently reported that allows the prediction of the hepatic clearance based on its governing processes (see section 2.5). The combination of both approaches could be used in early drug development for a first risk assessment of NMEs. Using statins as model drugs, this study therefore aimed to further validate the application of the mechanistic clearance concept to predict the hepatic clearance of statins and subsequently assess their DDI potential. In this context, the use of the Extended Clearance Concept Classification System to anticipate the major DDI potential of statins was assessed.

- **The assessment of the inhibitory potential of telaprevir on renal and hepatic drug transporters.**
  In clinical studies telaprevir, a new marketed drug, has been shown to be involved in drug-drug interactions as a perpetrator. *In vitro* studies demonstrated that telaprevir inhibits metabolic enzymes but data on its interaction with drug transporters are lacking. As illustrated in section 2.6, DDIs can be the result of drug transporter inhibition. Therefore, the purpose of this study was the application of cell-based *in vitro* systems to investigate the inhibitory potential of telaprevir on major human renal and hepatic SLC transporters.

Chapter 4

In vitro- in vivo extrapolation method to predict human renal clearance of drugs

Annett Kunze[a,b], Jörg Huwyler[b], Birk Poller[a], Heike Gutmann[a], Gian Camenisch[a]

[a] Division of Drug Metabolism and Pharmacokinetics, Drug-Drug Interaction Section
Novartis Institutes for Biomedical Research, CH-4056 Basel, Switzerland

[b] Department of Pharmaceutical Sciences, Division of Pharmaceutical Technology
University of Basel, CH-4056 Basel, Switzerland

This work is published in:

Journal of Pharmaceutical Sciences
2014 Mar;103(3): 994-1001
doi: 10.1002/jps.23851.
Epub 2014 Jan 13.

4.1 Abstract

Renal clearance is a key determinant of the elimination of drugs. To date, only few in *vitro- in vivo* extrapolation (IVIVE) approaches have been described to predict the renal organ clearance as the net result of glomerular filtration, tubular secretion, and tubular reabsorption. In this study, we measured in LLC-PK_1 cells the transport of 20 compounds that cover all four classes of the Biopharmaceutical Drug Disposition Classification System. These data were incorporated into a novel kidney model to predict all renal clearance processes in human. We showed that filtration and secretion were main contributors to the renal organ clearance for all compounds, whereas reabsorption was predominant for compounds assigned to classes 1 and 2. Our results suggest that anionic drugs were not significantly secreted in LLC-PK_1 cells, resulting in under-predicted clearances. When all study compounds were included a high overall correlation between the reported and predicted renal organ clearances was obtained (R^2 = 0.83). The prediction accuracy in terms of percentage within two-fold and three-fold error was 70% and 95%, respectively. In conclusion, our novel IVIVE method allowed to predict the human renal organ clearance and the contribution of each underlying process.

4.2 Introduction

Besides the liver, the kidney is the major organ responsible for the elimination of drugs from the systemic circulation. Renal elimination of drugs is considered to be a major clearance process, when the excretion of unchanged drug into the urine exceeds 25% of the absorbed dose (Morrissey et al., 2013). As summarized by Morrissey et al, 32% of the top 200 prescribed drugs in the United States in 2010 were cleared at least partially by renal elimination (Morrissey et al., 2013). Therefore, renal clearance should be considered as potentially important route of elimination for any new chemical entity.

Renal excretion describes the elimination process of unchanged drugs from the blood circulation into the urine and is the net result of glomerular filtration, tubular secretion, and tubular reabsorption. Glomerular filtration is a passive process and the filtration clearance $CL_{r,fil}$ equals the product of the glomerular filtration rate (GFR) and the unbound fraction of drug in blood fu_b. Tubular secretion describes the trans-epithelial permeation of drugs from the blood into the tubular fluid and the secretion clearance ($CL_{r,sec}$) is the sum of active secretion and passive permeation. Active tubular secretion of drugs is mediated by organic anion (OAT) and organic cation transport (OCT) systems. These systems contain various drug transporters that mediate the active cellular uptake of drugs from the blood into the proximal tubule and its subsequent efflux into the tubular fluid (Morrissey et al., 2013; Li et al., 2006). For example, the secretion of cationic drugs is mediated by the organic cation transporter OCT2, which is expressed at the basolateral membrane of proximal tubule cells,

and the apically expressed multidrug and toxin extrusion proteins MATE1 and MATE2K as well as the P-glycoprotein (P-gp) (Morrissey et al., 2013; Li et al., 2006). Weakly acidic drugs are secreted by the organic anion transporters OAT1 and OAT3, which are expressed at the basolateral membrane, and the multidrug resistance-associated proteins MRP2 and MRP4 as well as the breast cancer-resistant protein (BCRP) (Morrissey et al., 2013). The latter transporters are expressed at the apical membrane. Tubular reabsorption describes the back-flux of drugs from the tubular fluid into the blood. Although active reabsorption may occur (e.g. via the organic cation transporter proteins OCTN1 and OCTN2), this process is mainly dependent on the passive permeability of a compound (Feng et al., 2010; Masereeuw and Russel, 2001).

Tubular secretion and reabsorption involve both active, transporter-mediated processes, and passive permeation across the tubular epithelium. Consequently, an *in vitro* model that allows the determination of both processes is needed. The proximal tubule cell line LLC-PK_1, derived from pig (*Sus scrofa*) kidney, has been used in various studies to examine the renal disposition of compounds. When grown on permeable filter membranes, LLC-PK_1 cells form confluent, polarized cell monolayers that allow the the conduction of trans-epithelial transport studies. LLC-PK_1 cells were shown to be a suitable *in vitro* system for studying the active secretion of cationic compounds (Masago et al., 2010; Takaai et al., 2007; Urakami et al., 2005; Saito et al., 1992). Furthermore, expression of endogenous P-gp, MRP2, and BCRP in LLC-PK_1 cells was shown on mRNA and protein level (Kuteykin-Teplyakov et al., 2010; Takada et al., 2005). Following standard protein basic local alignment analysis (http://plast.ncbi.nlm.nih.gov) between *S. scrofa* and *Homo sapiens* revealed over 80% identity for OAT3, OCT1, P-gp, MRP2, and OCTN1; and 79% for BCRP.

The Biopharmaceutical Drug Disposition Classification System (BDDCS), established by Benet et al., classifies drugs according to their *in vivo* reported extent of metabolism (extensive >70%, poor <30%) and solubility to predict the disposition and potential drug-drug interactions of new chemical entities (Benet et al., 2011). Through *in vitro* studies, Camenisch and Umehara demonstrated that the BDDCS class assignments correlate with the major route of hepatic elimination of drugs (Umehara and Camenisch, 2012; Camenisch and Umehara, 2012).

In the current study, we aimed to establish a novel physiological-based *in vitro-in vivo* extrapolation (IVIVE) method to predict the human renal organ clearance based on filtration, secretion, and reabsorption processes. We used LLC-PK_1 cells as an *in vitro* tool to measure the bidirectional epithelial permeation of a set of 20 compounds with various physiochemical properties covering all four BDDCS classes. The obtained permeability data were incorporated in our model to predict $CL_{r,fil}$, $CL_{r,sec}$, the fraction of drug reabsorbed (f_{reab}), and following the total renal organ clearance ($CL_{r,org}$). We assessed the correlation between the *in vitro* predicted and *in vivo* reported renal clearances. Specifically, we investigated which underlying process is the major determinant for the overall renal organ clearance for all four BDDCS classes.

4.3 Materials and methods

Materials

[^{3}H]desipramine (80 Ci/mmol), [^{3}H]digoxin (40 Ci/mmol), [^{3}H]imipramine hydrochloride (47.5 Ci/mmol), [^{14}C]D-mannitol (0.0588 Ci/mmol), [^{3}H]propranolol (30 Ci/mmol), and [^{3}H]verapamil hydrochloride (65.6 Ci/mmol) were acquired from PerkinElmer (Boston, MA). [^{3}H]amantadine hydrochloride (0.2 Ci/mmol), [^{3}H]aten- olol (7.3 Ci/mmol), [^{14}C]creatinine hydrochloride (0.0573 Ci/mmol), [^{3}H](R,S)-fexo- fenadine hydrochloride (0.29 Ci/mmol), [^{3}H]fluconazole (9.9 Ci/mmol), [^{3}H]metho- trexate disodium (25.9 Ci/mmol), and [^{3}H]tetracycline (17.1 Ci/mmol) were purchased from Moravek Biochemicals, Inc (Brea, CA). [^{3}H]ketoconazole (10 Ci/mmol), [^{3}H]atorva- statin calcium (10 Ci/mmol), [^{3}H]chloroquine (20 Ci/mmol), [^{3}H]cimeti- dine (80 Ci/mmol), [^{14}C]metformin hydrochloride (80 Ci/mmol), [^{3}H]pravastatin sodium (5 Ci/mmol), and [^{3}H]quinidine (20 Ci/mmol) were obtained from American Radiolabeled Chemicals, Inc. (St. Louis, MO). [^{3}H]cyclosporine A (20 Ci/mmol) was purchased from Amersham (Buckinghamshire, UK) and [^{14}C]valsartan (39.6 Ci/mmol) was synthesized internally (Isotope Laboratories, Drug Metabolism and Pharmacolinetics, Novartis Pharma AG, Basel, Switzerland). All other compounds and reagents were of analytical grade and purchased from commercial sources.

Cell culture

The LLC-PK$_1$ cell line at passage 197 (ATCC CL-101TM) was obtained from the American Type Culture Collection (ATCC, Manassas VA). The cells were cultivated in medium 199 (Sigma-Aldrich, St. Louis, MO) supplemented with 10% fetal bovine serum (FBS), at 37°C under a humidified atmosphere containing 5% CO_2.The culture medium was changed every second to third day. The cells were cultivated for a maximum period of 6 weeks and were passaged 13 times.

Bidirectional permeability studies in LLC-PK$_1$ cells

We conducted the bidirectional transport studies in Corning Transwell cell culture inserts (Corning Inc., Corning, NY). The LLC-PK$_1$ cells were seeded on a microporous poly-carbonate membrane (0.4 µm pore size; 0.33 cm^2 surface area) at a density of $5 \cdot 10^5$ cells/cm^2. The cells were maintained for four days as described above. On the day of the experiment, we measured the trans-epithelial electrical resistance (TEER) with a Millicell Electrical Resistance System (Millipore, Bedfor, MA) according to the manufac-

turer's recommendations. The transport studies were carried out only with cell monolayers that exceeded a TEER value of 120 Ωcm^2.
To account for physiological conditions, a pH difference between blood (basolateral) and urine (apical) compartments was applied neglecting urinary pH variations. The experiments were performed in modified Krebs buffer adjusted to pH 7.4 and 6.8 for the basolateral (lower chamber, 1.0 mL) and apical compartment (upper chamber, 0.2 mL), respectively (Brown et al., 2008). We replaced the cell culture medium with prewarmed assay buffer (37°C) and preincubated the cell monolayers for 30 min. Subsequently, the buffer was aspirated and buffer containing the radio-labeled study compound was added to the donor compartment. All study compounds were prepared as a mixture of labeled and unlabeled substance to obtain a final concentration of 1 µM. The cell monolayers were incubated for 20 min at 37°C. Aliquots (0.1 mL) of both compartments were transferred into scintillation vials and the radioactivity was determined by liquid scintillation counting using a Packard Tri-Carb 2700TR (Westwood, MA). To evaluate the reproducibility of data in terms of active compound transport, we studied the basolateral to apical transport of creatinine (5 µM) in the presence and absence of N-methyl-4phenylpyridium acetate (MPP^+; 100 µM). Creatinine is known to be transported across the LLC-PK_1 monolayers by an active process which is inhibited by MPP^+ (Urakami et al., 2005). Furthermore, we measured the basolateral to apical transport of D-mannitol (1 µM) to evaluate the integrity of the cell monolayers.
The apparent permeability P_{app} (cm/min) was calculated with:

$$P_{app} = \frac{V_R \cdot C_R}{t \cdot A \cdot C_D} \tag{4.1}$$

where V_R determines the incubation volume (mL) in the receiver chamber, C_R refers to the substrate concentration (µM) in the receiver chamber at the end of the incubation time t (min), A is the surface area of the transwell filter membrane (cm^2), and C_D determines the initial substrate concentration (µM) in the donor chamber. From bidirectional transport experiments P_{app} values were determined in basolateral to apical ($P_{app,BA}$) and apical to basolateral ($P_{app,AB}$) directions.

Upscaling of *in vitro* parameters

The *in vitro* determined $P_{app,BA}$ and $P_{app,AB}$ values were upscaled to the human intrinsic clearances [$CL_{r,int,BA}$ and $CL_{r,int,AB}$, respectively; mL/(min· kg)] with:

$$CL_{r,int} = P_{app} \cdot \frac{\pi \cdot l_{PT} \cdot d_{PT} \cdot n_{nep} \cdot n_{kid}}{BW} \tag{4.2}$$

where the surface of the human proximal tubule is calculated as the product of its length l_{PT} (1.5 cm), its diameter d_{PT} ($7 \cdot 10^{-3}$ cm), and the number pi (= 3.141). n_{nep} is the number of nephrons per kidney ($1.5 \cdot 10^{6}$), n_{kid} the number of kidneys in human (2), and BW is the average human body weight (70 kg) (Lote, 2012).

Determination of human renal clearance

The renal organ clearance ($CL_{r,org}$), as descriptor of renal excretion, is a composed process involving glomerular filtration clearance ($CL_{r,fil}$), tubular secretion clearance ($CL_{r,sec}$), metabolic clearance, and reabsorption of a fraction of drug from the tubule fluid back into the blood (f_{reab}). Assuming that the contribution of renal metabolic clearance is negligible $CL_{r,org}$ can be expressed as (Okudaira and Sugiyama, 1996; Fagerholm, 2007; Kusuhara and Sugiyama, 2009):

$$CL_{r,org} = \left(CL_{r,fil} + CL_{r,sec}\right) \cdot (1 - f_{reab}) \tag{4.3}$$

The filtration clearance can be calculated as the product of GFR [1.79 mL/(min· kg)] and the unbound fraction of drug in blood (fu_b) provided in Table 4.1 (Dewoskin and Thompson, 2008):

$$CL_{r,fil} = fu_b \cdot GFR \tag{4.4}$$

In analogy to the well-stirred liver model, $CL_{r,sec}$ can be expressed as a function of the renal blood flow rate $Q_{r,b}$ [17.14 mL/(min· kg)], fu_b, and the intrinsic clearance of tubular secretion (Dewoskin and Thompson, 2008; Shitara et al., 2005). Assuming that secretion occurs exclusively in the renal proximal tubules, the intrinsic clearance of tubular secretion was approximated with $CL_{r,int,BA}$ (Eqs 4.1 and 4.2). Consequently, $CL_{r,sec}$ was calculated as follows:

$$CL_{r,sec} = \frac{Q_{r,b} \cdot fu_b \cdot CL_{r,int,BA}}{Q_{r,b} + fu_b \cdot CL_{r,int,BA}} \tag{4.5}$$

Reabsorption can be determined analogous to the secretion clearance. As it occurs from the tubule fluid into the blood, we substituted $Q_{r,b}$ in 4.5 with GFR, used $CL_{r,int,AB}$ instead of $CL_{r,int,BA}$, and assumed protein binding in the tubule fluid to be negligible (Dewoskin and Thompson, 2008). Consequently, the fraction of drug reabsorbed was calculated as follows:

$$f_{reab} = \frac{CL_{r,int,AB}}{GFR + CL_{r,int,AB}} \tag{4.6}$$

Finally, we obtained the predicted renal organ clearance ($CL_{r,org,in\ vitro}$) by substituting the variables from Eqs. (4.4-4.6) into Eq. 4.3.

Data analysis

We performed at least two independent bidirectional transwell experiments for each compound. Each experiment consisted of triplicate incubations (n = 3). The permeability ($P_{app,BA}$) of the reference compounds creatinine and mannitol was measured in 12 independent experiments. Data were expressed as the mean of all incubations and the differences between creatinine permeabilities in the presence and absence of MPP^+ was calculated by unpaired Student's *t*-test. Differences were considered statistically significant when *p* was < 0.05. The correlation between (*in vitro*) predicted and the (*in vivo*) observed clearances was investigated by linear regression analysis using Microsoft Excel. As the clearance values show a log-normal distribution, the linear regression analysis was performed with log-transformed values to obtain the regression equation and the correlation coefficient (R^2). To indicated the predictive accuracy, average fold errors (afe) between the observed and predicted clearances were calculated:

$$afe = 10^{\left|\frac{1}{N}\sum log\frac{predicted}{observed}\right|} \tag{4.7}$$

A perfect prediction would be indicated by an afe value of one and a successful prediction method is represented by an afe below two (Obach et al., 1997).

4.4 Results

Compound characteristics

We selected the 20 study compounds based on their physiochemical and pharmacokinetic properties, to generate a heterogeneous test set covering all four BDDCS classes as summarized in Table 4.1. A further selection criterion was the availability of reported clinical data such as protein binding, blood-to-plasma ratios, and renal clearances (Supplementary Information Table 6.3). The relative contributions of the *in vivo* renal organ clearance ($CL_{r,org,in\ vivo}$) to the total body clearance ($CL_{tot,in\ vivo}$) as reported in literature are illustrated in Figure 4.1. For all classes 1 and 2 compounds, renal clearance is a minor route of elimination with urinary excretion fractions (U_e) below 20%. In contrast, the contribution of renal clearance to total body clearance exceeds 20% for all classes 3

Table 4.1: Physiochemical and pharmacokinetic drug properties.

Compounds	BDDCS	pK_a	$LogD_{7.4}$	fu_b	Rb	$CL_{tot,in\ vivo}$ [mL/(min·kg)]	U_e (%)
Desipramine	Class1	10.2 (b)	1.40	0.21	0.857	12.05	2
Imipramine	Class1	9.5 (b)	2.20	0.13	1.100	9.92	2
Propranolol	Class1	9.5 (b)	1.20	0.11	1.182	20.81	1
Quinidine	Class1	4.3/8.5 (b)	1.82	0.27	0.444	7.30	19
Quinine	Class1	4.1/8.4 (b)	1.82	0.18	0.733	2.62	16
Verapamil	Class1	8.9 (b)	1.75	0.13	0.846	16.21	3
Atorvastatin	Class2	4.5 (a)	1.53	0.08	0.630	14.17	1
Cyclosporine A	Class2	n.a. (n)	2.92	0.03	2.333	4.88	1
Ketoconazole	Class2	2.9/6.5 (b)	4.05	0.02	0.500	4.46	3
Amantadine	Class3	10.1 (b)	-0.69	0.14	2.660	1.22	70
Atenolol	Class3	9.6 (b)	-1.03	0.89	1.070	2.18	91
Chloroquine	Class3	8.4 (b)	1.54	0.11	4.000	2.58	57
Cimetidine	Class3	6.8 (b)	0.33	0.84	0.952	7.43	84
Digoxin	Class3	n.a. (n)	1.26	0.82	0.915	3.58	66
Fexofenadine	Class3	4.3/9.5 (a)	2.68	0.56	0.550	11.00	13
Metformin	Class3	11.5 (b)	-5.41	1.00	1.000	6.56	99
Methotrexate	Class3	4.8/5.5 (a)	-2.52	0.65	0.830	2.63	74
Pravastatin	Class3	4.5 (a)	-0.23	0.97	0.536	25.19	47
Tetracycline	Class3	3.3/7.7/9.5 (a)	-1.41	0.84	0.900	2.37	85
Valsartan	Class4	3.9/4.7 (a)	-0.34	0.09	0.556	0.94	29

BDDCS refers to the Biopharmaceutics Drug Disposition Classification System according to Benet et al. (2011) fu_b refers tot he fraction of drug unbound in blood, $CL_{tot,\ in\ vivo}$ describes the total human body clearance, and U_e is the fraction of drug excreted into urine ($U_e = CL_{r,org,in\ vivo}/CL_{tot,in\ vivo} \cdot 100\%$). The letters b,a, and n refer to basic, acidic, and neutral, respectively. All literature references for the given values are listed in Table 6.3 of the Supplementary Information.

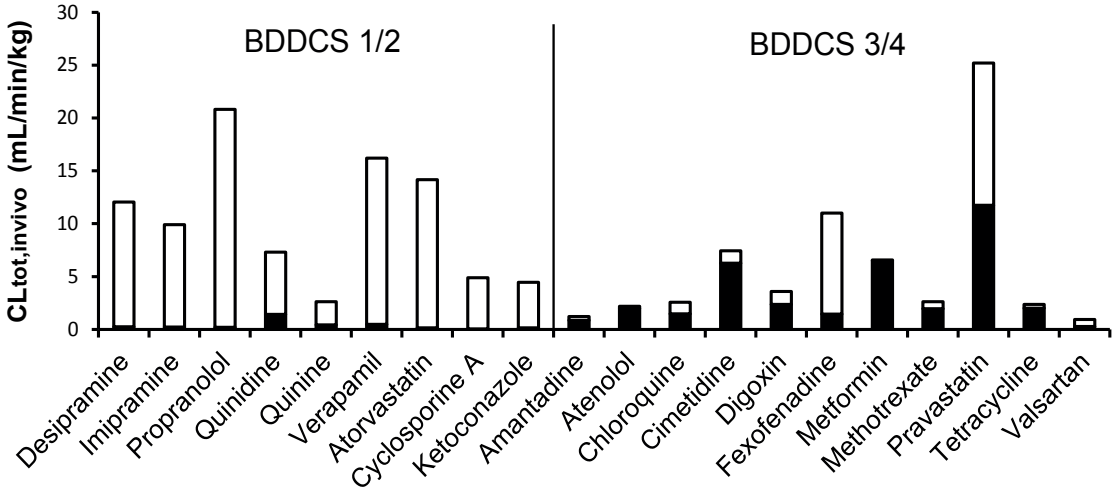

Figure 4.1: Relative contributions of the renal (black bars) and nonrenal (white bars) clearance pathways to the total body clearance for the study compounds according to Table 4.1. The line separates the study compounds assigned to BDDCS classes 1,2 and classes 3,4.

and 4 compounds except fexofenadine. For several class 3 compounds such as atenolol, cimetidine, or tetracycline, renal clearance is the predominant or exclusive (metformin) route of elimination with U_e above 80%. Literature references of all compounds including human physiochemical and pharmacokinetic parameters are provided as supplementary information.

Bidirectional permeability studies in LLC-PK$_1$ cells

For all compounds, bidirectional transport studies were performed at a concentration of 1 µM. It is assumed that this concentration is well below the K_m values of relevant basolateral uptake transporters allowing measurements of intrinsic transport properties for compounds that are actively secreted across the LLC-PK$_1$ monolayer (Morrissey et al., 2013). In addition, sink conditions were verified at the end of the bidirectional transport studies to assure linear transport conditions. For all study compounds, receiver chamber concentrations were below 10% of the donor chamber concentrations except for three compounds were deviations were assumed to be in an acceptable range (10%-13%).
To evaluate inter-assay variability of the LLC-PK$_1$ cell system regarding monolayer integrity and reproducibility of P_{app} values, we performed eight independent transport assays in basolateral to apical direction with creatinine and mannitol. We observed a mean $P_{app,BA}$ value of $28.6 \cdot 10^{-5} \pm 1.6 \cdot 10^{-5}$ cm/min for creatinine in the absence of an inhibitor. In the presence of MPP^+, creatinine transport was significantly reduced to a mean $P_{app,BA}$ of $16.5 \cdot 10^{-5} \pm 1.5 \cdot 10^{-5}$ cm/min ($p < 0.001$). For mannitol, we obtained a mean $P_{app,BA}$ value of $6.5 \cdot 10^{-5} \pm 0.5 \cdot 10^{-5}$ cm/min.
Table 4.2 lists the P_{app} values for all study compounds obtained from bidirectional transport experiments as well as the corresponding efflux ratios (ERs). The ERs ranged from 0.51 for atorvastatin to 8.99 obtained for cimetidine. Out of 20 study compounds, 15 exhibited ERs above 1, showing favored permeation in basolateral to apical direction. This might be caused by transporter-mediated active secretion and/or favored passive permeation based on lower degree of ionization of weak bases at pH 7.4 in the basolateral compartment (compared with apical of 6.8).

Renal clearance prediction

For all study compounds, the clearances for the individual renal elimination process ($CL_{r,fil}$, $CL_{r,sec}$, f_{reab}), as well as the overall renal organ clearances ($CL_{r,org,in\ vitro}$) were calculated as described in section 4.3. The resulting predictions are listed in Table 4.3.
For all BDDCS 1 and 2 study compounds with exception to quinidine, the reported *in vivo* renal organ clearances in humans ($CL_{r,org,in\ vivo}$) are below 1 mL/(min·kg). Our predicted filtration ($CL_{r,fil}$) and secretion ($CL_{r,sec}$) clearances were below 1 mL/(min·kg) for all

Table 4.2: Drug transmembrane permeation over the LLC-PK_1 monolayers.

Compounds	$P_{app,BA}$ (10^{-5} cm/min)	SD (10^{-5} cm/min)	$P_{app,AB}$ (10^{-5} cm/min)	SD (10^{-5} cm/min)	ER
Desipramine	199.82	2.72	89.38	5.05	2.24
Imipramine	273.75	9.08	142.15	7.46	1.93
Propranolol	408.82	53.31	241.75	11.54	1.69
Quinidine	178.10	10.10	39.11	6.14	4.55
Quinine	140.24	5.83	28.50	5.53	4.92
Verapamil	438.51	32.46	367.44	29.87	1.19
Atorvastatin	3.90	0.81	46.66	8.99	0.51
Cyclosporine A	165.18	31.37	81.94	4.6	2.02
Ketoconazole	138.44	3.90	96.78	13.09	1.43
Amantadine	128.17	6.38	15.86	1.02	8.08
Atenolol	7.92	0.43	9.49	1.12	0.83
Chloroquine	317.03	5.97	45.87	1.67	6.91
Cimetidine	201.59	18.22	22.43	1.26	8.99
Digoxin	41.42	2.55	15.46	1.89	2.68
Fexofenadine	12.04	1.11	13.05	3.02	0.92
Metformin	147.46	5.76	19.73	2.72	7.47
Methotrexate	10.27	0.62	10.13	2.09	1.01
Pravastatin	6.47	0.84	7.59	0.59	0.89
Tetracycline	106.25	4.54	97.29	11.09	1.09
Valsartan	30.46	1.62	40.73	1.15	0.75

$P_{app,BA}$ and $P_{app,AB}$ refer to the apparent permeabilities obtained from transport studies in basolateral to apical (BA) and apical to basolateral (AB) as described by Eq.4.1. The efflux ratio (ER) was calculated as the quotient of $P_{app,BA}$ and $P_{app,AB}$.

classes 1 and 2 compounds as well. The determined fraction reabsorbed ranged between 0.18 obtained for quinine and 0.74 obtained for verapamil.

For classes 3 and 4 compounds, $CL_{r,org,\ in\ vivo}$ ranged between 0.27 mL/(min·kg) reported for valsartan and 11.75 mL/(min·kg) reported for pravastatin. The predicted $CL_{r,fil}$ covered a range between 0.16 and 1.79 mL/(min·kg) for valsartan and metformin, respectively. The determined $CL_{r,sec}$ values ranged between 0.04 mL/(min·kg) for valsartan and 2.10 mL/(min·kg) for cimetidine. The calculated fractions reabsorbed were generally smaller for classed 3 and 4 compounds than observed for classes 1 and 2 with values below 0.2, except for valsartan (0.24), chloroquine (0.27), and tetracycline (0.43).

The correlation between the individual predicted clearance processes and $CL_{r,org,\ in\ vivo}$ is illustrated in Figure 4.2. When $CL_{r,org,in\ vivo}$ was correlated exclusively with $CL_{r,fil}$ (Fig. 4.2a), 14 compounds were within a three-fold error. Six compounds assigned to BDDCS classes 2 (namely ketoconazole) and 3 (namely amantadine, chloroquine, cimetidine, metformin, and pravastatin) were underpredicted though. Including all compounds, an afe of 1.94 was obtained, indicating a successful prediction of $CL_{r,org,\ in\ vivo}$ from $CL_{r,fil}$. When the dataset was separated into BDDCS classes 1/2 and 3/4, afe values of 1.40 and 2.54 were obtained, respectively. This analysis, indicated that BDDCS 1/2 compounds were well predicted by filtration only, in contrast to classes 3/4 compounds.

In Figure 4.2b, $CL_{r,org,in\ vivo}$ was correlated with $CL_{r,sec}$ showing that nine compounds (namely desipramine, imipramine, propranolol, quinidine, quinine, verapamil, cyclosporine A, cimetidine, and tetracycline) were within three-fold error and 11 compounds were un-

Table 4.3: Predicted human renal drug clearances from *in vitro* assays.

Compounds	$CL_{org,in\ vivo}$ [mL/(min·kg)]	$CL_{r,fil}$ [mL/(min·kg)]	$CL_{r,sec}$ [mL/(min·kg)]	$CL_{r,fil+sec}$ [mL/(min·kg)]	f_{reab}	$CL_{org,in\ vitro}$ [mL/(min·kg)]
Desipramine	0.26	0.38	0.57	0.95	0.41	0.56
Imipramine	0.23	0.23	0.49	0.72	0.53	0.34
Propranolol	0.21	0.20	0.61	0.81	0.66	0.28
Quinidine	1.42	0.48	0.65	1.13	0.24	0.86
Quinine	0.42	0.32	0.35	0.67	0.18	0.55
Verapamil	0.48	0.23	0.77	1.00	0.74	0.26
Atorvastatin	0.14	0.14	0.03	0.17	0.27	0.12
Cyclosporine A	0.05	0.05	0.07	0.12	0.39	0.07
Ketoconazole	0.14	0.04	0.04	0.08	0.43	0.05
Amantadine	0.86	0.25	0.25	0.50	0.11	0.45
Atenolol	1.99	1.59	0.10	1.69	0.07	1.57
Chloroquine	1.47	0.20	0.48	0.68	0.27	0.50
Cimetidine	6.26	1.50	2.10	3.60	0.15	3.06
Digoxin	2.38	1.47	0.47	1.94	0.11	1.73
Fexofenadine	1.44	1.00	0.09	1.09	0.09	0.99
Metformin	6.49	1.79	1.86	3.65	0.13	3.18
Methotrexate	1.95	1.16	0.09	1.25	0.07	1.16
Pravastatin	11.75	1.74	0.09	1.83	0.06	1.72
Tetracyline	2.02	1.50	1.18	2.68	0.43	1.53
Valsartan	0.27	0.16	0.04	0.20	0.24	0.15

$CL_{r,org,in\ vivo}$ denotes the *in vivo* reported renal blood clearance, $CL_{r,fil}$, $CL_{r,sec}$, $CL_{r,fil+sec}$, and $CL_{r,org,in\ vitro}$ denote the determined renal filtration clearance, the renal secretion clearance, the su of filtration and secretion clearances, and the predicted renal organc clearance according to Eqs.4.3-4.5. f_{reab} refers to the determined fraction of drug reabsorbed according to Eq. 4.6.

derpredicted including the majority of BDDCS classes 2,3, and 4 compounds. Including all compounds, an afe of 3.13 was obtained when $CL_{r,org,in\ vivo}$ was predicted from the secretion clearance. A separate analysis of classes 1/2 and 3/4 showed an excellent prediction for compounds assigned to classes 1/2 (afe = 1.04), whereas compounds, assigned to classes 3/4 were poorly predicted with an afe of 7.72.

When $CL_{r,org,in\ vivo}$ was correlated with the sum of filtration and secretion clearance ($CL_{r,sec+fil}$), the prediction was improved and 16 out of 20 study compounds were within a three-fold error (Fig. 4.2c). The BDDCS class 1 compounds desipramine, imipramine, and propranolol were slightly overpredicted, whereas the BDDCS class 3 compound pravastatin was underpredicted by more than six-fold. Following afe analysis including all compounds, an excellent prediction was obtained when $CL_{r,org,in\ vivo}$ was predicted from $CL_{r,sec+fil}$ (afe = 1.01). A separated analysis of classes 1/2 and 3/4 resulted in afe values of 1.80 (overpredicted) and 1.64 (underpredicted) for classes 1/2 and 3/4, respectively, thus indicating a successful prediction.

Figure 4.2d shows the correlation of $CL_{r,org,in\ vivo}$ and $CL_{r,org,in\ vitro}$. The incorporation of all renal clearance processes improved the prediction significantly and 14 out of 20 compounds were within a two-fold error and 19 out of 20 study compounds were within a three-fold error. Only pravastatin (class 3) was underpredicted. Including all study compounds, the prediction accuracy in terms of the two-fold and three-fold error expressed in percent was 70% and 95%, respectively. Afe analysis resulted in a value of 1.4 including

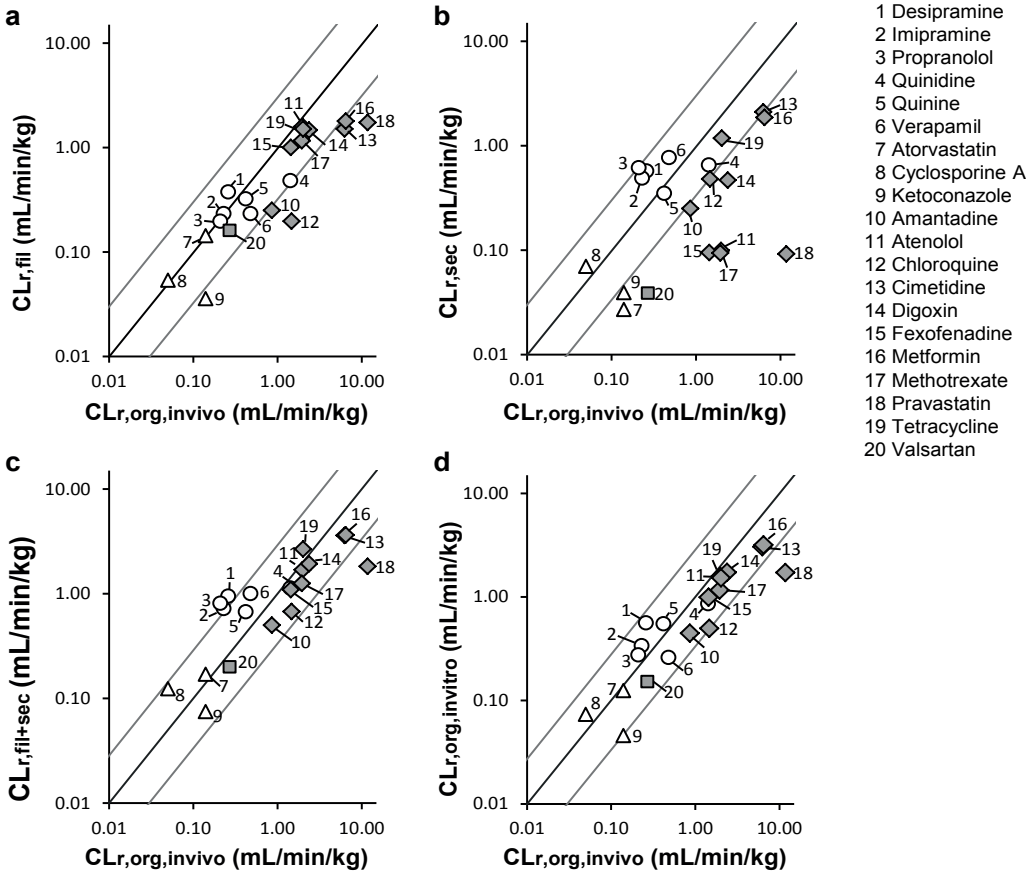

Figure 4.2: Correlation of the *in vivo* reported and the *in vitro* predicted renal clearances according to 4.3. $CL_{r,org,in\ vivo}$ was compared either with **(a)** the filtration clearance [$\log(CL_{r,org,in\ vivo}) = 0.72 \cdot \log(CL_{r,fil}) - 0.31$; $R^2 = 0.80$], **(b)** the tubular secretion clearance [$\log(CL_{r,org,in\ vivo}) = 0.37 \cdot \log(CL_{r,sec}) - 0.55$; $R^2 = 0.17$], **(c)** the sum of filtration and secretion clearance [$\log(CL_{r,org,in\ vivo}) = 0.62 \cdot \log(CL_{r,fil+sec}) - 0.04$; $R^2 = 0.71$], or **(d)** the predicted renal organ clearance taking all processes into account [$\log(CL_{r,org,in\ vivo}) = 0.75 \cdot \log(CL_{r,org,in\ vitro}) - 0.19$; $R^2 = 0.83$]. Circles, triangles, diamonds, and squares refer to BDDCS class assignments 1,2,3, and 4, respectively. White and gray represents BDDCS classes 1/2 and 3/4, respectively. The black line represents the line of unity and the gray lines the three-fold errors.

all compounds, 1.03 for classes 1/2 and 1.96 for classes 3/4. Thus, a successful prediction of $CL_{r,org,in\ vivo}$ from $CL_{r,org,in\ vitro}$ was obtained including all compounds as well as for compounds assigned to classes 1/2 and 3/4.

4.5 Discussion

Our present study aimed to establish a novel IVIVE method to predict the human renal organ clearance based on *in vitro* permeability studies in the LLC-PK_1 cell line. We performed bidirectional transepithelial permeation experiments for 20 compounds and calculated the resulting ERs (Table 4.2). For all basic compounds, except atenolol, the ERs were greater than 1.0 indicating secretion by an active transport process. The highest ER values were obtained for amantadine, cimetidine, and metformin. These compounds are

reported substrates for the OCT system and were shown to be actively secreted via OCT2 and MATE in humans (Morrissey et al., 2013; ITC, 2010). Moreover, we confirmed results by Urakami et al. indicating that LLC-PK_1 cells actively secrete creatinine (Urakami et al., 2005). Thus, our data were in line with findings that the relevant transporters of the renal OCT system are functionally active in the LLC-PK_1 cell line (Urakami et al., 2005; Saito et al., 1992). In contrast, the measured bidirectional permeabilities of the weakly acidic drugs such as pravastatin, fexofenadine, methotrexate, tetracycline, and valsartan were not significantly different resulting in ER values of approximately one or lower. As all of these compounds are reported to be actively secreted by transporters of the renal organic anion transport (OAT) system, including OAT1, OAT3, MRP2, and BCRP, our results appeared to support previous data indicating limited OAT activity in the LLC-PK_1 cell line (Hori et al., 1993).

For our study dataset, we scaled the measured permeability values up to human intrinsic clearances and incorporated these data into our new physiological-based model to determine $CL_{r,sec}$ and f_{reab} as well as $CL_{r,org,in\ vitro}$ (Table 4.3). Out of 20 compounds, nine are assigned to the BDDCS classes 1 and 2. According to the BDDCS, the major route of elimination for these compounds is hepatic metabolic clearance. Indeed, all classes 1 and 2 compounds in our dataset have reported $CL_{r,org,in\ vivo}$ below 1 ml/(min·kg). Because of the high protein binding, $CL_{r,fil}$ was low and $CL_{r,org,in\ vivo}$ were well predicted exclusively from $CL_{r,fil}$ for classes 1 and 2 compounds (Fig. 4.2a). Nevertheless, we could show that secretion processes occurred also for these two BDDCS classes. Consequently, $CL_{r,org,in\ vivo}$ was overpredicted for these compounds when predicted from either $CL_{r,sec}$ or $CL_{r,fil+sec}$ (Fig. 4.2b and 4.2c). The inclusion of the reabsorption process increased the predictability of classes 1 and 2 compounds and we obtained a good correlation between $CL_{r,org,in\ vivo}$ and $CL_{r,org,in\ vitro}$ when taking all physiological processes driving renal clearance into account (Fig. 4.1d). Extensive reabsorption is assumed to be a consequence of a high passive permeation over the tubular epithelial of highly lipophilic compounds (Li et al., 2006; Varma et al., 2009). Our study results confirmed that assumption and we predicted extensive reabsorption for the highly lipophilic compounds assigned to BDDCS classes 1 and 2. Thus, despite the significant contribution of secretion, the overall renal organ clearances for all classes 1 and 2 compounds were low. In conclusion, all renal clearance processes of BDDCS 1 and 2 compounds were well described with our new model and in line with literature data.

The major route of elimination for BDDCS 3 and 4 compounds is renal and biliary excretion of unchanged drug (Benet et al., 2011). Our study included 11 compounds assigned to the BDDCS classes 3 and 4. When $CL_{r,org,in\ vivo}$ was predicted either from $CL_{r,fil}$ or $CL_{r,sec}$, the majority of classes 3 and 4 compounds was underpredicted (Fig. 4.2a and Fig. 4.2b). Moreover, a cluster of four class 3 compounds, including the three acidic drugs methotrexate, pravastatin, and tetracycline, was strongly underpredicted when $CL_{r,org,in\ vivo}$ was correlated to $CL_{r,sec}$. As discussed above, the LLC-PK_1 might not functionally express major transporters of the OAT system. Consequently, our model might underpredict the

contribution of $CL_{r,sec}$ to $CL_{r,org,in\ vivo}$ for compounds whose tubular secretion clearance mainly depends on active secretion mediated by OAT. In contrast, we obtained highest $CL_{r,sec}$ values for all the basic class 3 compounds in our dataset, indicating that active secretion via OCT was contributing significantly to $CL_{r,org,in\ vivo}$. Taking all classes 3 and 4 compounds of our dataset into account, regardless of their physiochemical properties, we obtained a good correlation when $CL_{r,org,in\ vivo}$ was predicted from either $CL_{r,fil+sec}$ (Fig. 4.2c) or $CL_{r,org,in\ vitro}$ (Fig. 4.2d). These results suggest that the contribution of reabsorption to $CL_{r,org,in\ vivo}$ was negligible for most classes 3 and 4 compounds, which is reflected by the low f_{reab} values determined for these compound classes. Again, our new model well represented the underlying physiological determinants driving renal organ clearance and showed an overall good correlation between $CL_{r,org,in\ vivo}$ and $CL_{r,org,in\ vitro}$ for highly renally cleared classes 3 and 4 compounds.

Currently, reported IVIVE methods that allow the prediction of the overall renal organ clearance for compounds with various physiochemical and pharmacokinetic properties are limited. Recently, Neuhoff et al. introduced a new physiological-based pharmacokinetic kidney model for the prediction of renal elimination that includes glomerular filtration, secretion, reabsorption, and renal metabolism (Neuhoff et al., 2013). In comparison with our IVIVE method, this approach requires a multitude of input parameters including physiological, physiochemical, and *in vitro* data on drug transport and enzyme kinetics. Another approach has been used by Watanabe et al. to predict $CL_{r,sec}$ for anionic drugs based on *in vitro* uptake measurements in human kidney slices (Watanabe et al., 2011). A good prediction was obtained for eight out of nine compounds within a three-fold error. The predicted secretion clearance for valsartan was overestimated. Because of the experimental setup, studies in kidney slices only allow the assessment of cellular uptake though and the permeation over the epithelial layer cannot be determined. Consequently, IVIVE methods using kidney slices are limited to compounds whose major renal clearance contributor is active secretion and that do not undergo reabsorption. Major drawbacks of studies with kidney slices and human primary tissue in general are the limited availability of suitable donors and potential interdonor variability.

The ideal *in vitro* system would be a renal cell line of human origin, expressing all relevant transporters and forming tight monolayers. Yet to our knowledge, no cell line was reported to fulfill these requirements and therefore the LLC-PK_1 cell line was considered as the most suitable *in vitro* system. Our findings demonstrated that the LLC-PK_1 cells represented a valuable *in vitro* model to predict the renal organ clearance, especially for neutral and cationic compounds. However, the lack of a functional OAT system limited the predictability for anionic compounds that are mainly eliminated by tubular secretion.

As the distribution of of the 20 compounds had to fulfill a series of properties (described in section 4.4), the proportion of neutral compounds was rather underrepresented. Future application of this IVIVE approach to a larger set of compounds will be needed to investigate the predictability for neutral and zwitterionic compounds as well as for additional cationic compounds that are actively secreted. Future work will also be required to validate

the model in terms of its suitability for dynamic predictions. Although the present experimental setup using only single concentrations allows static renal clearance and drug-drug interaction predictions, concentration-dependent studies would allow the generation of kinetic parameters that can be incorporated into physiologically based pharmacokinetic models.

In summary, our novel IVIVE approach allows the prediction of all major renal clearance processes of drugs and the assessment of the contribution of each process to the human renal organ clearance. In this study, we demonstrated that our IVIVE method can be applied to low and high renally cleared drugs with various properties independent of their BDDCS class assignments. Moreover, our findings indicated that the contribution of the underlying clearance processes to the total renal organ clearance correlates well with the BDDCS class assignment. Consequently, renal clearance predictions based on the mechanistic renal elimination model discussed in this paper can be used, at least for neutral and cationic compounds, to identify the compound-class dependent rate-limiting step of renal elimination and therefore for static or dynamic drug-drug interaction predictions in the kidney.

Acknowledgements

The authors wish to acknowledge the many Novartis Drug Metabolism and Pharmacokinetic scientists of Basel Switzerland who have supported this work. Special thanks go to Felix Huth, Hilmar Schiller, Joel Krauser, and Ken-Ichi Umehrara for their critical evaluation of this manuscript.

4.6 Supplementary Information

Table 4.4: Literature references for physiochemical and human pharmacokinetic properties of the study compounds.

compound	pk_a (-)	$logD_{7.4}$ (-)	$CL_{tot,invivo,p}$ (mL/min/kg)	$CL_{tot,invivo,p}/F$ (mL/min/kg)	$CL_{r,org,invivo,p}$ (mL/min/kg)	fu (-)	fu_b (-)	Rb (-)	F (-)	Ue (%)
Amantandine	10.1 [1]	-0.69	3.24 -	3.77 [2]	2.29 [2]	0.37 [1]	0.14 -	2.660 [1]	0.86 [1]	71 -
Atenolol	9.6 [3]	-1.03	2.33 -	4.02 [4]	2.13 [4]	0.95 [4]	0.89 -	1.070 [5]	0.58 [6]	91 -
Atorvastatin	4.5 [7]	1.53 [7]	8.93 [7]	63.79 -	0.09 -	0.05 [8]	0.08 [9]	0.630 -	0.14 [7]	1 [7]
Chloroquine	8.4 [10]	1.54	10.31 [11]	11.58 -	5.89 [11]	0.43 [10]	0.11 -	4.000 [10]	0.89 [11]	57 -
Cimetidine	6.8 [12]	0.33	7.07 [12]	n.o.	5.96 [12]	0.80 [12]	0.84 -	0.952 -	n.o.	84 -
Cyclosporine A	n.a.	2.92	11.39 [13][c)]	25.77 -	0.11 -	0.07 [6]	0.03 [9]	2.333 -	0.22 [13]	1 [6]
Desipramine	10.2 [14]	1.40	10.33 [15]	27.18 -	0.22 [15]	0.18 [15]	0.21 [15]	0.857 -	0.38 [15]	2 -
Digoxin	n.a	1.26	3.28 [16]	4.69 -	2.18 [16]	0.75 [6]	0.82 [9]	0.915 -	0.70 [6]	66 -
Fexofenadine	4.3/9.5 [17]	2.67	6.05 -	18.33 [18]	0.79 [18]	0.31 [8]	0.56 -	0.550 [8]	0.33 [17]	13 -
Imipramine	9.5 [14]	2.20	10.91 -	40.42 [19]	0.25 [19]	0.14 [20]	0.13 -	1.100 [21]	0.27 [20]	2 -
Ketoconazole	2.9/6.5 [22]	4.05	2.23 -	2.75 [23]	0.07 -	0.01 [23]	0.02 [9]	0.500 -	0.81 [23]	3 [24]
Metformin	11.5 [25]	-5.41	6.56 [25]	12.62 -	6.49 [25]	1.00 [25]	1.00 -	1.000 [26]	0.52 [25]	99 -
Methotrexate	4.8/5.5 [27]	-2.52	2.18 [28]	3.11 -	1.62 [28]	0.54 [6]	0.65 -	0.830 [8]	0.70 [6]	74 -
Pravastatin	4.5 [29]	-0.23	13.50 [30]	75.00 -	6.30 [30]	0.52 [29]	0.97 [9]	0.536 -	0.18 [30]	47 -
Propranolol	9.5 [14]	1.20	24.61 -	94.61 [32]	0.25 -	0.13 [6]	0.11 [9]	1.182 -	0.26 [6]	1 [6]
Quinidine	4.3/8.5 [31]	1.82	3.24 -	4.05 [33]	0.63 [33]	0.12 [34]	0.27 [9]	0.444 -	0.80 [6]	19 -
Quinine	4.1/8.4 [31]	1.82	1.92 [35]	2.53 -	0.31 -	0.13 [6]	0.18 -	0.733 [36]	0.76 [6]	16 [6]
Tetracycline	3.3/7.7/9.5 [37]	-1.41	2.13 [38]	n.o.	1.82 [38]	0.76 [38]	0.84 -	0.900 [39]	n.o.	85 -
Valsartan	3.9/4.7 [40]	-0.34 [41][b)]	0.52 [40]	2.26 -	0.15 [40]	0.05 [40]	0.09 [9]	0.556 -	0.23 [40]	29 -
Verapamil	8.9 [14]	1.75 [43]	13.71 [44]	52.73 -	0.41 -	0.11 [44]	0.13 [9]	0.846 -	0.26 [44]	3 [6]

Note: CL_{tot} denotes the total body clearance, $CL_{r,org,invivo}$ refers to the renal organ clearance, F denotes the bioavailability, fu and fu_b refer to the fraction of drug unbound in plasma and blood, respectively, Rb denotes the blood to plasma partition coefficient, and Ue refers to the percentage of drug excreted in urine. If not indicated otherwise, all values refer to human plasma. Clearance values were corrected for the average human body weight which was assumed to be 70 kg. The literature references are shown in squared brackets.
[a)] if not stated otherwise the values are obtained from Benet et al.
[b)] reported value refers to $logD_{7.0}$
[c)] the reported value refers to blood
n.o. not obtained
n.a. not available (neutral compounds)
- calculated parameter

The calculated parameters reported in Table 6.3 were obtained according to the following equations:

$$Rb = fu/fu_b = CL/CL_b = C_b/C \tag{4.8}$$

$$CL_{tot,invivo} = CL_{tot,oral} \cdot F \tag{4.9}$$

$$CL_{r,org,invivo} = Ae/AUC \tag{4.10}$$

$$CL_{r,org,invivo} = Ue \cdot CL_{tot} \tag{4.11}$$

$$\tag{4.12}$$

where Rb denotes the blood to plasma partition coefficient, fu and fu_b denote the fraction of drug unbound in plasma and blood, respectively, CL and CL_b refer to clearance values and C and C_b to concentrations obtained in plasma and blood, respectively, $CL_{tot,invivo}$ denotes the total body clearance, $CL_{tot,oral}$ refers to the total body clearance reported from oral administered drug studies, F denotes the bioavailability, $CL_{r,org,invivo}$ refers to the renal organ clearance, Ae describes the amount of drug excreted unchanged in urine,

AUC denotes the area under the curve, and Ue refers to the percentage of drug excreted unchanged in urine. Equation 4.8 was used to convert the reported clearances from plasma to blood values.

Supplementary References

1. Aoki FY, Sitar DS 1988. Clinical pharmacokinetics of amantadine hydrochloride. Clinical pharmacokinetics 14(1):35-51.
2. Wong LT, Sitar, DS, Aoki FY 1995. Chronic tobacco smoking and gender as variables affecting amantadine disposition in healthy subjects. British journal of clinical pharmacology 39(1):81-84.
3. Boyd RA, Chin SK, Don-Pedro O, Williams RL, Giacomini KM 1989. The pharmacokinetics of the enantiomers of atenolol. Clinical pharmacology and therapeutics 45(4):403-410-
4. Lilja JJ, Raaska K, Neuvonen PJ 2005. Effects of orange juice on the pharmacokinetics of atenolol. European journal of clinical pharmacology 61(5-6):337-340
5. Paixao P, Gouveia LF, Morais JA 2009. Prediction of drug distribution within blood. European journal of pharmaceutical sciences: official journal of the European Federation for Pharmaceutical Sciences 36(4-5):544-554.
6. 2011. Goodman and Gilman's The Pharmacological Basis of Therapeutics. 12ed.: Mc Graw Hill Medical.
7. Lennernas H 2003. Clinical pharmacokinetics of atorvastatin. Clinical pharmacokinetics 42(13):1141-1160.
8. Watanabe T, Kusuhara H, Debory Y, Maeda K, Kondo T, Nakayama H, Horita S, Ogilvie BW, Parkinson A, Hu Z, Sugiyama Y 2011. Prediction of the overall renal tubular secretion and hepatic clearance of anionic drugs and a renal drug-drug interaction involving organic anion transporter 3 in humans by in vitro uptake experiments. Drug metabolism and disposition: the biological fate of chemicals 39(6):1031-1038
9. Camenisch G, Umehara K 2012. Predicting human hepatic clearance from in vitro drug metabolism and transport data: a scientific and pharmaceutical perspective for assessing drug-drug interactions. Biopharmaceutics & drug disposition 33(4):179-194
10. White NK 1985. Clinical pharmacokinetics of antimalarial drugs. Clinical pharmacokinetics 10(3):187-215
11. Gustafsson LL, Walker O, Alvan G, Beermaan B, Estevez F, Gleisner L, Lindstrom B, Sjoqvist F 1983. Disposition of chloroquine in man after single intravenous and oral doses. British journal of clinical pharmacology 15(4):471-479
12. Gisclon LG, Boyd RA, Williams RL, Giacomini KM 1989. The effect of probenecid on the renal elimination of cimetidine. Clinical pharmacology and therapeutics 45(4):444-453.
13. Ducharme MP, Warbasse LH, Edwards DJ 1995. Disposition of intravenous and oral cyclosporine after administration with grapefruit juice. Clinical pharmacology and therapeutics 57(5):485-491.
14. Lombardo F, Obach RS, Shalaeva MY, Gao F 2004. Prediction of human volume of distribution values for neutral and basic drugs. Jounral of medical chemistry 47(5):1242-1250.
15. Ciraulo DA, Barnhill JG , Jaffe JH 1988. Clinical pharmacokinetics of imipramine and desipramine in alcoholics and normal volunteers. Clinical pharmacology and therapeutics 43(5):509-518.
16. Pedersen KE, Dorph-Pedersen A, Hvidt S, Klitgaard NA, Nielsen-Kudsk f 1981. Digoxin-verapamil

interaction. Clinical pharmacology and therapeutics 30(3):311-316.

17. sanofi-aventis.2006. Product monograph Allegra (fexofenadine hydrochloride). http://prodructs.sanofi.ca/en/allegra.pdf.
18. Wang, Z, Hamman MA, Huang, SM, Lesko LJ, Hall SD 2002. Effect of St John's wort on the pharmacokinetics of fexofenadine. Clinical pharmacology and therapeutics 71(6):414-420.
19. Auprayoon P, Sukontason K, Na-Bangchang K, Banmairuroi V, Molunto P, Karbwang J, 1995. Pharmacokinetics of quinine in chronic liver disease. British journal of clinical pharmacology 40(5):494-497.
20. Abernethy DR, Greenblatt DJ, Shader RI 1984. Imipramine disposition in users of oral contraceptive steroids. Clinical pharmacology and therapeutics 35(6):792-797.
21. Obach RS 1999. Prediction of human clearance of twenty-nine drugs from hepatic microsomal intrinsic clearance data. An examination of in vitro half-life approach and nonspecific binding to microsomes. Drug metabolism and disposition: the biological fate of chemicals 27(11):1350-1359.
22. Skiba M, Skiba-Lahiani M, Marchais H, Duclos R, Arnaud P 2000. Stability assessment of ketoconazole in aqueous formulations. International journal of pharmaceutics 198(1):1-6.
23. Huang YC, Colaizzi JL, Bierman RH, Woestenborghs R, Heykants J 1986. Pharmacokinetcs and dose proportionality of ketoconazole in normal volunteers. Antimicrobial agents and chemotherapy 30(2):206-210
24. Como JA, Dismukes WE 1994. Oral azole drugs as systemic antifungal therapy. The New England journal of medicine 330(4):263-272.
25. Pentikainen PJ, Neuvonen PJ, Penttila A 1979. Pharmacokinetics of metformin after intravenous and oral administration to man. European journal of clinical pharmacology. 16(3):195-202.
26. Sambol NC, Chiang J, Lin ET, Goodman AM, Liu CY, Benet LZ, Cogan MG 1995. Kidney function and age are both predictors of pharmacokinetics of metformin. Journal of clinical pharmacology 35(11):1094-1102
27. Nagulu M KV, Reddy UY, Krishna DR 2009. Development and validation of rapid and sensitive HPLC method for the determination of methotrexate in human serum. Stamford Journal of Pharmaceutical Sciences 2(1):8-13.
28. Vakily M, Amer F, Kukulka MJ, Andhivarothai N 2005. Coadministration of Iansoprazole and naproxen does not affect the pharmacokinetic profile of methotrexate in adult patients with rheumatoid arthritis. Journal of clinical pharmacology 45(10):1179-1186.
29. Hatanaka T 2000. Clinical pharmacokinetics of pravastatin: mechanism of pharmacokinetics events. Clinical pharmacokintics 39(6):397-412.
30. Singhiv SM, Pan HY, Morrison RA, Willard DA 1990. Disposition of pravastatin sodium, a tissue-selective HMG-CoA reductase inhibitor, in healthy subjects. British journal of clinical pharmacology 29(2):239-243.
31. Notterman Da, Drayer DE, Metakis L, Reidenber MM 1986. Stereoselective renal tubular secretion of quinidine and quinine. Clinical pharmacology and therapeutics 40(5):511-517
32. Greenblatt DJ, Scavone JM, Harmatz JS, Engelhardt N, Shader RI 1993. Cognitive effects of beta-adrenergic antagonists after single doses: pharmacokinetics and pharmacodynamics of propranolol, atenolol, lorazepam, and placebo. Clinical pharmacology and therapeutics 53(5):577-584.
33. Edwards DJ, Lavoi R, Beckman H, Hlevins R, Rubenfire M 1987. The effect of coadministration of verapamil on the pharmacokinetics and metabolism of quinidine. Clinical pharmacology adn therapeutics 41(1):68-73.
34. Mihaly GW, Ching MS, Klejn MB, Paull J, Smallwood RA 1987. Differences in the binding of quinidine to plasma proteins. British journal of clincial pharmacology 24(6):769-774.

35. White NJ, Chanthavanich P, Krishna S, Bunch C, Silamut K 1983. Quinine disposition kinetics. British journal of clinical pharmacology 16(4):399-403.
36. Vieira JL, Gomes AL, Borges LM, Guimaraes ER 2009. Relationship between plasma and red blood cell concentrations of quinine in Brazilian children with uncomplicated Plasmodium falciparum malaria on oral therapy. Revista do Instituto de Medicina Tropical de Sao Paulo 51(2):109-110.
37. Benet LZ, Goyan JE 1965. Determination of stability constants of tetracycline complexes. Journal of pharmaceutical sciences 54(7):993-987
38. Kunin CM, Dornbush AC, Finland M 1959. Distribution and excretion of four tetracycline analogues in normal young men. The Journal of clinical investigation 38:1950-1963.
39. Jun HW, Lee BH 1980. Distribution of tetracycline in red blood cells. Journal of pharmaceutical sciences 69(4):455-457.
40. Flesch G, Muller P, Llyod P 1997. Absolute bioavailability and pharmacokinetics of valsartan, an angiotensin II receptor antagonist, in man. European journal of clinical pharmacology 52(2):115-120.
41. Yamashiro W, Maeda K, Hirouchi M, Adachi Y, Hu Z, Sugiyama Y 2006. Involvement of transporters in the hepatic uptake and biliary excretion of valsartan, a selective antagonist of the angiotensin II AT1-receptor, in humans. Drug metabolism and disposition: the biological fate of chemicals 34(7):1247-1254.
42. Poulin P, Theil FP 2002. Prediction of pharmacokinetics prior to in vivo studies 1. Mechanism-based prediction of volume of distribution. Journal of pharmaceutical sciences 91(1):129-156.
43. Zachariah PK, Moyer TP, Theobald HM, Frantz RP, Kurtz SB, McCarthy JT, Smith RL 1991. The pharmacokinetics of racemic verapamil in patients with impaired renal function. Journal of clincial pharmacology 31(1):45-53.
44. Barbarash RA, Baumann JL, Fischer JH, Kondos GT, Batenhorst RL 1988. Near-total reduction in verapamil bioavailability by rifampin. Electrocardiographic correlates. Chest 94(5): 954-959.

Chapter 5

Prediction of Organic Anion-Transporting Polypeptide 1B1- and 1B3-mediated hepatic uptake of statins based on transporter protein expression and activity data

Annett Kunze[a,b], Jörg Huwyler[b], Gian Camenisch[a], Birk Poller[a],

[a] Division of Drug Metabolism and Pharmacokinetics, Drug-Drug Interaction Section
Novartis Institutes for Biomedical Research, CH-4056 Basel, Switzerland

[b] Department of Pharmaceutical Sciences, Division of Pharmaceutical Technology
University of Basel, CH-4056 Basel, Switzerland

This work is published in:

Drug Metabolism and Disposition
2014 Sep;42(9): 1514-21
doi: 10.1124/dmd.114.058412.
Epub 2014 Jul 2.

5.1 Abstract

Organic anion transporting polypeptides (OATP)1B1 and OATP1B3 are drug transporters mediating the active hepatic uptake of their substrates. Since they exhibit overlapping substrate specificities the assessment of the contribution of each isoform to the net hepatic uptake needs to be considered when predicting drug-drug interactions. The relative contribution of OATP1B1 and OATP1B3-mediated uptake of statins into hepatocytes was estimated based on either relative transporter protein expression data or relative activity data. Therefore, uptake kinetics of eight statins and OATP1B1 and OATP1B3-specific reference substrates were determined in OATP1B1 and OATP1B3-expressing HEK293 cells and in human cryopreserved hepatocytes. Absolute OATP1B1 and OATP1B3 protein abundance was determined by liquid chromatography-tandem mass spectrometry in all expression systems. Transporter activity data generated in recombinant cell lines were extrapolated to hepatocyte values using relative transporter expression factors (REF) or relative activity factors (RAF). Our results showed a pronounced OATP1B1 and comparatively low OATP1B3 protein expression in the investigated hepatocyte lot. Based on REF-scaling, we demonstrated that the active hepatic uptake clearance of reference substrates, atorvastatin, pravastatin, rosuvastatin, and simvastatin was well predicted within two-fold error demonstrating that OATP1B1 and OATP1B3 were major contributors. For other statins, the net hepatic uptake clearance was underpredicted, suggesting the involvement of other hepatic uptake transporters. Summarized, we showed that REF and RAF-based predictions were highly similar indicating a direct transporter expression-activity relationship. Moreover, we demonstrated that the REF-scaling method provided a powerful tool to quantitatively assess the transporter-specific contributions to the net uptake clearance of statins in hepatocytes.

5.2 Introduction

Human drug uptake transporters are membrane-bound proteins that facilitate the active cellular uptake of compounds which due to their physiochemcial properties cannot cross cellular membranes by passive diffusion. Expressed at the basolateral membrane of hepatocytes, organic anion transporting polypeptides (OATPs) mediate the uptake of mainly anionic drugs from the blood into the liver. OATP inhibition due to drug-drug interactions (DDIs) can lead to increased plasma concentration levels of drugs thus posing a potential risk for toxicity in peripheral organs. Following co-medications involving hydroxymethylglutaryl-coenzyme A (HMG-CoA) reductase inhibitors (statins), muscle toxicity and severe myopathy are reported risks that have been partially attributed to the inhibition of OATPs (Staffa et al., 2002; Shitara and Sugiyama, 2006; Neuvonen et al., 2006). Thus, predicting the transporter-mediated DDI risk is a necessity for the development of

new molecular entities.

Cryopreserved human hepatocytes are a common tool to assess the hepatic uptake of compounds. Hepatocytes express various uptake transporters including OATP1B1 (*SLCO1B1*), OATP1B3 (*SLCO1B3*), OATP2B1 (*SLCO2B1*), the organic anion transporter 2 (OAT2; *SLC22A7*), the organic cation transporter 1 (OCT1; *SLC22A1*), and the sodium taurocholate co-transporting polypeptide (NTCP; *SLC10A1*). Since a variety of compounds including statins exhibit an overlap of transporter specificity, compound uptake in hepatocytes reflects the sum of all transporter-specific contributions (Shitara and Sugiyama, 2006; Neuvonen et al., 2006; Noe et al., 2007; Shitara et al., 2013; Kalliokoski and Niemi, 2009; Knauer et al., 2010; Bi et al., 2013).

To assess the relative contribution of specific transporters to the net hepatic uptake, methods based on relative transporter expression and activity have been introduced. Hirano et al., established a method that allows the estimation of the contribution of OATP1B1 and OATP1B3 mediated uptake in hepatocytes based on relative activity factors (RAF) (Hirano et al., 2004). Determined as ratios of the uptake of transporter-specific substrates in hepatocytes relative to the uptake in recombinant cell lines, the RAF method has been widely used to estimate the contribution of OATP1B1 and OATP1B3 to the hepatic uptake of various compounds (Shitara and Sugiyama, 2006; Hirano et al., 2004; Shimizu et al., 2005; Kitamura et al., 2008). In addition, Hirano et al. used protein expression data from Western Blot analysis to estimate relative expression factors (REFs) to determine the contribution of OATP1B1, OATP1B3, and OATP2B1 to the net hepatic uptake of pitavastatin and estradiol 17β-D-glucuronide (Hirano et al., 2004, 2006). While the predicted transporter contributions based on RAFs and REFs were within a comparable range, net hepatic uptake clearances estimated from REFs were significantly over-predicted compared to observed values. Recently, the contribution of OATP1B1-mediated hepatic uptake of five substrates was investigated using a gene knockdown approach (Williamson et al., 2013). Compared with a RAF-based method highly similar results were obtained in predicting the transporter-specific contributions to the net hepatic uptake. Yet, extending the described approaches to any transport protein of interest is challenging due to practical limitations, such as the need for specific antibodies for Western Blots, transporter-specific substrates for RAFs, and genespecific knockdown. Moreover, the RAF-based and siRNA-based approaches are restricted to investigated cell systems (i.e. hepatocytes) and do not allow the extrapolation of transporters activities to any tissue based on *in vitro* experiments.

Recently, novel established quantitative targeted absolute proteomics (QTAP) methods, based on liquid chromatography-tandem mass spectrometry (LC-MS/MS) have been used to determine the absolute transporter amount in plasma membrane samples of various human tissues including liver and brain (Ohtsuki et al., 2012; Kamiie et al., 2008; Sakamoto et al., 2011; Uchida et al., 2011; Schaefer et al., 2012). Moreover, REFs determined by LC-MS/MS based approaches are used in first studies to determine the specific contribution of hepatic uptake transporters in cryopreserved hepatocytes and human liver (Karlgren et al., 2012; Kimoto et al., 2012; Bi et al., 2013; Vildhede et al., 2014).

It was the aim of the present study to determine the contribution of OATP1B1 and OATP1B3 to the net hepatic uptake clearance of atorvastatin, cerivastatin, fluvastatin, lovastatin, pitavastatin, pravastatin, rosuvastatin, and simvastatin. For this purpose protein expression levels of OATP1B1 and OATP1B3 were measured in cryopreserved human hepatocytes and in recombinant HEK293 cell lines. Subsequently, we determined the uptake clearances of statins and used REFs derived from QTAP analysis to extrapolate OATP1B1 and OATP1B3 activities obtained in recombinant cells to hepatocyte values. Finally, in order to further validate the REF-based scaling method, we assessed the correlation between uptake transporter activity and their relative protein abundance by comparing RAF and REF-based predictions.

5.3 Materials and Methods

Compounds

$[^3H]$atorvastatin calcium (0.37 MBq/nmol), $[^3H]$cerivastatin sodium (0.19 MBq/nmol), $[^3H]$cholecystokinin octapeptide (CCK8; 3.65 MBq/nmol), $[^3H]$fluvastatin sodium (0.74 MBq/nmol), $[^3H]$lovastatin acid (0.37 MBq/nmol), $[^3H]$rosuvastatin calcium (0.37 MBq/nmol), $[^3H]$pitavastatin calcium (0.37 MBq/nmol), and $[^3H]$simvastatin acid (0.37 MBq/nmol) were obtained from American Radiolabeled Chemicals, Inc. (Saint Louis, MO). $[^3H]$estrone-3-sulfate ammonium (E3S; 1.67 MBq/nmol) was purchased from PerkinElmer (Boston, MA). All other compounds and reagents were of analytical grade and purchased from commercial sources.

Cell systems

LiverPool^{TM} cryopreserved human hepatocytes (lot PQP) were obtained from Celsis, In Vitro Technologies (Brussels, Belgium). The hepatocyte pool was derived from non-transplantable fresh liver tissues of twenty donors (gender: 10 male and 10 female; age: 17-75, average age: 52; ethnic background: 16 Caucasians, 2 Blacks, and 2 Hispanics). A HEK293 cell line stably expressing human OATP1B3 (polybrene transfection method) was purchased from DKFZ (Deutsches Krebsforschungszentrum; Heidelberg, Germany) (König et al., 2000). A recombinant HEK293 cell line with stable expression of human OATP1B1 was generated in-house using the Flp-In^{TM} system (Invitrogen by Life Technologies, Paisley, United Kingdom) as previously described (Kunze et al., 2012). All HEK293 cell lines were cultivated in DMEM supplemented with 10% FBS, 1% L-glutamine, and 1% penicillin/streptomycin. For HEK293 cells expressing OATP1B1 or OATP1B3, 100 ng/µL hygromycin B or 800 ng/µL geneticin, respectively, was added to the cultivation medium.

The protein content of solubilized cells (solved in 0.2 N NaOH) was determined using the Bio-Rad Protein Assay kit (Bio-Rad Laboratories AG, Hercules, CA) according to the manufacturer's recommendations.

Determination of absolute transporter protein abundance

Absolute protein expression levels of human OATP1B1 and OATP1B3 in the membrane fractions of recombinant HEK293 cells and human cryopreserved hepatocytes were determined by peptide-based LC-MS/MS. The preparation of the membrane fractions as well as the QTAP analysis was performed by BertinPharma (Montigny le Bretonneux, France) according to established methods by the group of Terasaki, Sakamoto, and Ohtsuki et al. (Ohtsuki et al., 2012; Sakamoto et al., 2011).
Three samples containing each approximately 80 million HEK293-OATP1B1 or HEK293-OATP1B3 cells were quickly harvested in ice-cold lysis buffer [Tris-HCl 10 nM, 250 mM sucrose, Complete Protease Inhibitor (Roche, Basel, Switzerland)]. Subsequently, the samples were centrifuged (537 g, 4°C, 5 min) and the supernatant was aspirated. Two samples of human cryopreserved hepatocytes (approximately 30 million cells per sample) were thawed and immediately resuspended in *InVitro*GRO^{TM} HT Medium (BioreclammationIVT; Baltimore, MD). Samples were then centrifuged (50 g; 4°C; 5 min) and the supernatant was aspirated. All cells were stored as dry pellet at 80°C and were shipped to BertinPharma on dry ice.
All samples were processed by BertinPharma following the published protocols from the Terasaki group (Ohtsuki et al., 2012; Sakamoto et al., 2011). The cell pellets were suspended in lysis buffer followed by homogenization. Thereafter, sub-mitrochondrial fractions were isolated by centrifugation (25 min; 10'800 g; 4°C). The supernatant was collected and the microsomal fractions were obtained by centrifugation (60 min; 100'000 g; 4°C). The microsomal pellet was suspended in 10 mM Tris-HCl buffer (pH 7.4; 250 mM sucrose). The plasma membrane fractions were obtained by ultracentrifugation of the microsomal fractions through a 38% (w/v) sucrose solution (Ohtsuki et al., 2012; Sakamoto et al., 2011).
Total protein contents were determined by Lowry's method before and after each fractionation step. The absolute transporter protein abundance in the respective plasma membrane fractions were determined using simultaneous QTAP based on LC-MS/MS with multiple reactions monitoring (MRM) (Ohtsuki et al., 2012; Sakamoto et al., 2011). The same reference peptides were selected as previously published by Uchida et al. : LNTVGIAK for OATP1B1; IYNSVFFGR for OATP1B3; VLLQTLR for OATP2B1; NVALLALPR for OAT2M LSPSFADLFR for OCT1; and GIYDGDLK for NTCP (Uchida et al., 2011).
The respective transporter protein expression (exp) was obtained as the amount of transporter protein (fmol) per amount of plasma membrane protein (µg $prot_{mem}$). To determine the transporter expression per amount of total protein [fmol/(µg prot)], exp was multi-

plied with the amount of plasma membrane protein obtained per amount of total sample protein.

Uptake studies in suspended human hepatocytes

Hepatocyte uptake of reference compounds (E3S; CCK8) and the statins was assessed by the oil spin method as previously described (Umehara and Camenisch, 2012). Frozen hepatocytes were thawed and directly suspended in *InVitro*Gro^{TM} HT Medium. After centrifugation (537g, 5 min, low brakes), the supernatant was aspirated and the cells were immediately suspended in 1 mL of prewarmed Krebs-Henseleit-Buffer (KHB). Subsequently, cells were counted and the suspension was adjusted to a concentration of 1.0 - 1.5·10^5 viable cells/mL (viability: 83-95%).
Hepatocyte uptake studies initiated by adding 50 µL of hepatocyte suspension to 100 µL of a substrate solution (KHB containing a mixture of radiolabeled and non-labeled study compound at specific concentrations). All incubations were carried out at 37°C and 4°C following preincubation times of 5 min and 15 min at 37°C and 4°C, respectively. At designated time-points incubations were terminated transferring the sample to a mineral oil/NaOH containing tube [Hepatocyte Transporter Suspension Assay Kit (BD Biosciences, Woburn MA)], followed by immediate centrifugation (10'000 rpm; 1 min). The tubes were cut and the radioactivity in the cell pellets as well as in the supernatants (for mass balance studies) was analyzed by liquid scintillation counting (LSC; Packard Tri-Carb 2700TR; PerkinElmer Inc, Waltham MA).
All hepatocyte incubations were performed for 90 s. In time-dependent uptake experiments (1, 2, 3, 5 min) for E3S (0.1 µM), pitavastatin (0.5 µM, CCK8 (0.5 µM), and rosuvastatin (0.5 µM), the rate of uptake was found to lie in a time linear-uptake phase and was consequently applied to all statin incubations. For concentration-dependent kinetic studies, a broad concentration range was defined for all substrates (0.01–300 µM; 5-10 concentration points). To demonstrate uptake transporter activity, E3S (0.03 µM) uptake was measured in the absence and presence of an OATP inhibitor cocktail [a combination of atorvastatin (10 µM) and rifamycin (20 µM)] in all hepatocyte studies.

Uptake studies in human HEK293-OATP1B1 and HEK293-OATP1B3 expressing cell lines

Cellular uptake studies using plated HEK293-OATP1B1, HEK293-OATP1B3 cells, and HEK293 parental cells, were performed as previously described (Kunze et al., 2012). Uptake studies at 37°C were initiated by incubating the cells with the substrate solution at the respective concentrations (mix of radiolabeled and unlabeled study compound in KHB). To determine mass balances of the study compounds, aliquots of the incubation

solution were taken from each well prior to the termination of the incubation. Afterwards, the incubation was terminated by aspirating the remaining incubation solution followed by washing the cells twice with ice-cold PBS. Subsequently, the cells were lysed in NaOH (0.2 N). The protein contents of the solubilized cells were determined as described above. The amount of radiolabeled compound in the cell samples and in the incubation solution was quantified using LSC as described in the previous section.
Time-dependent experiments in OATP1B1 and OATP1B3-expressing HEK293 cells were performed to define the time-linear range for subsequent concentration-dependent studies (0.01-300 µM; 6-9 concentration points). An incubation time of 3 min was chosen for all cell lines and compounds, except for E3S (1 min). Uptake of each study compound (0.01 µM) was measured in the absence and presence of an OATP inhibitor cocktail [a combination of atorvastatin (10 µM) and rifamycin (20 µM)]. Functional activity of OATP1B1 and OATP1B3 in the recombinant cell lines was confirmed in each experiment as previously described (Kunze et al., 2012).

Data analysis

The uptake kinetics of the investigated compounds were calculated by normalizing the measured radioactivity to the incubation time and protein content. Consequently, these uptake rates (V_{app}; pmol·min^{-1}·mg^{-1}) were divided by the applied substrate concentrations to obtain the apparent uptake clearances (PS_{app}; µL·min^{-1}·mg^{-1}). Results are presented as uptake clearances throughout the whole manuscript to simplify the visualization of kinetic data.
As previously described, PS_{app} values determined in suspended hepatocytes are potentially affected by nonspecific binding (NSB) of the compound to plastic surfaces of the assay device or to cellular structures (Umehara and Camenisch, 2012). To account for plastic binding, total compound recoveries were calculated for all incubations and PS_{app} values were multiplied by a respective correction factor (total theoretical recovery divided by obtained recovery). In a second step, control incubations were performed at 4°C to correct PS_{app} obtained at 37°C ($PS_{app,tot,37°C}$) for saturable NSB processes to cells (Umehara and Camenisch, 2012):

$$PS_{tot} = PS_{app,tot,37°C} - (PS_{app,tot,4°C,Cmin} - PS_{app,tot,4°C,Cmax}) \tag{5.1}$$

where the difference between the apparent clearances determined from 4°C incubations at the lowest and highest substrate concentrations ($PS_{app,tot,4°C,Cmin}$ and $PS_{app,tot,4°C,Cmax}$, respectively) was used to describe saturable nonspecific cell binding. For incubations with OATP1B1 and OATP1B3 expressing HEK293 cells, none of the studied compounds showed significant NSB to plastic (recoveries > 90%). Moreover, no relevant saturable

NSB to cells was observed in control incubations using HEK293 parental cells. Consequently, no correction of uptake clearances was required for studies with cell lines and PS_{tot} equals PS_{app}. The different experimental setups between HEK293 cells (plated) and hepatocytes (suspension) and the resulting difference in cell surface exposed to the incubation medium might explain the lack of saturable NSB in HEK293 parental cells. Moreover, as discussed previously, a difference in NSB between HEK293 cells and hepatocytes could be a result of different cell membrane compositions (e.g. lipids and protein contents), between HEK293 cells and hepatocytes (Mateus et al., 2013).
The total uptake clearance (PS_{tot}) is the sum of the active uptake clearance for saturable, transporter-mediated and passive permeation processes (PS_{act} and PS_{pas}, respectively):

$$PS_{tot} = PS_{act} + PS_{pas} = \frac{PS_{act,max} \cdot Km}{Km + S} + PS_{pas} \tag{5.2}$$

where the active transporter-mediated process is following Michaelis-Menten kinetics with Km and S representing the Michaelis-Menten constant (µM) and the substrate concentration µM), respectively. For initial uptake rates and clearances at very low substrate concentration (S « Km), PS_{act} can be approximated with $PS_{act,max}$ representing a measure of the transporter activity. Kinetic parameters were estimated by fitting Eq. 5.2 to the measured data using a nonlinear least square method.

Estimation of OATP contribution in human hepatocytes

The relative contribution of OATP1B1 and OATP1B3 to the hepatic uptake of compounds can be assessed by determining a relative activity factor (RAF) or a relative expression factor (REF) for a specific transporter. In brief, RAFs for OATP1B1 and OATP1B3 were determined by comparing the transporter activities of transporter specific reference substrates (E3S for OATP1B1; CCK8 for OATP1B3) in recombinant cell lines and hepatocytes, as described by Hirano et al. (2004); Kimoto et al. (2012):

$$RAF_{1B1} = \frac{PS_{act,max,ES\ HEP}}{PS_{act,max,ES\ HEK\ OATP1B1}} \tag{5.3}$$

$$RAF_{1B3} = \frac{PS_{act,max,CCK8\ HEP}}{PS_{act,max,CCK8\ HEK\ OATP1B3}} \tag{5.4}$$

Subsequently, RAF_{1B1} and RAF_{1B3} were applied to predict the combined uptake transporter activity of OATP1B1 and OATP1B3 co-substrates into hepatocytes ($PS_{act,max,HEP}$) based on the transporter activities measured in recombinant cells ($PS_{act,max,1B1;1B3}$):

$$PS_{act,max,HEP} = PS_{act,max,HEK\ OATP1B1} \cdot RAF_{1B1} + PS_{act,max,HEK\ OATP1B3} \cdot RAF_{1B3} \quad (5.5)$$

Alternatively, we used absolute OATP1B1 and OATP1B3 protein expression data in hepatocytes and recombinant HEK293 cells to derive the REFs for OATP1B1 and OATP1B3:

$$REF_{1B1} = \frac{exp_{OATP1B1,HEP}}{exp_{OATP1B1,HEK\ OATP1B1}} \quad (5.6)$$

$$REF_{1B3} = \frac{exp_{OATP1B3,HEP}}{exp_{OATP1B3,HEK\ OATP1B3}} \quad (5.7)$$

where exp represents the specific transporter expression [fmol/(µg prot)] determined as described in section 5.3. In analogy to equation 5.5, the net transporter activity of compounds in hepatocytes was calculated from recombinant cells using the REF values:

$$PS_{act,max,HEP} = PS_{act,max,HEK\ OATP1B1} \cdot REF_{1B1} + PS_{act,max,HEK\ OATP1B3} \cdot REF_{1B3} \quad (5.8)$$

Statistics

All incubations for kinetic studies were performed in triplicates (n = 3) where values are given as the mean and standard deviation. Statistical significance for the differences in uptake clearances obtained in incubations in the presence and absence of transporter inhibitors was assessed by unpaired, two-tailed Student's *t*-test. Differences were considered to be statistically significant for p-values below 0.05. For parameter estimation based on data fitting the coefficients of determination (R^2) were determined to assess the goodness of fit. Moreover, fold-error deviations between the observed and predicted hepatic $PS_{act,max}$ values were calculated to assess the performance of the REF and RAF-based prediction methods.

5.4 Results

Transporter abundance

The transporter protein abundance in plasma membrane fractions of HEK293-OATP1B1 and HEK293-OATP1B3 cells and pooled human cryopreserved hepatocytes (lot PQP) was

Table 5.1: Absolute transporter protein expression.

expression system	transporter protein	protein expression	
		(fmol/µg $prot_{mem}$)	(fmol/µg prot)
human hepatocytes	OATP1B1	15.85	0.230
human hepatocytes	OATP1B3	0.35	0.005
human hepatocytes	OATP2B1	1.57	0.022
human hepatocytes	OAT2	1.03	0.014
human hepatocytes	NTCP	2.62	0.036
human hepatocytes	OCT1	6.94	0.095
HEK OATP1B1	OATP1B1	23.97	0.269
HEK OATP1B3	OATP1B3	1.44	0.028

The absolute transporter protein expression was normalized to the amount of plasma membrane protein (fmol/µg $prot_{mem}$) or total protein (fmol/µg prot) in the respective expression system.

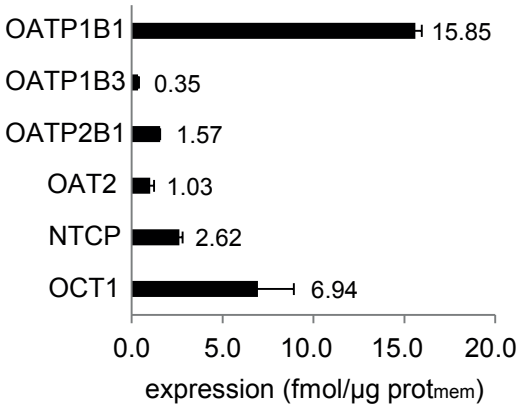

Figure 5.1: Transporter protein expression in plasma membrane fractions of pooled cryopreserved human hepatocytes. The bars represent mean values of two independent measurements performed in triplicates and errorbars represent standard deviations.

determined by the QTAP method. Figure 5.1 and Table 5.1 show the measured abundances of the uptake transporters OATP1B1, OATP1B3, OATP2B1, NTCP, OAT2, and OCT1 in cryopreserved human hepatocytes. Significant differences in expression levels were found between the specific transporters, ranging from 0.35 fmol/(µg $prot_{mem}$) for OATP1B3 to 15.85 fmol/(µg $prot_{mem}$) for OATP1B1. OATP2B1, NTCP, and OAT2 showed similar expression levels [1.03 to 2.62 fmol/(µg $prot_{mem}$)] while the expression of OCT1 was comparatively higher [6.94 fmol/(µg $prot_{mem}$)]. In plasma membranes of recombinant HEK293 cells, the protein expression levels of OATP1B1 and OATP1B3 were measured at 23.97 fmol/(µg $prot_{mem}$) and 1.44 fmol/(µg $prot_{mem}$) (Table 5.1). Transporter protein expression levels shown in Table 5.1, are either normalized to the amount of total plasma membrane (µg $prot_{mem}$) or to the total sample protein (µg prot).

Determination of pharmacokinetic parameters

We performed concentration-dependent incubations in HEK293-OATP1B1 and OATP1B3 over-expressing cells, and in suspended hepatocytes to subsequently estimate pharmacokinetic parameters of our study compounds. Control incubations in the presence of the OATP inhibitors atorvastatin and rifamycin resulted in a significant decrease in PS_{tot} values in recombinant cell lines and hepatocytes, confirming transporter functionality in all uptake experiments (data not shown).

Figure 5.2 shows the uptake clearances of the OATP1B1 and OATP1B3-specific reference compounds E3S and CCK8, respectively, into recombinant cell lines and suspended hepatocytes. E3S uptake clearances in HEK293-OATP1B1 were decreased in a concentration-dependent manner and PS_{tot} was significantly reduced in the presence of the OATP inhibitors. Also HEK293-OATP1B3 cells showed transport activity for E3S, which however, was significantly lower compared to HEK293-OATP1B1 cells (Fig.5.2A). For CCK8, a concentration dependent decrease in uptake clearances and inhibition in presence of OATP inhibitors were found in recombinant HEK293-OATP1B3 but not in HEK293-OATP1B1 cells (Fig.5.2B).

Compound recoveries in hepatocytes studies above 85% were obtained for E3S, CCK8, atorvastatin, lovastatin, pitavastatin, and rosuvastatin. In contrast, substantial concentration-dependent NSB to the experimental device was found for cerivastatin (69%), fluvastatin (79%), pravastatin (56%), and simvastatin (71%).

As illustrated in Figures 5.2C and 5.2D, experiments with E3S and CCK8 using human hepatocytes showed a concentration-dependent decrease in PS_{app} values at 4°C incubations. As previously described, such a profile indicates saturation of temperature-independent NSB of the compound to cellular structures. Consequently, uptake clearances determined from 37°C incubations were corrected according to Equation 5.1. The resulting PS_{tot} values showed a concentration-dependent decrease for E3S and CCK8 indicating that both compounds were actively transported into hepatocytes. The observed PS_{tot} value for E3S was more than ten-fold higher than the value observed for CCK8.

Figure 5.3 shows representative kinetic profiles for rosuvastatin and cerivastatin. For both compounds, OATP1B1 or OATP1B3 uptake clearances were significantly reduced in the presence of the OATPs inhibitors (Figure 5.3A and 5.3B). Moreover, saturation of transporter activities at high concentrations of both statins were observed in HEK293-OATP1B1 and HEK293-OTAP1B3 cells. However, in both cell lines the concentration-dependent decrease in PS_{tot} was more pronounced for rosuvastatin than for cerivastatin, probably due to the comparatively high passive uptake clearance obtained for the latter compound.

Atorvastatin, fluvastatin, pravastatin and pitavastatin were also actively transported by OATP1B1 and OATP1B3, while lovastatin was found to be a substrate for only OATP1B1 but not for OATP1B3. The simvastatin uptake clearances decreased in a concentration-dependent manner in OATP1B1 and OATP1B3 cells but co-incubation with the OATP inhibitors did not affect the total uptake clearance in either cell line.

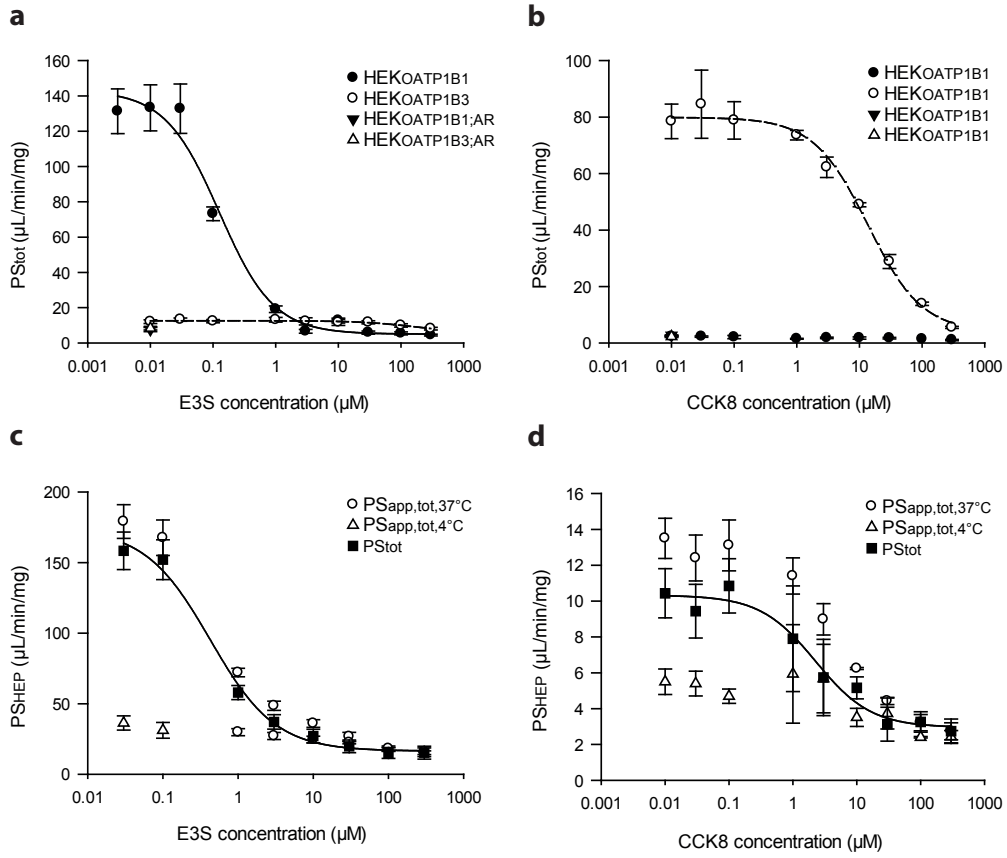

Figure 5.2: Uptake clearance of reference compounds in recombinant HEK293-OATP1B1 ($HEK_{OATP1B1}$) or HEK203-OATP1B3 ($HEK_{OATP1B3}$)cells **(a,b)** and human CCK8 **(b)** in recombinant cell lines in the presence and absence of OATP inhibitors atorvastatin and rifamycin (AR). The total uptake clearance of E3S **(c)** and CCK8 **(d)** and apparent clearances determined from 4°C and 37°C incubations, ($PS_{app,tot,\ 7°C}$ and $PS_{app,tot,4°C}$, respectively). Data are presented as triplicates with the error bars representing the standard deviation.

Hepatocyte uptake profiles of rosuvastatin and cerivastatin are shown in Figure 5.3C and 5.3D. The uptake clearances of both compounds were decreased in a concentration-dependent manner. Compared to the PS_{tot} value of rosuvastatin observed at initial concentrations, a very high PS_{tot} of cerivastatin was obtained. However, at high substrate concentrations, PS_{tot} of cerivastatin was significantly higher compared to the value determined for rosuvastatin, indicating a high contribution of the passive uptake clearance to the total cerivastatin uptake clearance.

Table 5.2 summarizes the estimated maximal activities ($PS_{act,max}$), the ratios between active to passive compound clearances, and the global goodness of fit (R^2) for parameter estimations according to equation 5.2. In recombinant cell lines highest $PS_{act,max}$ values were obtained for E3S and CCK8 in HEK293-OATP1B1 and OATP1B3-expressing cells, respectively. While E3S also exhibited the highest $PS_{act,max}$ value in hepatocytes, active CCK8 transport was comparatively low. For the statins, comparable activities ($PS_{act,max}$) of OATP1B1 and OATP1B3 were derived from recombinant cells while higher activities were generally obtained in human hepatocytes. The ratios between active and passive uptake clearances ($PS_{act,max}/PS_{pas}$) represent a measure of the contribution of the

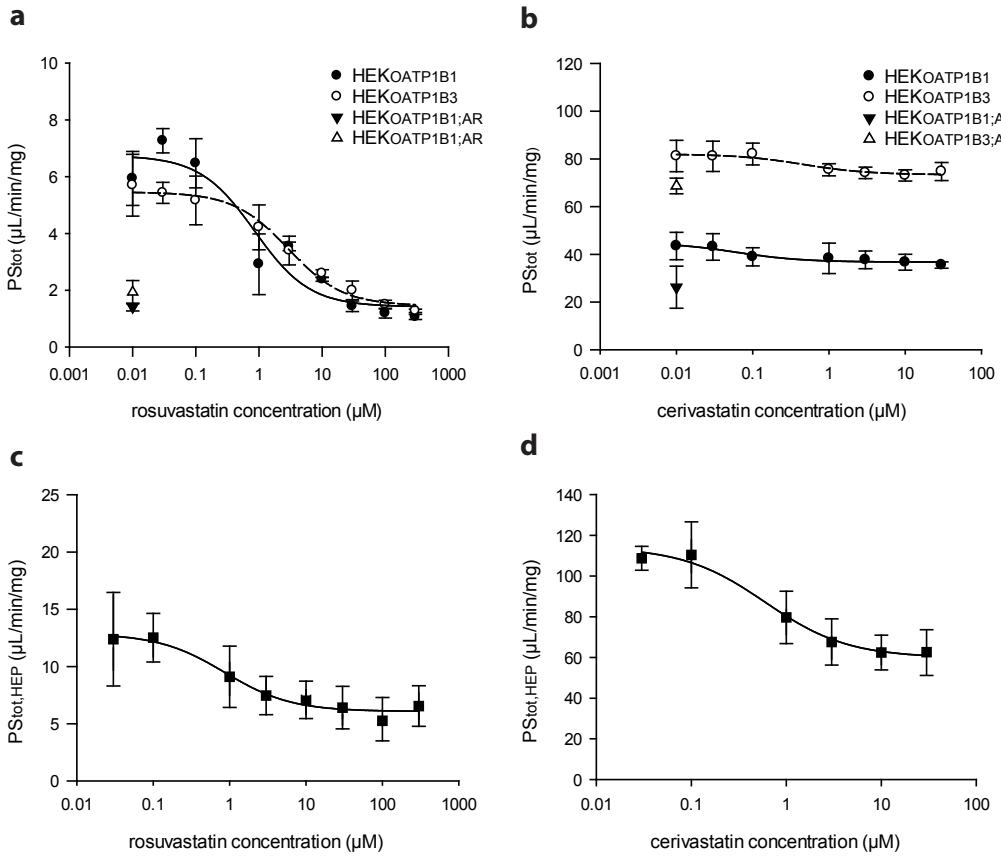

Figure 5.3: Uptake clearance of statins in recombinant HEK293-OATP1B1 ($HEK_{OATP1B1}$) or HEK293-OATP1B3 ($HEK_{OATP1B3}$) cells **(a,b)** and human cryopreserved hepatocytes (Hep; **c,d**). The total clearance (PS_{tot}) of rosuvastatin **(a,c)** and cerivastatin **(b,d)** in recombinant cell lines in the presence and absence of OATP inhibitors atorvastatin and rifamycin (AR) **(a,b)** or cryopreserved human hepatocytes (c,d). Data are presented as triplicates with the error bars representing the standard deviation.

transporter-mediated process to the total uptake clearance. E3S exhibited the highest ratios in HEK293-OATP1B1 cells and in hepatocytes. Among the statins, the highest ratio was measured for pravastatin in hepatocytes. Together with atorvastatin and rosuvastatin, pravastatin also showed highest ratios in recombinant cell lines. Ratios below one were obtained for simvastatin, fluvastatin, and cerivastatin in all expression system, indicating an extensive contribution of passive permeation to the total uptake clearance for these compounds.

REF and RAF based prediction of compound uptake in suspended hepatocytes

Table 5.3 lists the observed and predicted hepatic $PS_{act,max}$ values as well as the determined scaling factors. We obtained very similar transporter specific scaling factors with values of 0.853 and 1.112 for REF_{1B1} and RAF_{1B1} (1.3-fold deviation), respectively, and of 0.181 and 0.113 for REF_{1B3} and RAF_{1B3} (1.6-fold deviation), respectively. Consequently, the

Table 5.2: *In vitro* determined pharmacokinetic parameters of statins.

compounds	HEK OATP1B1				HEK OATP1B3				HEP PQP			
	$PS_{act,max}$ ($\mu L \cdot min^{-1} \cdot mg\ prot^{-1}$)	SD	$PS_{act,max}/PS_{pas}$ (-)	R^2 (-)	$PS_{act,max}$ ($\mu L \cdot min^{-1} \cdot mg\ prot^{-1}$)	SD	$PS_{act,max}/PS_{pas}$ (-)	R^2 (-)	$PS_{act,max}$ ($\mu L \cdot min^{-1} \cdot mg\ prot^{-1}$)	SD	$PS_{act,max}/PS_{pas}$ (-)	R^2 (-)
E3S	138.11	7.20	27.68	0.99	6.74	1.98	1.16	0.93	157.74	6.13	9.61	0.99
CCK8	no substrate				76.09	2.81	19.97	0.99	7.38	0.53	2.50	0.98
atorvastatin	26.26	0.45	5.48	1.00	31.88	1.77	6.39	0.99	45.13	11.61	1.30	0.96
cerivastatin	8.20	1.88	0.22	0.91	8.65	1.11	0.12	0.94	54.42	3.45	0.91	0.99
fluvastatin	20.48	1.81	0.46	0.96	29.75	2.02	0.49	0.98	53.72	12.11	0.67	0.88
lovastatin	8.89	1.04	0.38	0.92	no substrate				40.55	4.11	1.13	0.96
pitavastaitn	33.50	3.17	1.78	0.97	14.51	3.52	0.48	0.82	89.49	11.14	1.41	0.97
pravastatin	10.35	3.24	6.27	0.96	2.22	0.28	1.33	0.93	13.43	1.47	7.42	0.93
rosuvastatin	5.33	0.62	3.75	0.92	4.01	0.18	2.77	0.99	6.68	0.52	1.10	0.97
simvastatin	14.42	4.98	0.29	0.75	14.26	5.41	0.26	0.65	28.52	3.08	0.39	0.98

$PS_{act,max}$ refers to the total maximal active uptake in the respective expression system, PS_{pas} refers to the passive permeation, $PS_{act,max}/PS_{pas}$ describes the ratio of active to passive uptake clearance, and R^2 determines the coefficient of determination.

Table 5.3: Observed and predicted hepatic $PS_{act,max}$ values.

	observed	REF-based scaling			RAF-based scaling		
	$PS_{act,max}$	$PS_{act,max}$			$PS_{act,max}$		
	total	1B1	1B3	1B1 + 1B3	1B1	1B3	1B1 + 1B3
	(µL/min/mg)	(µL/min/mg)			(µL/min/mg)		
E3S	157.7	117.8	1.2	119.0	n.a.	n.a.	n.a.
CCK8	7.4	0.0	13.8	13.8	n.a.	n.a.	n.a.
Atorvastatin	45.1	22.4	5.8	28.2	30.0	3.1	33.1
Cerivastatin	54.4	7.0	1.6	8.6	9.4	0.8	10.2
Fluvastatin	53.7	17.5	5.4	22.8	23.4	2.9	26.3
Lovastatin	40.6	7.6	0.0	7.6	10.2	0.0	10.2
Pitavastatin	89.5	28.6	2.6	31.2	38.3	1.4	39.7
Pravastatin	13.4	8.8	0.4	9.2	11.8	0.2	12.0
Rosuvastatin	6.7	4.5	0.7	5.3	6.1	0.4	6.5
Simvastatin	28.5	12.3	2.6	14.9	16.5	1.4	17.9

$PS_{act,max}$ refers to the maximal observed or predicted active uptake in hepatocytes. 1B1 and 1B3 determine OATP1B1 and OATP1B3, respectively. According to Eqs. 5.3 and 5.4 for RAFs and Eqs. 5.6 and 5.7 for REFs the followig scaling factors were applied: REF_{1B1} = 0.853; REF_{1B3} = 0.181; RAF_{1B1} = 1.142; RAF_{1B3} = 0.097.

$PS_{act,max}$ values predicted from the RAF and REF-methods were highly comparable. Given the high similarity between the two scaling methods, only the results for REF-based scaling are discussed in the following.

$PS_{act,max}$ values in hepatocytes were predicted from the extrapolated sum of OATP1B1 and OATP1B3 activities (Equation 5.8). A good resulting prediction accuracy between the observed and predicted values for E3S, CCK8, atorvastatin, pravastatin, rosuvastatin, simvastatin was obtained with errors below two-fold. In contrast, poor predictability was observed for cerivastatin, fluvastatin, lovastatin, and pitavastatin with errors between two to six-fold, thus indicating a significant under-prediction.

Figure 5.4 illustrates the contribution of OATP1B1 and OATP1B3 to the observed active uptake clearance of statins in suspended hepatocytes predicted from REF-scaling. For all statins, OATP1B1-mediated uptake into hepatocytes was significantly higher than active uptake by OATP1B3. Moreover, the contribution of OATP1B1 and OATP1B3 to the hepatic uptake clearance of atorvastatin, pravastatin, rosuvastatin, and simvastatin was above 50% indicating that both isoforms were the major contributors to the hepatic uptake of these compounds. In contrast, OATP1B1 and OATP1B3-mediated uptake of cerivastatin, fluvastatin, lovastatin, and pitavastatin was not the major determinant of the active hepatic uptake clearance determined in hepatocyte lot PQP.

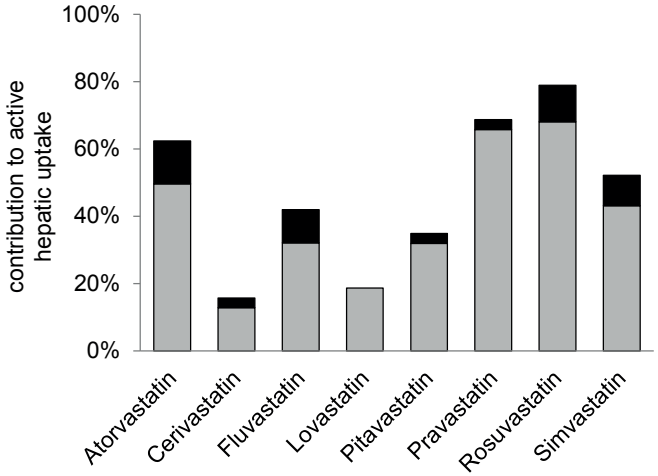

Figure 5.4: Fractional contribution of OATP1B1 (gray) and OATP1B3 (black) to the observed active uptake clearance of statins in suspended hepatocytes (lot PQP), where $PS_{act,max}$ measured in hepatocytes represents 100%. The transporter contributions were predicted with the REF-method based on data listed in Table 5.1 and Table 5.2.

5.5 Discussion

In the present study we determined the OATP1B1 and OATP1B3-mediated uptake clearances of statins in single-transporter expressing HEK293 cells. Based on relative transporter protein expression data, we used the transporter activities to estimate the OATP1B1 and OATP1B3-mediated uptake of statins into hepatocytes.

Recently, QTAP methods were established to quantify low abundant proteins, and first expression levels in cryopreserved hepatocytes and liver samples were reported for the major hepatic uptake transporters OATP1B1, OATP1B3, OATP2B1, OAT2, OCT1, and NTCP (Bi et al., 2012; Kimoto et al., 2012; Ohtsuki et al., 2012; Bi et al., 2013). Literature data on OATP transporter expression show high inter-individual differences. For OATP1B1 values between 2-12 fmol/(µg $prot_{mem}$) in human liver samples and 2-7 fmol/(µg $prot_{mem}$) in cryopreserved hepatocytes are reported (Karlgren et al., 2012; Kimoto et al., 2012; Ohtsuki et al., 2012; Vildhede et al., 2014).

For OATP1B3 reported values vary between 1-6 fmol/(µg $prot_{mem}$) in human liver samples and 1-2 fmol/(µg $prot_{mem}$) in cryopreserved hepatocytes (Karlgren et al., 2012; Ohtsuki et al., 2012; Vildhede et al., 2014). Reported values for other uptake transporters in human liver tissues vary between 1-4 (OATP2B1), 1-10 (NTCP), 1-3 (OAT2), and 3-15 fmol/(µg $prot_{mem}$) (OCT1) (Karlgren et al., 2012; Kimoto et al., 2012; Ohtsuki et al., 2012; Vildhede et al., 2014).

In the present study, transporter protein expression was quantified for pooled (20 donors) human cryopreserved hepatocytes. Measured protein expression levels were within the range of reported values, with 16 (OATP1B1), 0.4 (OATP1B3), 2 (OATP2B1), 3 (NTCP), 1 (OAT2), and 7 fmol/(µg $prot_{mem}$) for OCT1 (Table 5.1). In the tested lot of human hepatocytes, OATP1B1 protein was found to be expressed at a substantially higher level than OATP1B3. Such a pronounced OATP1B1 abundance with a concomitant low OATP1B3 expression has not yet been reported for protein levels in cryopreserved hepatocytes. In contrast, comparatively high differences in OATP1B1 and OATP1B3 expression levels

were observed in human liver samples (Vildhede et al., 2014). Thus, the level of OATP1B1 protein expression is in agreement with reported values in human liver samples while generally lower values are reported in human cryopreserved hepatocytes.

On a functional level, high variability in active uptake values determined in different cryopreserved hepatocytes is shown for statins and our reference substrates (Hirano et al., 2004; Watanabe et al., 2010; Kimoto et al., 2012). Hirano et al. reported maximum transporter activities between 36-84 $\mu L \cdot min^{-1} \cdot mg^{-1}$ for E3S and 1-5 $\mu L \cdot min^{-1} \cdot mg^{-1}$ for CCK8 in three different cryopreserved human hepatocyte lots (Hirano et al., 2004). While our CCK8 results were comparable, we obtained a significantly higher maximal activity for E3S uptake in hepatocytes. These findings are in-line with the high OATP1B1 protein expression level obtained in the hepatocyte lot PQP.

Differences in reported transporter activities and protein expression levels might be a result of substantial inter-individual variation in transporter protein abundances observed in human liver samples (Nies et al., 2013; Vildhede et al., 2014). Furthermore, differences in hepatocyte isolation or transporter protein quantification procedures, as well as in the selection of reference peptides for QTAP analysis were attributed to impact determined transporter protein abundances (Balogh et al., 2012; Lundquist et al., 2014). All studied statins are reported substrates of OATP1B1, and fluvastatin, rosuvastatin, pravastatin, and pitavastatin are substrates of OATP1B3 (Hirano et al., 2004; Neuvonen et al., 2006; Noe et al., 2007; Kalliokoski and Niemi, 2009). Our results confirmed that all statins were substrates of OATP1B1. Only lovastatin was not identified as an OATP1B3 substrate. Simvastatin demonstrated concentration-dependent uptake kinetics in OATP1B1 and OATP1B3 cells but no significant inhibition was observed upon co-administration with OATP inhibitors. We assume that its extensive passive permeation might have masked the contribution of the active transport process.

To investigate the correlation between transporter activity and expression level, we predicted the OATP1B1 and OATP1B3 activities in hepatocytes from studies in cell lines expressing the respective transporter, using RAF and REF based methods. In the ideal case, where measured activity of a specific transporter is directly proportional to its protein expression level, the transporter specific REF, would be equal to the respective RAF. Our determined REF and RAF values for OATP1B1 (0.853 and 1.112) and for OATP1B3 (0.181 and 0.113) showed a high similarity indicating a direct correlation between expression levels and activity for OATP1B1 and OATP1B3. These results should neither be affected by individual variation in transporter protein expression, nor by variation in the hepatocyte preparation as absolute protein abundance measurements, as well as kinetic experiments, were performed for the same batch of human hepatocytes. Thus, even if transporter protein expression in cryopreserved hepatocytes would not represent transporter expression levels in freshly-isolated or human liver samples, as indicated in studies by Kimoto et al. and Lundquist et al., the correlation between transporter protein expression and activity should not be affected as protein abundances and transporter activities were determined for the same lot of hepatocytes in the present study (Lundquist et al., 2014). In contrast, given the

substantial variation in reported transporter protein abundances between different hepatocyte lots or liver samples, it is crucial to characterize transporter expression in hepatocytes in order to compare with the respective activities.

Using protein expression based REF-scaling, the observed hepatic $PS_{act,max}$ for the reference compounds E3S and CCK8 were predicted within two-fold error. For statins, the REF-based predicted $PS_{act,max}$ values were in good agreement with the observed values with fold error deviation below two for atorvastatin, pravastatin, rosuvastatin, and simvastatin, indicating that their active hepatic uptake was mainly described by OATP1B1 and OATP1B3 mediated transport. In contrast, the active hepatic uptake of cerivastatin, fluvastatin, lovastatin, and pitavastatin was under-estimated.

Within the scope of this study, the hepatic uptake activities were only extrapolated using OATP1B1 and OATP1B3 values. Therefore, a potential explanation could be the involvement of other transporters in the hepatic uptake of these compounds. Recently, Bi et al. showed that NTCP is significantly involved in the hepatic uptake of fluvastatin, pitavastatin, and rosuvastatin (Bi et al., 2013). NTCP protein abundance in our hepatocyte pool was about two-fold higher than the reported value by Bi et al. Hence a significant contribution of NTCP to the net hepatic uptake of the respective statin is likely to be expected for our investigated hepatocyte lot. Moreover, atorvastatin, fluvastatin, pravastatin and rosuvastatin, as well as E3S, were shown to be substrates of OATP2B1 (Noe et al., 2007; Kalliokoski and Niemi, 2009; Knauer et al., 2010). OATP2B1 was found to be expressed at a comparable level to reported human liver data (Kimoto et al., 2012; Vildhede et al., 2014). Therefore, we assumed that OATP2B1 might has contributed to the uptake of statins in the studied hepatocyte lot. Thus, comparing REF-based extrapolation of specific hepatic transporter activities with measured hepatic net uptake provides information about the potential involvement of other transporters in the net hepatic uptake activity.

It is expected that REF-based scaling will represent a powerful tool for *in vitro-in vivo* extrapolation of OATP1B1 and OATP1B3 activities to subsequently predict their contribution to the net hepatic uptake clearance and to assess the impact of OATP1B1 and OATP1B3-mediated DDIs. Recently Karlgren et al. and Vildhede et al. predicted the contribution of OATP1B1, OATP1B3, OATP2B1, and NTCP to the atorvastatin uptake clearance based on protein expression data determined for human liver samples and recombinant cell lines by an LC-MS method. Subsequently, the impact on isoform-specific inhibition to the atorvastatin clearance was assessed (Karlgren et al., 2012; Vildhede et al., 2014). Based on the substantial variation in transporter protein abundance among the investigated liver samples (twelve donors), the predicted transporter-specific uptake clearances showed high inter-individual variability ranging between 26-89% and 1.8-60% for OATP1B1 and OATP1B3, respectively. Moreover, Nies et al., demonstrated that genetic polymorphism significantly contributed to variation in OATP1B1 protein expression and functionality, observed among 82 individuals (Nies et al., 2013). The high inter-individual variability in transporter-protein expression observed in these studies clearly needs to be considered when REF-based methods are used for *in vitro-in vitro* extrapolation of

transporter activities. This aspect becomes especially important when results from DDI studies with relatively small numbers of subjects are compared with IVIVE approaches.

In summary we demonstrated as a proof-of-concept that the OATP1B1 and OATP1B3 activity in hepatocytes can be extrapolated from recombinant cell lines based on absolute transporter protein measurements. We further assessed the relative contribution of OATP1B1 and OATP1B3 to the total hepatic uptake. Moreover, in contrast to RAF-based scaling methods, this approach is expected to allow scaling of transporter activities from *in vitro* incubations in recombinant cell lines to any tissues, given the respective transporter abundance is known. Therefore, future research will be required to strengthen the evidence that scaling of transporter activities based on absolute protein abundance data represents a powerful tool to predict transporter-mediated *in vivo* clearance processes and DDI effects.

Acknowledgments

The authors wish to acknowledge the many Novartis Drug Metabolism and Pharamcokinetic scientists of Basel Switzerland who have supported this work. Special thanks go to Francis Heitz for technical assistance and Joel Krauser for critical evaluation of this manuscript.

Chapter 6

Application of the extended clearance concept classification system (ECCCS) to predict the victim drug-drug interaction potential of statins

Annett Kunze[a,b], Birk Poller[a], Jörg Huwyler[b] , Gian Camenisch[a]

[a] Division of Drug Metabolism and Pharmacokinetics, Drug-Drug Interaction Section
Novartis Institutes for Biomedical Research, CH-4056 Basel, Switzerland

[b] Department of Pharmaceutical Sciences, Division of Pharmaceutical Technology
University of Basel, CH-4056 Basel, Switzerland

This work is submitted for publication.

6.1 Abstract

During drug development, it is an important safety factor to identify the potential of any new molecular entity to become a victim of drug-drug interactions (DDI). Especially in preclinical development, anticipation of clinical DDIs remains a difficult challenge mainly because of the lack of *in vivo* human pharmacokinetic data. We therefore applied a recently developed *in vitro-in vivo* extrapolation method, including hepatic metabolism and transport processes, to predict the human hepatic clearance and the DDI potential of eight statins. For atorvastatin, cerivastatin, fluvastatin, lovastatin acid, pitavastatin, pravastatin, rosuvastatin, and simvastatin acid all processes driving the hepatic clearance were determined *in vitro*. Application of the recently established Extended Clearance Concept Classification System (ECCCS), demonstrated a good predictability of the human hepatic clearance with six out of eight statins projected within a two-fold deviation to reported values. Furthermore, the DDI potential of the statins was assessed with respect to the impact of possible perpetrator drugs on hepatic uptake, metabolism, and biliary secretion and subsequently compared with reported clinical DDI effects. The predicted AUC ratios for statins showed excellent quantitative correlations with clinical observations. In addition, the mechanistic interplay of hepatic transport and metabolism processes was well-reflected by our model. The ECCCS thus represents a powerful tool to anticipate the DDI potential of victim drugs based on *in vitro* drug metabolism and transport data.

6.2 Introduction

Statins are 3-hydroxy-3-methylglutaryl-coenzyme A (HMG-CoA) reductase inhibitors indicated for the treatment of hypercholesterolemia (Shitara and Sugiyama, 2006). They are widely used to lower the risk of cardiovascular disease. In 2012, rosuvastatin, simvastatin, and atorvastatin were among the 15 most prescribed drugs in the United States. Myotoxicity and rare cases of severe rhabdomyolysis are reported adverse events following statin treatment though. In 2001, cerivastatin was therefore withdrawn from the market due to incidents of fatal rhabdomyolysis, which were partially attributed to drug-drug interactions (DDI) following comedication with gemfibrozil (Staffa et al., 2002). For several statins hepatic elimination is described as interplay of drug transport and metabolism processes. Expressed at the basolateral membrane of hepatocytes, the organic anion transporting polypeptides (OATP) 1B1, 1B3 and 2B1 as well as the organic anion transporter (OAT) 2 and the sodium taurocholate co-transporting polypeptide (NTCP) are known to be involved in the hepatic uptake of various statins. Subsequent biliary secretion is mediated by apically expressed efflux transporters including P-glycoprotein (P-gp), the multidrug-resistance associated protein (MRP) 2, and the breast cancer resistance protein (BCRP) (Li et al., 2011). Hepatic metabolism of statins is predominantly mediated by enzymes of the

cytochrome P450 (CYP) family including CYP3A4, CYP2C8, and CYP2C9 (Shitara and Sugiyama, 2006). Moreover, glucuronidation mediated by UDP-glucuronosyltransferase (UGT) is involved in the metabolism of several statins (Prueksaritantont et al., 2002a). Thus, each statin exhibits a unique and complex pharmacokinetic profile due to specific transporter- and/or enzyme-mediated clearance mechanisms. Inhibition of one or several of these clearance pathways upon co-medication of the statins (so-called victim drug) with a perpetrator compound might therefore ultimately result in alterations of drug exposure.

Recently, our group established a novel method to predict the human hepatic drug clearance based on a mechanistic i*n vitro-in vivo* extrapolation (IVIVE) model (Umehara and Camenisch, 2012; Camenisch and Umehara, 2012). The approach is based on incorporation of *in vitro* data for all physiological hepatic drug elimination processes into the extended mechanistic hepatic clearance model, allowing the determination of the rate-limiting hepatic clearance step. Based on this approach, drugs can be classified according to their *in vitro* determined major clearance mechanism, referred as Extended Clearance Concept Classification System (ECCCS). Similar to the Biopharmaceutics Drug Disposition Classification System (BDDCS), which is based on the extent of *in vivo* observed drug metabolism and *in vitro* solubility data (Benet et al., 2008), the ECCCS categorizes drugs into four classes. For highly permeable class 1 and 2 compounds, metabolism is projected as the major hepatic clearance process. While passive hepatic uptake is the rate-limiting step for class 1 compounds, the sum of metabolism and efflux transporter-mediated biliary elimination is predicted to be rate-limiting for class 2 compounds. Active hepatic uptake is predicted to be the rate-determining step for class 3 compounds, while the clearance of class 4 compounds is dependent on the interplay of all processes involved in hepatic elimination (namely metabolism, uptake, and efflux). Thus, based on the extended mechanistic clearance concept, application of the ECCCS allows for a compound-class dependent assessment of the DDI potential of (new) chemical entities. In this study, we used statins as model drugs to further validate our new *in vitro* data-based extended mechanistic hepatic clearance model. Human hepatic clearances were predicted for all marketed statins: atorvastatin, fluvastatin, lovastatin acid, pitavastatin, pravastatin, rosuvastatin, and simvastatin acid as well as for cerivastatin. Subsequently, we assessed the DDI potential of each statin by simulating inhibition of the relevant hepatic clearance processes. The predicted DDI effects were compared with reported AUC changes from clinical studies (Sharma et al., 2012; Yoshida et al., 2012; Neuvonen et al., 2006) and the underlying mechanisms driving the DDI potential for each statin were discussed within the frame of the ECCCS.

6.3 Materials and Methods

Compounds

[^{3}H] atorvastatin calcium (0.37 MBq/nmol), [^{3}H] cerivastatin sodium (0.19 MBq/nmol). [^{3}H] fluvastatin sodium (0.74 MBq/nmol), [^{3}H] lovastatin acid (0.37 MBq/nmol), [^{3}H] pitavastatin calcium (0.37 MBq/nmol), [^{3}H] pravastatin sodium (0.19 MBq/nmol), [^{3}H] rosuvastatin calcium (0.37 MBq/nmol), and [^{3}H] simvastatin acid (0.37 MBq/nmol) were obtained from American Radiolabeled Chemicals, Inc. (Saint Louis, MO). [^{3}H] taurocholic acid (TCA; 1.67 MBq/nmol) was purchased from PerkinElmer (Boston, MA). All other compounds and reagents were of analytical grade and purchased from commercial sources. Human sandwich-cultured hepatocytes were purchased as B-CLEAR® kits from Qualyst, Inc. (Durham, NC).

Hepatic clearance prediction

According to the extended mechanistic clearance concept, the overall apparent hepatic intrinsic clearance can be described as follows (Camenisch and Umehara, 2012):

$$CL_{h,int} = \frac{(PS_{inf,act} + PS_{inf,pas}) \cdot (CL_{int,sec} + CL_{int,met})}{(PS_{eff,act} + PS_{eff,pas} + CL_{int,sec} + CL_{int,met})} \tag{6.1}$$

Where $PS_{inf,act}$ and $PS_{inf,pas}$ are the active and passive hepatic influx clearances from the blood, respectively, $CL_{int,sec}$ is the intrinsic biliary secretion clearance, and $CL_{int,met}$ is the intrinsic metabolic clearance. $PS_{eff,act}$ and $PS_{eff,pas}$ describe the active and passive sinusoidal efflux from the hepatocytes back into the blood, respectively.
All above parameters can be determined experimentally (Umehara and Camenisch, 2012; Camenisch and Umehara, 2012). For present assessment, all *in vitro* transport and metabolism data for atorvastatin and pravastatin were taken from a previous work (Camenisch and Umehara, 2012). For the other statins, we used $PS_{inf,act}$ and $PS_{inf,pas}$ data as recently assessed in suspended hepatocytes (Kunze et al., 2014a). $CL_{int,sec}$ was determined in human sandwich-cultured hepatocyte incubations using the B-CLEAR® assay (single concentration determinations at 0.1 µM) assuming that metabolism was negligible (Camenisch and Umehara, 2012). All values for $CL_{int,met}$ determined in human liver microsomal incubations were taken from literature (Table 6.1). Moreover, we assumed that efflux over the sinusoidal membrane from hepatocytes back into the blood occurred via passive diffusion only (i.e. $PS_{eff,act} = 0$) and that the passive sinusoidal efflux was equal to the passive influx (i.e. $PS_{eff,pas} = PS_{inf,pas}$). Subsequently, the hepatic *in vivo* clearance

(CL_h) was predicted based on the "well-stirred liver" model as follows (Camenisch and Umehara, 2012):

$$CL_h = \frac{Q_h \cdot f_{u,b}(PS_{inf,act} + PS_{inf,pas}) \cdot (CL_{int,sec} + CL_{int,met})}{Q_h \cdot (PS_{inf,pas} + CL_{int,sec} + CL_{int,met}) + f_{u,b} \cdot (PS_{inf,act} + PS_{inf,pas}) \cdot (CL_{int,sec} + CL_{int,met})} \tag{6.2}$$

Where Q_h is the hepatic blood flow [20.7 mL/(min·kg)] and $f_{u,b}$ is the unbound fraction of drug in blood as reported in literature (Table 6.1).

DDI assessment

A perpetrator drug may inhibit all active clearance pathways contributing to the total hepatic elimination of a substrate compound. Accordingly, based on equation 6.1, the overall apparent hepatic intrinsic clearance in the presence of a perpetrator ($CL_{h,int,i}$) can be expressed as follows (Camenisch and Umehara, 2012):

$$CL_{h,int,i} = \frac{((1 - f_{i,inf}) \cdot PS_{inf,act} + PS_{inf,pas}) \cdot ((1 - f_{i,sec}) \cdot CL_{int,sec} + (1 - f_{i,met}) \cdot CL_{int,met})}{(PS_{inf,pas} + (1 - f_{i,sec}) \cdot CL_{int,sec} + (1 - f_{i,met}) \cdot CL_{int,met})} \tag{6.3}$$

Where $f_{i,inf}$, $f_{i,sec}$, and $f_{i,met}$ denote the inhibited fractions of active influx, secretion, or metabolism, respectively. A value of zero thereby indicates no inhibition whereas a value of one refers to complete inhibition. Based on this relationship the hepatic *in vivo* clearance in the presence of any perpetrator compound ($CL_{h,i}$) can be calculated in accordance with equation 6.2.

Following oral administration of a drug and its perpetrator, assuming the presence of hepatic and a non-hepatic (e.g. renal) elimination pathways and that the perpetrator drug only affects active processes in the liver, the exposure (AUC) fold-change (expressed as $AUC_{po,i}/AUC_{po}$) can be described as follows (Boulenc and Barberan, 2011):

$$\frac{AUC_{po,i}}{AUC_{po}} = \frac{F_{h,i}}{F_h} \cdot \frac{1}{f_{n,h} \cdot CL_{h,i}/CL_h + 1 - f_{n,h}} \tag{6.4}$$

Where, $f_{n,h}$ is the fractional contribution of hepatic clearance to overall clearance. F_h (= 1-CL_h/Q_h) and $F_{h,i}$ (= 1-$CL_{h,i}/Q_h$) are the fractions of the oral dose escaping hepatic first-pass in the absence and presence of a perpetrator, respectively.

Under the additional assumption that the liver is the only clearance organ (i.e. $f_{n,h}$ = 1)

equation 6.4 simplifies with (Einolf, 2007):

$$\frac{AUC_{po,i}}{AUC_{po}} = \frac{CL_{h,int}}{CL_{h,int,i}} \tag{6.5}$$

Statistical Analysis

Linear correlation analysis were performed to obtain the regression equation and the correlation coefficient (R^2) using Microsoft Excel. Average fold errors (afe), predicting the accuracy between the observed and predicted parameters were calculated accordingly:

$$= 10^{\frac{1}{N}\sum log\frac{predicted}{observed}} \tag{6.6}$$

Where a value below two indicates a good prediction accuracy (Kunze et al., 2014b).

Table 6.1: *In vitro* pharmacokinetic parameters.

compounds	measured in house			obtained from literature[a]	
	$PS_{inf,act,invitro}$ ($\mu L \cdot min^{-1} \cdot 10^6 cells$)	$PS_{inf,pas,invitro}$ ($\mu L \cdot min^{-1} \cdot 10^6 cells$)	$CL_{int,sec,invitro}$ ($\mu L \cdot min^{-1} \cdot mg_{prot}^{-1}$)	$CL_{int,met,invitro}$ ($\mu L \cdot min^{-1} \cdot mg_{prot}^{-1}$)	$f_{u,b}$ (-)
lovastatin acid	64.88	57.17	bld	337.00	0.08
simvastatin acid	45.63	117.09	0.50	564.71	0.11
cerivastatin	87.07	95.82	bld	34.40	0.02
fluvastatin	85.95	127.94	bld	107.79	0.04
pitavastatin	143.18	101.70	bld	12.96	0.07
atorvastatin	55.15	22.69	3.75	47.41	0.08
pravastatin	22.78	14.13	0.71	0.68	0.97
rosuvastatin	10.69	9.73	1.90	1.13	0.17

[a)] Literature references are provided as "Supplementary Information" (Supplementary Table 6.3)
[bld)] below limit of detection (zeroed for all subsequent calculations)

6.4 Results and Discussion

The experimentally determined *in vitro* parameters for hepatic influx, metabolism, and biliary secretion are listed in Table 6.1. The up-scaled process parameters, the projected

overall apparent hepatic intrinsic clearances according to equation 6.1 and the predicted *in vivo* hepatic organ clearances ($CL_{h,pre}$) according to equation 6.2 are given in Table 6.2. Moreover, Table 6.2 lists the *in vivo* observed hepatic clearances ($CL_{h,obs}$) which were derived from human mass balance studies taking the *in vivo* determined renal clearances into account.

As shown in Table 6.2, the values for the different physiological processes driving hepatic elimination differ significantly for the eight statins in our dataset. Highest net hepatic influx values, exceeding 500 mL/(min·kg), were obtained for pitavastatin and fluvastatin, while pravastatin and rosuvastatin showed comparatively low values [< 100 mL/(min·kg)]. Simvastatin acid, cerivastatin, and fluvastatin exhibited a high contribution of passive influx to the total net influx ($PS_{inf,pas} > PS_{inf,act}$). The up-scaled $CL_{int,met}$ ranged from 0.9 mL/(min·kg) for pravastatin to 769.2 mL/(min·kg) for simvastatin acid. Up-scaled $CL_{int,sec}$ was highest for atorvastatin [11.8 mL/(min·kg)] whereas no biliary secretion at all could be experimentally determined for lovastatin acid, cerivastatin, fluvastatin and pitavastatin. The predicted intrinsic clearances ranged from 7.4 mL/(min·kg) measured for pravastatin to 298.6 mL/(min·kg) obtained for simvastatin acid.

Anticipation of hepatic clearance

The correlation between the *in vitro* predicted and *in vivo* observed hepatic clearances is illustrated in Figure 6.1. Six out of eight statins (atorvastatin, fluvastatin, lovastatin acid, pitavastatin, pravastatin, and simvastatin acid) were predicted within two-fold deviation from the clinically observed value, while cerivastatin and rosuvastatin were under-predicted by more than two- and six-fold, respectively. Excluding rosuvastatin a good overall ac-

Table 6.2: Predicted pharmacokinetc parameters

compounds	ECCCS	PS_{act} mL/(min·kg)	PS_{pas} mL/(min·kg)	$CL_{int,met}$ mL/(min·kg)	$CL_{int,sec}$ mL/(min·kg)	$CL_{h,int}$ mL/(min·kg)	$CL_{h,pred}$ mL/(min·kg)	$CL_{h,obs}$ [a] mL/(min·kg)
lovastatin acid	class 1	165.1	145.5	459.0	0.0	235.8	9.9	11.4
simvastatin acid	class 1	116.1	297.9	769.2	1.7	298.6	12.7	25.2
cerivastatin	class 2	221.5	243.8	46.9	0.0	75.0	1.4	3.4
fluvastatin	class 2	218.7	325.5	146.8	0.0	169.2	5.1	7.0
pitavastatin	class 2	364.3	258.7	17.7	0.0	39.8	2.5	3.5
atorvastatin	class 4	140.4	7.7	64.6	11.8	112.9	6.5	5.9
pravastatin	class 4	57.9	36.0	0.9	2.2	7.4	5.4	10.4
rosuvastatin	class 4	27.2	24.8	1.5	5.7	11.8	1.8	12.2

Notes: Up-scaling of the *in vitro* clearances (Table 6.1) to human *in vivo* organ level was performed with the help of the following scaling factors: 1.6 (mg protein)/($1 \cdot 10^6$ cells) and $99 \cdot 10^6$ cells/(g liver) for suspended hepatocytes; 53 (mg protein)/(g liver) for liver microsomes; 116 (mg protein)/(g liver) for sandwich-cultured hepatocytes and 25.7 (g liver)/(kg body weight) for liver weight (Carlile et al., 1997; Swift et al., 2010). $CL_{h,int}$ and $CL_{h,pred}$ were calculated according to equations 6.1 and 6.2, respectively. Compound categorization according to the ECCCS was performed as previously described (Camenisch and Umehara, 2012).

[a] Literatur references and calculation details are provided as "Supplementary Information" (Supplementary Table 6.4).

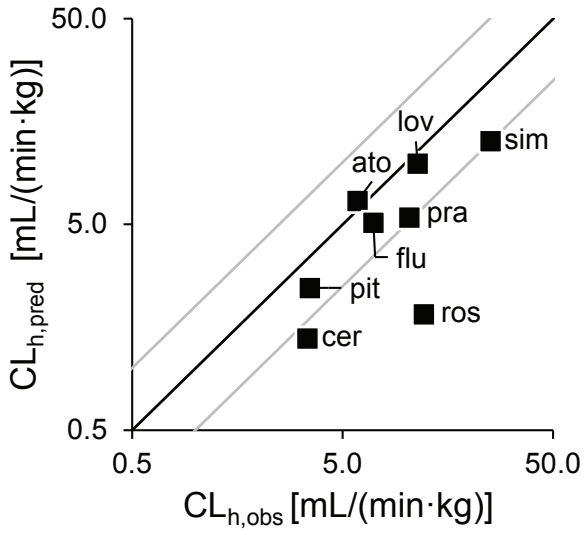

Figure 6.1: Correlation between the predicted ($CL_{h,pred}$) and observed ($CL_{h,obs}$) hepatic clearances. Abbreviations: ato, atorvastatin; cer, cerivastatin, flu, fluvastatin; lov, lovastatin acid; pit, pitavastatin; pra, pravastatin; ros, rosuvastatin, and sim, simvastatin acid. The black and gray lines represent the line of unity and the two-fold deviations, respectively.

curacy of prediction was indicated by an average fold error (afe) of 1.5. However, a trend towards a slight under-estimation of the *in vivo* observed hepatic clearances was observed (linear regression slope: 0.47, intercept: 1.72, $R^2 = 0.80$). Down-regulated transporter/enzyme expression in our *in vitro* systems and/or intracellular pH effects potentially impacting the basolateral passive efflux out of hepatocytes are possible mechanistic/physiological explanations for this general observation as discussed in more detail elsewhere (Umehara and Camenisch, 2012; Camenisch and Umehara, 2012). Possible other reasons eventually leading to significant IVIVE disconnects are discussed below.

Drug-drug interaction potential projections

Figure 6.2 depicts the predicted DDI potential of all statins in our dataset following oral administration according to equation 6.5, generally assuming significant (almost complete) process inhibition of 90% (i.e. $f_{i,inf} = f_{i,met} = f_{i,sec} = 0.9$) (Camenisch and Umehara, 2012). As illustrated, the impact of simultaneous inhibition of multiple clearance processes can for some statins (such as cerivastatin, fluvastatin, lovastatin acid, pitavastatin, and simvastatin acid) be anticipated from the product of the AUC ratios of the individual processes (i.e. inhibition of only influx, metabolism, or biliary secretion) whereas for another category of statins (such as atorvastatin, pravastatin, and rosuvastatin) the projected overall AUC change increases over-proportionally compared to the single process contributions. The power of the extended hepatic clearance model for providing mechanistic insight into the (rate-limiting) processes driving hepatic elimination and, ultimately, for assessing qualitatively and quantitatively the compound-dependent DDI risks is subsequently discussed for each statin separately.

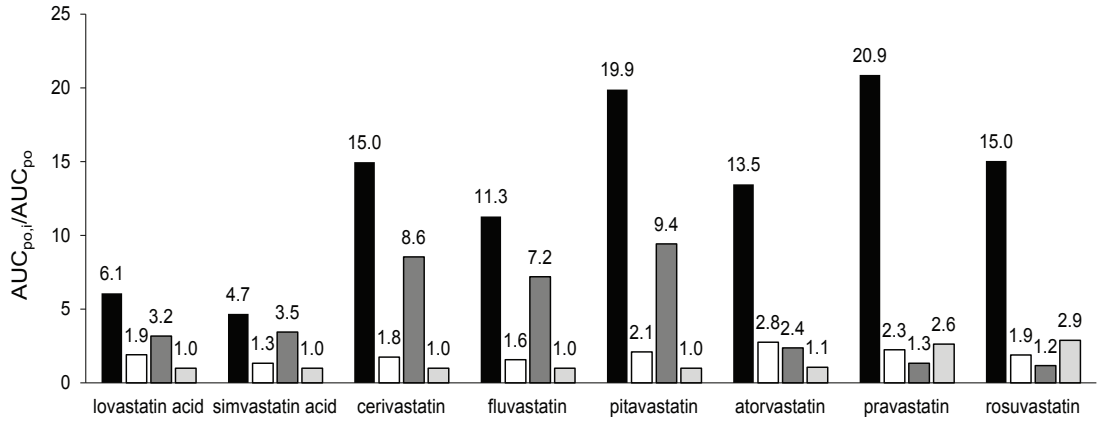

Figure 6.2: Prediction of the hepatic DDI potential of statins. Using equation 6.5, the AUC fold-change was determined for the following scenarios (Camenisch and Umehara, 2012): black, total hepatic inhibition ($f_{i,inf} = f_{i,met} = f_{i,sec} = 0.9$); white, inhibition of active hepatic influx ($f_{i,inf} = 0.9$); dark gray, inhibition of metabolism ($f_{i,met} = 0.9$); light gray, inhibition of biliary secretion ($f_{i,sec} = 0.9$).

Lovastatin acid and simvastatin acid

Lovastatin and simvastatin are both administered as lactone pro-drugs, which are rapidly converted to their active acid forms either by spontaneous chemical reactions or by carboxylesterase-mediated metabolism in the intestine, liver, and plasma (Neuvonen et al., 2006; Elsby et al., 2012). Renal clearance represents a minor elimination pathway for both, lovastatin acid and simvastatin acid, with 10% and 13% parent drug excreted in urine, respectively. Both drugs are mainly eliminated by metabolism via CYP3A4, CYP2C8, and UGTs (Prueksaritantont et al., 2002a; Neuvonen et al., 2006; Elsby et al., 2012). Lovastatin acid was *in vitro* identified to be transported by OATP1B1 and simvastatin acid is a substrate of OATP1B1 and OATP1B3 (Kunze et al., 2014a).

Following co-medication with gemfibrozil in clinics, AUC ratios of 2.8 and 2.9 were reported for lovastatin acid and simvastatin acid, respectively (Backman et al., 2000; Kyrklund et al., 2001). Gemfibrozil is a well-known inhibitor of OATP1B1, NTCP, CYP2C8, and UGTs (Prueksaritantont et al., 2002b; Shitara et al., 2004). Accordingly, applying equation 6.5 with $f_{i,inf} = f_{i,met} = 0.9$, AUC ratios of 6.1 and 4.7 are predicted for lovastatin acid and simvastatin acid, respectively (Figure 6.2). Both projections slightly over-predict the *in vivo* findings though (2.2-fold for lovastatin acid and 1.6-fold for simvastatin acid). However, static DDI prediction methods are generally expected to be over-predictive for the *in vivo* situation as they do not account for the real inhibitor concentration and consequently for partial inhibition effects at the sites of interaction (i.e. any process inhibition fractions below 0.9 in this study). In addition, recent studies in our laboratories have revealed the involvement of at least one additional not yet identified transporter system in the hepatic uptake of both compounds (its contribution to overall active uptake is estimated with about 80% and 40% for lovastatin acid and simvastatin acid, respectively) (Kunze et al., 2014a). Provided that gemfibrozil is not inhibiting this additional transport system,

the fractional contributions for active OATP1B1-mediated influx would be significantly lower than assumed above ($f_{i,inf}$ = 0.2 and 0.6 for lovastatin acid and simvastatin acid, respectively) and, as a consequence, a lower DDI potential following simultaneous inhibition of OATP1B1-mediated hepatic uptake and overall metabolism is projected (3.5-fold for lovastatin acid and 4.2-fold for simvastatin acid).
Nevertheless, based on their high passive permeability characteristics, both compounds were assigned to ECCCS class 1. In this class the uptake into the hepatocytes becomes the rate-limiting step of hepatic elimination and metabolism is anticipated to be the major source for DDIs. Applying the mechanistic extended hepatic clearance model, inhibition of only metabolism resulted in AUC ratio projections of 3.2 and 3.5 for lovastatin acid and simvastatin acid, respectively. This DDI prediction is in excellent agreement with the *in vivo* interaction results (less than 1.2-fold over-predictive for both lovastatin acid as well as simvastatin acid). Consequently, in alignment with the ECCCS class 1 assignment, transporter effects (if any) are projected to be minimal and the product of the individual AUC ratio changes driving hepatic elimination (namely hepatic uptake and metabolism) can be used to anticipate the overall DDI risk following simultaneous inhibition of both processes together (Figure 6.2).

Cerivastatin

Cerivastatin, administered as free acid, is exclusively eliminated in the liver where primary OATP1B1 (20%) and a yet unknown transporter system (probably NTCP, 80%) are involved in its active hepatic uptake (Kunze et al., 2014a). Metabolism is the only reported clearance pathway of cerivastatin, with a contribution of 61% CYP2C8 and 37% of CYP3A4 (Shitara et al., 2004; FDA, 2014).
As shown in Table 6.2, cerivastatin was assigned to ECCCS class 2. In this class the sum of metabolism and biliary clearance represents the rate-limiting step of hepatic elimination and inhibition of metabolism is generally projected as the major source of drug-drug interactions (Figure 6.2). In clinical studies, an AUC-ratio of 5.6 has been observed following co-administration of cerivastatin and gemifbrozil (Yoshida et al., 2012). Based on *in vitro* studies gemfibrozil inhibits the OATP1B1- and NTCP-mediated hepatic uptake as well as the CYP2C8-mediated metabolism of cerivastatin while its inhibitory effect on CYP3A4 is expected to be of minor clinical relevance (Shitara et al., 2004; Prueksaritantont et al., 2002c). Thus, taking into account above inhibitory potential of gemfibrozil ($f_{i,inf}$ = 0.9, $f_{i,met}$ = 0.61) the liver-based static DDI model (equation 6.5) predicted an AUC ratio of 4.1. Furthermore, in clinics, cyclosporine A (CsA, an OATP family, NTCP and CYP3A4 inhibitor with no relevant CYP2C8 effect) was shown to increase the AUC of cerivastatin by 3.8-fold (Yoshida et al., 2012). Accordingly, with $f_{i,inf}$ = 0.9 and $f_{i,met}$ = 0.37, an AUC ratio of 2.6 is anticipated from *in vitro* data. Consequently, for both scenarios DDI effects within a comparable range to the observed AUC ratios were predicted with a general trend towards a slight under-prediction (about 1.5-fold) of the effective DDI potential. One reason for systematic under-predictions with the extended clearance concept approach is

the possibility that the fractional process contributions as estimated from *in vitro* investigations might not absolutely reflect the ultimate *in vivo* situation correctly (e.g. wrong fractional contributions of known pathways, existence of additional not yet identified pathways and/or time-dependent changes of pathway contributions as e.g. observed following auto-induction/inhibition). And indeed, being a prominent CYP3A4, BCRP and P-gp substrate (Matsuhima et al., 2005), for cerivastatin a possible existence of an extra-hepatic elimination pathway such as pre-systemic intestinal metabolism and/or efflux ultimately contributing to the overall clinical DDI risk in the range of our under-predictions was discussed in literature (Yoshida et al., 2012). Nevertheless, similar to ECCCS class 1, transporter effects for ECCCS class 2 drugs are anticipated to contribute minimally to their hepatic interaction risk and the overall DDI potential as victim drug in the liver can easily be projected from the AUC changes of the individual processes (Figure 6.2).

Fluvastatin

Fluvastatin is predominately cleared by the liver. Administered as free acid, about 90% of a fluvastatin dose undergoes metabolism while only 2% and 6% of parent drug are recovered in feces and urine, respectively. *In vitro* studies indicate that metabolism is primarily mediated by CYP2C9 (75%) and to a lower extent by CYP3A4 (20%) and CYP2C8 (5%) (Scripture and Pieper, 2001). Moreover, OATP1B1, OATP2B1, OATP1B3, and NTCP contribute to the active hepatic uptake of fluvastatin (Kunze et al., 2014a; Bi et al., 2013; Fujino et al., 2003).

Fluvastatin was assigned to ECCCS class 2 and, in agreement with this classification, the overall DDI potential can be projected from the individual process contributions as discussed above (Figure 6.2). Inhibition of metabolism is predicted as the major pathway causing DDIs while inhibition of hepatic uptake transporters is expected to have a minor impact. This conclusion is supported by a clinical observation demonstrating that co-administration of the OATP transporter family inhibitor erythromycin (no CYP inhibition potency) did not significantly alter the exposure of fluvastatin (predicted and observed AUC) ratio of 1.6 and 1.2, respectively) (Scripture and Pieper, 2001).

As illustrated in Figure 6.2, an AUC ratio of 11.3 was projected assuming simultaneous inhibition of active uptake and metabolism ($f_{i,inf} = f_{i,met} = 0.9$). In clinical trials, maximal DDI effects resulted generally in AUC ratios below four though. However, as multiple transporters and metabolic enzymes are involved in the hepatic elimination of fluvastatin, it is likely that perpetrators used in clinical studies did not concomitantly inhibit all active clearance processes involved in its elimination. For example, AUC-increases of up to 3.5-fold have been reported for co-administration of fluvastatin with CsA (potent inhibitor of OATPs, NTCP, BCRP, and CYP3A4 (Yoshida et al., 2012)). Assuming inhibition of hepatic uptake ($f_{i,inf} = 0.9$) and simultaneously of only CYP3A4-mediated metabolism ($f_{i,met} = 0.2$) the anticipated change in AUC is 1.8-fold which, in contrast to above projections, slightly under-predicts the *in vivo* observed value. Thus, the discrepancy between the predicted and observed clinical DDI effect could eventually be attributed to an additional (partial)

inhibition of CYP2C8 and/or CYP2C9 by CsA. Recent investigations, however, are more supportive for the hypothesis that BCRP-mediated intestinal efflux might have a significant role in modulating the absorption of fluvastatin (Elsby et al., 2012). Integrating into above assessment an experimentally determined *in vivo* exposure increase of 72% (1.72-fold) following complete BCRP inhibition, the overall static DDI risk projection for fluvastatin in the presence of CsA would be 3.1-fold which is in excellent compliance with the clinical observations.

Pitavastatin

Administered as free acid, pitavastatin is exclusively eliminated via the liver, and 79% of the dose is recovered in feces as unchanged parent drug, indicating direct biliary secretion (Elsby et al., 2012). Thus, metabolism of pitavastatin, mainly mediated by CYP2C9 (45%) and UGT (55%), is a minor hepatic elimination pathway (Shitara and Sugiyama, 2006; Fujino et al., 2003). Moreover, pitavastatin is an *in vitro* substrate of OATP1B1, OATP1B3, NTCP, and BCRP (Kunze et al., 2014a; FDA, 2014; Bi et al., 2013; Hirano et al., 2005).

In contrast to the described clinical observations, no active biliary secretion of pitavastatin was measured in our *in vitro* experiments which is in alignment with recent clinical findings that pitavastatin disposition is not influenced by BCRP *in vivo* (Elsby et al., 2012). Metabolism was predicted as the predominant hepatic elimination pathway of pitavastatin (Table 6.2) and the anticipated hepatic clearance based on the extended clearance concept equation was similar to the measured clinical data. This observation suggests that the reported value for biliary parent drug secretion (79%) might not correctly reflect the effective mechanism of pitavastatin elimination (Elsby et al., 2012). *In vitro* studies demonstrated that direct glucuronidation contributes significantly to pitavastatin metabolism providing evidence that *in vivo* pitavastatin might be substantially biliary secreted as its direct glucuronide metabolite (Shitara and Sugiyama, 2006; Fujino et al., 2003). Since glucuronide metabolites are often found to be cleaved in the gastrointestinal tract (e.g. by enterobacteria), the amount of unchanged pitavastatin found in human feces might consequently not fully represent the actual amount of secreted parent drug. The contribution of direct biliary pitavastatin secretion *in vivo* might therefore be significantly overestimated while hepatic metabolism is in fact representing the most relevant clearance mechanism.

Using the ECCCS categorization approach pitavastatin was assigned to class 2. Inhibiting all hepatic pitavastatin clearance mechanisms as a worst-case scenario (i.e. $f_{i,inf} = f_{i,met} = 0.9$) we predicted an AUC ratio of 19.9 (Figure 6.2). In a clinical study, co-administration with CsA led to a 4.6-fold increased AUC of pitavastatin (Yoshida et al., 2012). Based on *in vitro* inhibition data, CsA is expected to inhibit active hepatic uptake and UGT-mediated metabolism of pitavastatin while it has no clinically significant inhibitory potential on CYP2C9 (Yoshida et al., 2012; Liu et al., 2011). Thus, applying the known inhibitory properties of CsA ($f_{i,inf} = 0.9$ and $f_{i,met} = 0.55$) we forecast an AUC increase of 4.5-fold. In a different study, co-administration of pitavastatin with erythromycin (inhibitor of OATPs

but not of CYPs) resulted in an observed AUC increase of 380% (Elsby et al., 2012). Assuming inhibition of active hepatic influx only ($f_{i,inf}$ = 0.9) we project an AUC ratio of 2.1-fold. Our predictions indicate that clinically observed DDI effects are mechanistically well-reflected by our model. These observations further support the above mentioned hypothesis that clinical data might represent an over-estimation of the actual *in vivo* observed biliary pitavastatin clearance.

Atorvastatin

In clinics, atorvastatin is administered as pharmacologically active acid. About 70% of administered atorvastatin is metabolized (mainly by CYP3A4), and about 28% are actively biliary secreted. With 2% of unchanged drug recovered in urine, renal elimination is a minor excretion pathway for atorvastatin. *In vitro* studies demonstrated that atorvastatin is a substrate for OATP1B1, OATP1B3, P-gp, BCRP, and MRP2 (Li et al., 2011; Kunze et al., 2014a; Lau et al., 2006).

Based on *in vitro* data, atorvastatin was assigned to ECCCS 4 (Table 6.2). As shown in Figure 6.2, inhibition of either active influx ($f_{i,inf}$ = 0.9) or metabolism ($f_{i,met}$ = 0.9) is predicted to result in moderate AUC changes of about 2- to 3-fold, while no significant increase in AUC was anticipated when only biliary clearance was inhibited ($f_{i,sec}$ = 0.9). Upon simultaneous inhibition of all hepatic clearance processes, an AUC change of 13.5-fold is projected. Clinical studies, following oral co-administration of atorvastatin with CsA, reported AUC changes of up to 15-fold (Yoshida et al., 2012; Elsby et al., 2012). CsA is a well-known (*in vitro*) inhibitor of OATP1B1, OATP2B1, OATP1B3, NTCP, P-gp, BCRP and MRP2 transporters, as well as of CYP3A4 and UGT metabolic enzymes (Liu et al., 2011; Cummins et al., 2002; El-Sheikh et al., 2013; Ho et al., 2006; Xia et al., 2007). Hence, the present total hepatic worst case DDI prediction of about 14-fold is in excellent agreement with the reported clinical observations. Similarly, when clinically co-administered with a combination of lopinavir and ritonavir a 5.9-fold AUC increase of atorvastatin was observed (Yoshida et al., 2012; Elsby et al., 2012). Lopinavir is a potent OATP1B1 and OATP1B3 inhibitor while ritonavir also inhibits CYP3A4 metabolism (Annaert et al., 2010; Eagling et al., 1997). Assuming concomitant significant inhibition of active influx and metabolism ($f_{i,inf}$ = $f_{i,met}$ = 0.9), the extended clearance concept anticipates an exposure increase of around 6.5-fold. Moreover, an AUC ratio of 3.3 was reported for atorvastatin when given together with the potent CYP3A4 inhibitor itraconazole (has no effect on OATPs), which is also in good agreement with the projected value of 2.4-fold (Yoshida et al., 2012; Elsby et al., 2012).

In contrast to the ECCCS class 1 and 2 compounds discussed before, the overall DDI potential for atorvastatin cannot be projected from the AUC changes of the individual processes though, as nicely illustrated in Figure 6.2. Hence, for ECCCS class 4 compounds the substantial over-proportional increase in AUC upon simultaneous inhibition of uptake, efflux and metabolism derives from the essential interplay and inter-dependencies of all hepatic elimination pathways together. It is noteworthy to mention here, that in current

DDI risk assessment potential involvement of basolateral hepatic and/or apical intestinal efflux transporters as well as of intestinal enzymes was not considered and that significant coincidental *in vivo* inhibition of any of these active processes by perpetrators drugs would ultimately result in over-predictions of the effective interaction potential for this ECCCS class 4 compound.

Pravastatin

Administered as free acid, the major route of hepatic pravastatin elimination is biliary secretion of parent drug mediated by BCRP and MRP2. Hepatic oxidative metabolism via CYPs is considered to be of minor importance since less than 10% of the dose are recovered as metabolites in feces (Elsby et al., 2012; Hirano et al., 2005; Everett et al., 1991; Sasaki et al., 2002). Furthermore, active hepatic uptake of pravastatin is mediated by OATP1B1, OATP1B3, and OATP2B1 (Shitara and Sugiyama, 2006; Kunze et al., 2014a).

Applying equation 6.4, inhibition of all hepatic clearance processes ($f_{i,inf} = f_{i,met} = f_{i,sec} = 0.9$) resulted in a maximal AUC increase projection of more than 20-fold (Figure 6.2). However, in contrast to other statins, pravastatin exhibits a unique pharmacokinetic profile due to a significant contribution of renal clearance (47%) to the total body clearance which represents a significant deviation from the assumptions made for equation 6.5 (Elsby et al., 2012). Hence, the fractional contribution of the hepatic pathway to overall pitavastatin elimination is only about 53% ($f_{n,h} = 0.53$) and, as a consequence according to equation 6.4, complete blockage of the hepatic elimination pathway is not expected to result in AUC changes beyond 2.6-fold. Clinical DDI studies with pravastatin and gemfibrozil, a selective OATP inhibitor, reported 2-fold AUC changes (Nakagomi-Hagihara et al., 2007). Assuming only inhibition of active hepatic influx ($f_{i,inf} = 0.9$), we calculated an AUC ratio of 1.6 with equation 6.4. Furthermore, no significant AUC increases were observed in clinics following co-administration of pravastatin with either itraconazole or fluconazole both compounds potent CYP3A4 and CYP2C9 inhibitors (Yoshida et al., 2012). This observation was also reflected by our model since inhibition of metabolism alone did not predict any relevant AUC changes (1.1-fold).

However, in clinics an AUC ratio of 23 was reported upon co-administration of pravastatin with CsA (inhibitor of OATPs, NTCP, CYP3A4, UGTs, MRP2, and BCRP) exceeding the theoretically possible hepatic DDI potential by about 9-fold (Yoshida et al., 2012). Yet, in human the renal excretion process is known to involve active transporter-mediated secretion as indicated by the estimated renal clearance (9.2 mL/(min·kg) corresponding to 47% of total clearance) significantly exceeding (about 5-6-fold) the projected renal filtration clearance [~ 1.7 mL/(min·kg)] calculated from the product of glomerular filtration rate [1.8 mL/(min·kg)] and the fraction unbound in blood ($f_{u,b} = 0.97$) (Kunze et al., 2014b). The most likely reason for the obvious contradiction in data is therefore the contribution of a transporter mediated active tubular secretion pathway coincidentally also inhibited by CsA. In literature, OAT3 has been suggested to be responsible for the basolateral uptake of pravastatin, whereas the transporter involved in its luminal efflux is yet to be

identified (Nakagomi-Hagihara et al., 2007). MRP2 and/or BCRP are likely candidate transporters though, both well-known to be effectively inhibited by CsA. Assuming a 80% simultaneous inhibition of both hepatic as well as renal elimination pathways the anticipated overall exposure increase can be estimated with around 9-fold (details are given as "Supplementary Information" (equation 6.16, Table 6.5)). Following a 90% inhibition of the overall clearance the AUC increase is projected with already 19-fold ("Supplementary Information" (equation 6.16, Supplementary Table 6.6)). This would be in excellent agreement with the observed *in vivo* DDI effect (measured *in vivo* AUC ratio/predicted *in vitro* AUC ratio $\approx$ 1.2). Owing the complex inhibition profile of CsA a final assessment is difficult to develop though notably because of a potentially reduced pravastatin absorption due to intestinal MRP2 as discussed in literature (Elsby et al., 2012). The restriction of pravastatin absorption was quantified with 67% reflecting the observed AUC increase in individuals with a synonymous c1446C > G single nucleotide polymorphism in the ABCC2 (MRP2) gene (Niemi et al., 2006). In any case, the hepatic DDI projections according to equation 6.5 provided above are therefore just accidentally reflecting the *in vivo* observations stressing out the need for a careful and integrated (pre)clinical data analysis for more complex chemical entities such as the ECCCS class 4 compound pravastatin.

Rosuvastatin

Rosuvastatin is administered as free acid. The hepatic clearance of rosuvastatin accounts for approximately 70% ($f_{n,h}$ = 0.7) of the net body clearance while 30% are attributed to renal secretion of unchanged drug. Direct biliary secretion of unchanged rosuvastatin is reported as the major hepatic route of elimination. Thereby, OATP1B1, OATP1B3, OATP2B1, and NTCP are assumed to mediate active hepatic uptake, while secretion of rosuvastatin into bile is primary mediated via BCRP (Elsby et al., 2012; Martin et al., 2003a). Metabolic clearance, mainly by CYP2C9 and UGTs, is considered to play a minor role in rosuvastatin elimination (Elsby et al., 2012; Prueksaritantont et al., 2002c; Martin et al., 2003a).

A clinical AUC ratio of 2.1-fold was reported when co-administering rosuvastatin together with lopinavir (OATP family inhibitor) and ritonavir (CYP3A4 inhibitor) (Yoshida et al., 2012). Since rosuvastatin is not metabolized by CYP3A4, the observed DDI effect is expected to result exclusively from inhibition of active hepatic uptake. Assuming significant inhibition of hepatic influx ($f_{i,inf}$ = 0.9) and applying due to a significant renal clearance contribution equation 6.4, we foresee an 1.5-fold AUC change with this static model approach. Moreover, a triple combination of rosuvastatin, azatanavir (OATP inhibitor) and ritonavir (OATP and CYP inhibitor) resulted *in vivo* in a 3.1-fold increased rosuvastatin AUC (Yoshida et al., 2012). Both perpetrators do not affect canalicular efflux of rosuvastatin. The corresponding static DDI projection predicts an AUC ratio of 1.7. Furthermore, maximum clinical AUC increases of 7.1-fold were observed upon co-administration of rosuvastatin with CsA, which is expected to inhibit all active hepatic elimination processes

of rosuvastatin (Yoshida et al., 2012). Simulating inhibition of all possibly involved hepatic clearance processes in our model, using equation 6.5 (which neglects the clearance pathway via the kidney), an exposure increase of up to 15-fold is projected (Figure 6.2). Also taking into consideration a renal clearance contribution according to equation 6.4, we predict a 3.1-fold AUC increase though. BCRP eventually plays a relevant role in the absorption of rosuvastatin in humans which was demonstrated to be 50% (Elsby et al., 2012; Keskitalo et al., 2009). With that, the maximal exposure increase following intestinal BCRP inhibition is two-fold (probably significantly less though as the physiochemical properties of this hydrophilic statin are unlikely accounting for a complete absorption even in the absence of any efflux transporter activity). Consequently, the static DDI projection for CsA, taking into account DDI effects in the liver and intestine, would be 6.2-fold maximum, which is in good agreement with the clinical observations. However, also for rosuvastatin a substantial active tubular secretion via the OAT1, OAT3, MRP2, BCRP as well as P-gp was demonstrated (Verhulst et al., 2008; Windass et al., 2007). Accounting for such an active tubular secretion pathway, similar to the pravastatin case above (i.e. 80% inhibition of overall systemic clearance without considering a potential intestinal interaction on BCRP), the overall DDI risk would be only slightly over-estimated (1.5-fold) (details are given as "Supplementary Information" [equation 6.16, Supplementary Table 6.5)].

Rosuvastatin was assigned to ECCCS class 4. This is in line with clinical observations, demonstrating that concomitant inhibition of sinusoidal uptake, biliary secretion as well as metabolism pathways significantly define the complex hepatic DDI potential of rosuvastatin. Although the mechanism-based DDI assessment for the liver seems to reflect the clinical observations pretty well (all hepatic projections based on equation are only slightly under-predictive (1.6-fold maximum)), the experimentally determined *in vivo* hepatic clearance of rosuvastatin was significantly under-predicted (> 6-fold) by the extended clearance concept model (Figure 6.1). One possible explanation for this IVIVE disconnect would be an overestimation of the *in vivo* hepatic clearance pathway as derived from experimental clinical data. Hypothetically, the presence of an additional extra-hepatic/extra-renal elimination pathway (such as e.g. active BCRP-mediated intestinal secretion) could have resulted in such an over-estimation of the effective hepatic clearance without really impacting above static DDI assessments for the unspecific cross-reactive inhibitor CsA (Martin et al., 2003b). Yet, present hypothesis is in partial contradiction to above discussed (major) involvement of BCRP in rosuvastatin absorption as it would rather support a significant involvement of this efflux pump in hepatic, renal and intestinal systemic elimination, largely accounting for the 2.4-fold exposure difference observed in healthy volunteers and BCRP-deficient individuals (Keskitalo et al., 2009). Fractional process contributions as experimentally determined from *in vitro* investigations not correctly reflecting the ultimate *in vivo* situation might provide an alternative explanation for the observed data discrepancy. Recently, Jamei et al. developed an IVIVE-based PBPK model for rosuvastatin (Jamei et al., 2014). Since experimental hepatic uptake data did not accurately predict the reported *in vivo* clearance of rosuvastatin the authors used

a top-down (fitted) value [$PS_{inf,act}$ = 222 µL/(min·10^6 cells)] which was 21-fold higher compared to our experimental data (Table 6.1). Replacing our in-house active hepatic uptake results with this tailored value the current IVIVE model (equation 6.2) would have predicted a hepatic clearance of 10.8 mL/(min·kg) being in excellent agreement with the observed *in vivo* clearance (Table 6.2). In addition, using equation 6.4 (i.e. not considering a possible interaction on the active renal tubular secretion pathway and not taking into account a possible intestinal BCRP inhibition), static DDI predictions including this new data point would have provided DDI estimations reflecting above *in vivo* observations very well (8.8-fold following complete process inhibition as observed with CsA, 4.1-fold for an OATP and CYP inhibition profile as seen with the azatanavir/ritonavir combo, and 3.8-fold following OATP inhibition with lopinavir). But, although intriguing prima facie, the potential role of renal and/or intestinal transporter inhibition as discussed above remains to be clarified. In addition, this hypothesis would need to be substantiated by the involvement of a not yet identified sinusoidal active solute-carrier system (as most other statins can reasonably well predicted with current approach the candidate transporters are unlikely OATP1B1, OATP1B3 or NTCP) which in course of the isolation and/or preparation process is ultimately heavily down-regulated in the in vitro hepatocyte systems and which *in vivo* is similarly subject to inhibition by above perpetrators.

6.5 Conclusion

In agreement with previous findings, by applying the extended mechanistic hepatic organ model, a very good *in vitro-in vivo* projection of the effective hepatic clearances for all marketed statins could be demonstrated. Similarly, using clinical *in vivo* observations and *in vitro* information about drug transport and metabolism characteristics, the DDI potential of these statins was successfully assessed and quantitatively evaluated in several retrospective analysis. The correlation between observed and predicted AUC ratios for different combinations of the investigated statins and perpetrator drugs is given in Figure 6.3 summarizing all relevant DDI predictions according to equations 6.4 and 6.5 as discussed above. Overall, the observed interaction effects were well-predicted by the extended mechanistic hepatic clearance model as indicated by an afe of 1.3. Out of 16 DDIs 14 were predicted within a two-fold error and linear regression analysis revealed an almost 1-to-1 correlation (slope: 0.857, intercept: -0.2677, R^2: 0.84). Excluding the interaction predictions for the ECCCS class 4 compounds pravastatin and rosuvastatin in the presence of CsA as perpetrator (legitimated by the evident and significant under-prediction of the overall DDI risk due to cross-reactivity with renal and/or intestinal transporters as discussed above) all clinical DDI effects were projected within a two-fold error maximum (R^2 of 0.89) underlying the validity of this static DDI prediction approach to appropriately

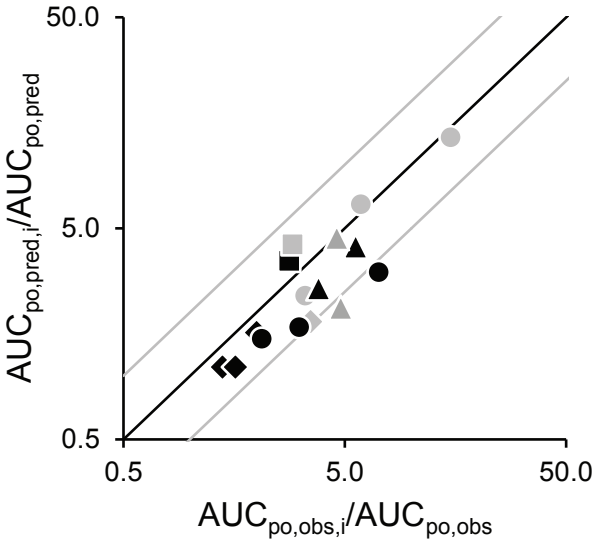

Figure 6.3: Correlation of all observed ($AUC_{po,obs,i}/AUC_{po,obs}$) vs. predicted ($AUC_{po,pred,i}/AUC_{po,pred}$) DDIs between statins and different perpetrator drugs according to equation 6.4 [applied for pravastatin (black diamonds) and rosuvastatin (black circles)] and equation 6.5 [used for lovastatin acid (black squares), simvastatin acid (gray squares), fluvastatin (gray diamonds), cerivastatin (black triangles), pitavastatin (gray triangles) and atorvastatin (gray circles)]. For effective numbers please refer to text. Predictions prone to misjudgment of the effective DDI potential while underlying some vital assumptions (such as the presence of alternative renal and/or intestinal active processes as discussed in the manuscript) were not considered. The black and gray lines represent the line of unity and the two-fold deviations, respectively.

anticipate the DDI potential of victim drugs in the liver.

For the five statins assigned to ECCCS class 1 (lovastatin acid, and simvastatin acid) and ECCCS class 2 (fluvastatin, cerivastatin and pitavastatin) metabolism was anticipated as major clearance mechanism primary responsible for causing DDIs. For compounds assigned to these classes the overall DDI potential can easily be anticipated from the product of the AUC changes of the individual process. A similar overall DDI behavior would be anticipated for ECCCS class 3 statins with sinusoidal transporter inhibition being the major mechanism causing the interaction though. However, none of the statins in this study could be assigned to this ECCCS class which, besides a significant active uptake contribution, is characterized by a low passive permeability and a comparatively high intrinsic (metabolic and/or sinusoidal efflux) clearance. For the three ECCCS class 4 compounds in the dataset (pravastatin, rosuvastatin and atorvastatin), we predicted highest AUC changes upon concomitant inhibition of hepatic uptake, biliary secretion and metabolism whereas inhibition of the single clearance pathways results in comparatively moderate AUC ratios. This concept was well reflected by our DDI predictions and is in good agreement with clinical DDI data. Nevertheless, it noteworthy to mention at this point that present analysis bases on transport and metabolism data determined in pools of human hepatocytes and liver microsomes from multiple donors (Camenisch and Umehara, 2012; Kunze et al., 2014a). Differences in protein expression levels due to genetic polymorphism were therefore not actively taken into consideration. As polymorphism for some variants ultimately translates into activity changes, it is evident, that such alterations might impact the ECCCS class categorization, hepatic clearance prediction and/or the DDI projections for some statins in our dataset. Susceptibility towards this effect was e.g. reported for

atorvastatin (144% greater mean AUC for the SLCO1B1 (OATP1B1) c.521CC genotype (Pasanen et al., 2007)), fluvastatin (up to 3-fold differences in mean AUC according to the number of CYP2C9*3 alleles (Kirchheiner et al., 2003), or rosuvastatin (AA haplotype individuals on ABCG2 (BCRP) c.421 exhibited 2.4-fold higher AUC compared with individuals carrying the control (CC) haplotype (Keskitalo et al., 2009)).
In summary, we have demonstrated the validity of the ECCCS as a bottom-up assessment for hepatic clearance and as a static model for DDI predictions purely from *in vitro* data. The ECCCS is therefore expected to be of great value for preclinical Drug Development, at a time when no human pharmacokinetic data are available. In addition, in combination with clinical (DDI) data applying a top-down approach, the ECCCS concept can be extremely helpful in identifying IVIVE disconnects and in revealing alternative elimination pathways. As such pathways are passively (by altering the individual fractional pathway contributions) and/or actively (by involvement of metabolism and/or transporter processes likewise being subject to interferences) contributing to the ultimate drug-drug interaction risk of victim drugs their quantitative integration into static or even dynamic (e.g.with help of the population-based simulator Simcyp®) pharmacokinetic models might be crucial for an appropriate assessment and final interpretation of clinical study results.

Acknowledgments

The authors wish to acknowledge the many Novartis Drug Metabolism and Pharmacokinetic scientists of Basel, Switzerland, who have supported this work. Special thanks go to Francis Heitz for technical assistance.

6.6 Supplementary Information

Literature references for reported *in vitro* data and calculations of pharmacokinetic parameters

In order to obtain intrinsic secretion clearances $CL_{int,sec,invitro}$ (provided in Table 6.1 of the manuscript), the measured apparent secretion clearances from sandwich-cultured hepatocyte incubations ($CL_{app,sec,invitro}$) were corrected for the unbound fraction of drug in hepatocytes ($f_{u,hep}$, Supplementary Table 6.3) as described previously [1]:

$$CL_{int,sec,invitro} = CL_{app,sec,invitro} / f_{u,hep} \tag{6.7}$$

with:

$$log(f_{u,hep}) = 0.9161 - 0.2567 \cdot logD_{7.4} \tag{6.8}$$

Similarly, the intrinsic metabolic clearances $CL_{int,met,invitro}$ were calculated from reported apparent metabolic clearances from liver microsomal incubations ($CL_{app,met,invitro}$) taking the unbound fraction of drug in microsomes ($f_{u,mic}$; Supplementary Table 6.3) into account [1]:

$$CL_{int,met,invitro} = CL_{app,met,invitro} / f_{u,mic} \tag{6.9}$$

Table 6.3: Physiochemical and pharmacokinetic parameters of statins.

compound	$logD_{7.4}$ (-)	$f_{u,hep}$ (-)	$f_{u,mic}$ (-)	$f_{u,p}$ (-)	R_b (-)	$CL_{app,met,invitro}$ ($\mu L \cdot min^{-1} mg_{prot}^{-1}$)	$CL_{app,sec,invitro}$ ($\mu L \cdot min^{-1} mg_{prot}^{-1}$)
lovastatin acid	1.51 [2][a)]	0.050	0.096 [3]	0.05 [2]	0.57 [4]	32.35 [2]	bld [m]
simvastatin acid	1.88 [2]	0.040	0.051 [3]	0.06 [2]	0.57 [4]	28.80 [2]	0.02 [m]
cerivastatin	1.90 [5]	0.039	0.689 [3]	0.01 [6]	0.60 [7]	23.70 [2]	bld [m]
fluvastatin	1.60 [8]	0.047	0.308 [9]	0.02 [6]	0.52 [7]	33.20 [2]	bld [m]
pitavastatin	1.50 [10]	0.050	0.432 [9]	0.04 [7]	0.58 [7]	5.60 [2]	bld [m]
atorvastatin	1.30 [5]	0.056	0.510 [1]	0.05 [1]	0.63 [-]	24.18 [1]	0.21 [1]
pravastatin	-0.40 [11]	0.154	0.880 [1]	0.52 [1]	0.54 [-]	0.60 [1]	0.11 [1]
rosuvastatin	-0.89 [10]	0.205	0.975 [3]	0.12 [9]	0.69 [9]	1.10 [12]	0.40 [m]

Notes: $f_{u,p}$ refers to the fraction of unbound drug in plasma, R_b denotes the blood-to-plasma partition coefficient. The literature references are shown in brackets. [-], calculated parameter, [m], parameter determined in this study. bld, below limit of detection.

[a)] the reported value refers to $logD_{7.0}$

Table 6.4: Literature references for the human pharmacokinetic properties of statins.

compound	$CL_{tot,obs,p}$ (mL/min/kg)	$CL_{tot,obs,oral,p}$ (mL/min/kg)	$CL_{h,obs,p}$ (mL/min/kg)	$CL_{r,obs,p}$ (mL/min/kg)	Ue (-)	F (-)
lovastatin acid	7.20 [13]	144.00 [-]	6.48 [-]	0.72 [-]	0.10 [2]	0.05 [2]
simvastatin acid	16.53 [-]	330.69 [14]	14.39 [-]	2.15 [-]	0.13 [6]	0.05 [6]
cerivastatin	2.04 [-]	3.04 [2]	2.04 [-]	0.00 [-]	0.00 [7]	0.60 [6]
fluvastatin	3.88 [-]	16.17 [15]	3.65 [-]	0.23 [-]	0.06 [15]	0.24 [6]
pitavastatin	2.02 [-]	3.97 [2]	2.02 [-]	0.00 [-]	0.00 [7]	0.51 [6]
atorvastatin	3.73 [-]	26.62 [-]	3.69 [1]	0.04 [-]	0.01 [16]	0.14 [16]
pravastatin	10.60 [-]	58.89 [-]	5.62 [1]	4.98 [-]	0.47 [16]	0.18 [16]
rosuvastatin	11.64 [17]	58.02 [-]	8.40 [-]	3.24 [17]	0.28 [-]	0.20 [2]

Notes: Clearance values were corrected for the average human body weight assuming 70 kg.
The literature references are shown in brackets. [-], calculated parameters.

Literature references for clinical data

Supplementary Table 6.4 provides the literature references for all described clinical pharmacokinetic parameters. All reported clearances in supplementary Table 6.4 represent plasma clearances. Hepatic clearances ($CL_{h,obs,p}$) were obtained from reported total body clearances after oral ($CL_{tot,obs,oral,p}$) or i.v. ($CL_{tot,obs,p}$) administration according to the following equations:

$$CL_{tot,obs,p} = CL_{tot,obs,oral,p} \cdot F \tag{6.10}$$

$$CL_{r,obs,p} = Ue \cdot CL_{tot,obs,p} \tag{6.11}$$

$$CL_{h,obs,p} = CL_{tot,obs,p} - CL_{r,obs,p} \tag{6.12}$$

$$\tag{6.13}$$

where F denotes the absolute oral bioavailability, $CL_{r,obs,p}$ refers to the renal organ clearance, and Ue refers to fraction of drug excreted unchanged in urine.

In the main manuscript all pharmacokinetic parameter are referring to blood, in order to compare with predicted hepatic blood clearances. Consequently, plasma-based parameters in Supplementary Table 6.4 were converted to the respective blood parameters by the following equation:

$$R_b = f_{u,p}/f_{u,b} = CL_p/CL_b = C_b/C_p \tag{6.14}$$

where R_b denotes the blood-to-plasma partition coefficient, $f_{u,p}$ and $f_{u,b}$ denote the fraction of drug unbound in plasma (p) and blood (b), respectively, CL_p and CL_b refer to clearance values and C_p and C_b to concentrations obtained in plasma and blood, respectively.

DDI predictions taking into account inhibition of renal secretion

The degree of change in AUC caused by drug-drug interaction following oral (p.o.) administration can be expressed as follows:

$$\frac{AUC_{po,i}}{AUC_{po}} = \frac{\frac{F_a \cdot F_{g,i} \cdot F_{h,i} \cdot D}{CL_{h,i}+CL_{r,i}}}{\frac{F_a \cdot F_g \cdot F_h \cdot D}{CL_h+CL_r}} \tag{6.15}$$

where F_a, F_g and F_h represent the fraction of drug absorbed, the fraction of drug escaping gut-wall metabolism and the fraction of drug escaping hepatic extraction. D represents the administered dose. The corresponding parameters in the presence of a perpetrator drug are denoted "i".

Assuming that: (i) the substrate is not metabolized and/or transported in the intestine (F_g = 1), and (ii) F_a does not change in the presence of inhibitor, the $AUC_{po,i}/AUC_{po}$ ratio can be described as follows:

$$\frac{AUC_{po,i}}{AUC_{po}} = \frac{F_{h,i} \cdot (CL_h + CL_r)}{F_h \cdot (CL_{h,i} + CL_{r,i})} \tag{6.16}$$

Equation 6.16 was be applied for the two statins in our dataset (pravastatin, rosuvastatin), which are subject to concomitant hepatic as well as renal process inhibition by CsA. The corresponding input parameters assuming 80% or 90% process inhibition on hepatic and renal clearance and DDI anticipations are summarized in Supplementary Table 6.5 and 6.6, respectively.

Table 6.5: Hepatic and renal elimination contributions in clinics in absence and presence of a 80% process inhibitor.

compound	$CL_{h,obs}$ (mL/min/kg)	F_h (-)	$CL_{r,obs}$ (mL/min/kg)	$CL_{h,i,pre}$ (mL/min/kg)	$F_{h,i}$ (-)	$CL_{r,i,pre}$ (mL/min/kg)	$AUC_{po,i}/AUC_{po}$ (-)
pravastatin	10.4 [1]	0.50 [-]	9.2 [-]	2.08 [-]	0.90 [-]	1.84 [-]	9.0
rosuvastatin	12.2 [17]	0.42 [-]	5.2 [7]	2.44 [-]	0.88 [-]	1.04 [-]	10.5

Notes: All clearance parameters represent human blood clearances. [-], calculated parameters.

Table 6.6: Hepatic and renal elimination contributions in clinics in absence and presence of a 90% process inhibitor.

compound	$CL_{h,obs}$ (mL/min/kg)	F_h (-)	$CL_{r,obs}$ (mL/min/kg)	$CL_{h,i,pre}$ (mL/min/kg)	$F_{h,i}$ (-)	$CL_{r,i,pre}$ (mL/min/kg)	$AUC_{po,i}/AUC_{po}$ (-)
pravastatin	10.4 [1]	0.50 [-]	9.2 [-]	1.04 [-]	0.95 [-]	0.92 [-]	19.0
rosuvastatin	12.2 [17]	0.42 [-]	5.2 [7]	1.22 [-]	0.94 [-]	0.52 [-]	22.4

Notes: All clearance parameters represent human blood clearances. [-], calculated parameters.

Supplementary References

1. Camenisch G and Umehara K 2012. Predicting human hepatic clearance from in vitro drug metabolism and transport data: a scientific and pharmaceutical perspective for assessing drug-drug interactions. Biopharm Drug Dispos. 33(3):179-94.
2. Shitara Y and Sugiyama Y 2006. Pharmacokinetic and pharmacodynamic alterations of 3-hydroxy-3-methylglutaryl coenzyme A (HMG-CoA) reductase inhibitors: drug-drug interactions and interindividual differences in transporter and metabolic enzyme functions. Pharmacol Ther. 112(1):71-105
3. Austin RP, Barton P, Cockroft SL, Wenlock MC, Riley RJ 2012. The influence of nonspecific microsomal binding on apparent intrinsic clearance, and its prediction from physiochemical properties. Drug Metab Dispos. 30(12):1497-503.
4. Gertz M, Harrison A, Houston JB, Galetin A 2010. Prediction of human intestinal first-pass metabolism of 25 CYP3A4 substrates from in vitro clearance and permeability data. Drug Metab Dispos. 38(7):1147-58.
5. Yabe Y, Galetin A, Houston JB 2011. Kinetic characterization of rat hepatic uptake of 16 actively transported drugs. Drug Metab Dispos. 39(10):1808-14.
6. Drugs@FDA database: www.accessdata.fda.gov/scripts/cder/drugsatfda/
7. Shitara Y, Maeda K, Ikejiri K, Yoshida K, Horie T, Sudiyama Y 2013. Clinical significance of organic anion transporting polypeptides (OATPs) in drug disposition: their roles in hepatic clearance and intestinal absorption. Biopharm Drug Dispos. 34(1):45-78.
8. Jones HM, Barton HA, Lai Y, Bi YA, Kimoto E, Kempshall S, Tate SC, El-Kattan A, Houston JB, Galetin A, Fenner KS 2012. Mechanistic pharmacokinetic modeling for the prediction of transporter-mediated disposition in humans from sandwich culture human hepatocyte data. Drug Metab Dispos. 40(5):1007-17.
9. Watanabe T, Kusuhara H, Maeda K, Kanamaru H, Saito Y, Hu Z, Sugiyama Y 2010. Investigation of the rate-determining process in the hepatic elimination of HMG-CoA reductase inhibitors in rats and humans. Drug Metab Dispos. 38(2):215-22.
10. Benet LZ, Broccatelli F, Oprea TI 2011. BDDCS applied to over 900 drugs. AAPS J. 13(4):519-47.
11. Umehara K and Camenisch G 2012. Novel in vitro- in vivo extrapolation (IVIVE) method to predict hepatic organ clearance in rat. Pharm Res. 29(2):603-17.
12. Fujino H, Saito T, Tsunenari Y, Kojima J, Sakaeda T 2004. Metabolic properties of the acid and lactone forms of HMG-CoA reductase inhibitors. Xenobiotica 34(11-12):961-71.
13. Obach RS, Lombardo F, Waters NJ 2008. Trend analysis of a database of intravenous pharmacokinetic parameters inhumans for 670 drug compounds. Drug Metab Dispos. 36(7):1385-405.
14. Lilja JJ, Kivistoe KT, Neuvonen PJ 2000. Duration of effect of grapefruit juice on the pharmacokinetics of the CYP3A4 substrate simvastatin. Clin Pharmacol Ther. 68(4):384-90.
15. Corsini A, Bellosta S, Baetta R, Fumagalli R, Paoletti R, Bernini F 1999. New insights into the pharmacodynamic and pharmacokinetic properties of statins. Pharmacol Ther. 84(3):413-28.
16. Kunze A, Huwyler J, Poller B, Gutmann H, Camenisch G 2014. In vitro- in vivo extrapolation method to predict human renal clearance of drugs. J Pharm Sci. 103(3):994-1001.
17. Martin PD, Warwick MJ, Dane AL, Brindley C, Short T 2003. Absolute oral bioavailability of rosuvastatin in healthy white adult male volunteers. Clin Ther. 25(10):2553-63.

Chapter 7

Interaction of the antiviral drug telaprevir with renal and hepatic drug transporters

Annett Kunze[a,b], Jörg Huwyler[b], Gian Camenisch[a], Heike Gutmann[a]

[a] Division of Drug Metabolism and Pharmacokinetics, Drug-Drug Interaction Section
Novartis Institutes for Biomedical Research, CH-4056 Basel, Switzerland

[b] Department of Pharmaceutical Sciences, Division of Pharmaceutical Technology
University of Basel, CH-4056 Basel, Switzerland

This work is published in:

Biochemical Pharmacology
2012 Oct 15;84(8): 1096-102
doi: 10.1016/j.bcp.2012.07.032.
Epub 2012 Aug 4.

7.1 Abstract

Telaprevir is a new, direct-acting antiviral drug that has been approved for the treatment of chronic hepatitis C viral infection. First data on drug-drug interactions with co-medications such as cyclosporine, tacrolimus, and atorvastatin have been reported recently. Drug transporting proteins have been shown to play an important role in clinically observed drug-drug interactions. The aim of this study was therefore to systematically investigate the potential of telaprevir to inhibit drug transporting proteins. The effect of telaprevir on substrate uptake mediated by drug transporters located in human kidney and liver was investigated on a functional level in HEK293 cell lines that over-express single transporter. Telaprevir was shown to exhibit significant inhibition of the human renal drug transporters OCT2 and MATE1 with IC_{50} values of 6.4 µM and 23.0 µM, respectively, whereas no inhibitory effect on OAT1 and OAT3 mediated transport by telaprevir was demonstrated. Liver drug transporters were inhibited with an IC_{50} of 2.2 µM for OATP1B1, 6.8 µM for OATP1B3, and 20.7 µM for OCT1. Our data show that telaprevir exhibited significant potential to inhibit human drug transporters. In view of the inhibitory potential of telaprevir, clinical co-administration of telaprevir together with drugs that are substrates of renal and hepatic transporters should be carefully monitored.

7.2 Introduction

Hepatitis C (HVC) is a major burden to public health in industrialized as well as developing countries. The prevalence of HCV infection is estimated to 2-3% worldwide, affecting 130-170 million people (Lavanchy, 2009; Shepard et al., 2005). In 2011 a new class of compounds, direct acting-antiviral agents (DAA), such as telaprevir were approved by the FDA. Triple therapy with these new protease inhibitors in combination with pegylated inteferon (peg-IFN) and ribavirin has significantly increased the sustained virologic response (SVR) rates in patients with HCV genotype 1. Combining peg-IFN with ribavirin increased the SVR by about 50%, whereas triple therapy resulted in an increase in SVR about 70% (Asselah and Marcellin, 2011). This combination therapy is therefore a promising new tool to treat chronic hepatitis C infections and is expected to lead to increased usage in the future.

Patients treated with these new DDA are often co-medicated with several other drugs. The potential for drug-drug interactions (DDI) due to these compounds should therefore be carefully investigated. DDIs with telaprevir and co-medications such as cyclosporine, tacrolimus, and atorvastatin were recently reported, demonstrating significant increases in blood concentrations of the co-administered drugs (Garg et al., 2011; Lee et al., 2011). Co-administration with steady-state telaprevir increased dose-normalized cyclosporine

exposure by 4.6-fold and tacrolimus 70-fold. In an open-label clinical study with 21 healthy volunteers, co-administration of telaprevir increased the C_{max} of atorvastatin 10.6-fold and its AUC 7.88-fold.

Cyclosporine, tacrolimus, and atorvastatin were reported to be substrates of P-glycoprotein (P-gp). Furthermore, atorvastatin is known to be a substrate of breast cancer resistance protein (BCRP), of the organic anion transporting polypeptide 1 (OATP1B1), and of the organic anion transporting polypeptide 2B1 (OATP2B1) (Fricker et al., 1996; Grube et al., 2006; Keskitalo et al., 2009; Lau et al., 2006; Wu et al., 2000). The fact that DDI led to changes in the pharmacokinetics of co-medications with telaprevir was attributed mainly to cytochrome P450 enzymes (Kiser et al., 2012). However, besides metabolic enzymes, interactions with drug transporters should not be neglected and can also play an important role.

Drug transporters expressed in the kidney mediate the cellular transport of endogenous and exogenous organic anions and cations. Tubular section of many organic cations is mediated by uptake across the basolateral membrane by organic cation transporter 2 (OCT2) and by efflux across the apical membrane by multidrug and toxin extrusion transporters (MATE) (Nakamura et al., 2010). Human organic anion transporter 1 (OAT1) and human organic anion transporter 3 (OAT3) have been localized at the basolateral membrane of renal proximal tubule cells, where they mediate the cellular uptake of a number of drugs such as thiazides, cephalosporin antibiotics, and loop diuretics as well as toxic compounds (Nigam et al., 2007; Ueo et al., 2005). OAT1, OAT3, OCT2, and MATE1 are expressed predominantly in the kidney. Organic anion transporting polypeptides (OATPs) such as OATP1B1 and OATP1B3 are liver-specific drug transporters selectively expressed at the basolateral membrane of hepatocytes, where they mediate the cellular uptake of several drugs, including statins (Hagenbuch and Meier, 2004; König et al., 2006; Matsushima et al., 2008). Expressed at the basolateral membrane as well, the organic cation transporter 1 (OCT1) has been shown to transport HIV drugs and anti-diabetic drugs (Jung et al., 2008; Shu et al., 2008).

Telaprevir is reported to be a substrate and inhibitor of P-gp (Vertex, 2011). To date, no information is available on potential interactions of telaprevir with other drug transporters located in kidney or liver. It was therefore the aim of the present study to test *in vitro* the inhibitory effect of telaprevir on drug transporters and quantify the specific impact on each transporter by determining corresponding IC_{50} values. In particular, using cell lines transfected with single transporters of the solute carrier (SLC) family, the effect of telaprevir on cellular uptake of substrates of OCTs, MATE1, OATs, and OATPs was systematically investigated.

7.3 Materials and methods

Materials

[^{3}H]aminohippuric acid (PAH; 4.53 Ci/mmol), [^{3}H]estradiol 17β-D-glucuronide (34.3 Ci/mmol) were acquired from PerkinElmer (Waltham, MA).[^{3}H]atorvastatin calcium (10 Ci/mmol), [^{3}H]N-methyl-4-phenyl pyridinium iodide (MPP$^+$; 85 Ci/mmol), and [^{14}C]metformin HCl were purchased from American Radiolabeled Chemicals, Inc. (Saint Louis, MO). Metforfmin HCl, estradiol 17β-D-glucuronide sodium salt, 1,1'-diethyl-2,2'-cyanine iodide (decynium), probenecid, phenoxybenzamine hydrochloride, MPP$^+$ iodide, PAH, dimethyl sulfoxide (DMSO), formic acid, and acetonitirle were purchased from Sigma-Aldrich (Saint Louis, MO). Atorvastatin calcium was obtained from AKScientific (Union City, CA) and telaprevir (VX 950) was purchased from APIchem Chemical Technology Co. (Shanghai, China). Irgarsafe Plus liquid scintillator was purchased from Zinsser Analytic (Frankfurt, Germany). Trypsin-EDTA (0.05%), DMEM, GlutaMAX^{TM}, Dulbecco's phosphate-buffered saline (PBS), fetal bovine serum (FBS), geneticin (50 mg/mL), Hank's balanced salt solution (HBSS), and hygromycin B (50 mg/mL) were obtained from Invitrogen by Life Technologies (Paisly, UK). Penicilin/streptomycin (10,000 IU/mL Str) was acquired from BioConcept (Allschwil, Switzerland). All unlabeled solid compounds were dissolved in DMSO.

Mass spectrometry

According to the certificate of analysis provided by the manufacturer, telaprevir used for the present study had a purity of 99.2% as determined by HPLC-analysis. In addition, identity of telaprevir (10 µg/mL) used as a freshly prepared stock solution in 0.1% (v/v) formic acid in acetonitrile, was confirmed by mass spectrometry. Mass spectra were recorded by direct infusion at a rate of 10 µL/min (infusion pump 11, Harvard Apparatus, MA) into an API 365 triple-quadrupole mass spectrometer (PE Biosystems, Foster City, CA) equipped with a turbo ion spray interface, operated in positive or negative ionization mode (Duthaler et al., 2011). The analyte was detected by either single-quadrupole mode or selected reaction monitoring (SRM). Instrumentation control and data analysis were performed with Analyst 1.4.2. software (PE Biosystems). Results were in accordance with published data (Farnik et al., 2009): Positive mode, protonated molecular [M+H]$^+$ ions at *m/z* 680; negative mode, deprotonated [M-H]$^-$ at 678; mass transition (collision energy of 15eV) *m/z* 680 $\geq$ 322. The mass spectrometer was operated in unit resolution mode with a precision of $\pm$ 0.1 mass units.

Cell culture

Recombinant HEK293 cell lines with stable expression of human OATP1B1, OCT1, OCT2, OAT1, OAT3, or MATE1 were generated by using the Flp-In^{TM} system according tho the manufacturer's recommendations (Invitrogen by Life Technologies, Paisley, UK). Briefly, HEK293 Flp-In cells were transfected with human OATP1B1, OCT1, OCT2, OAT1, OAT3, or MATE1 cDNAs subcloned into pFRTV5-Dest plasmid vector and pOG44 or with the respective vector alone using FuGene according to the manufacturer's recommendations (Roche, Basel, Switzerland). Transporter-expressing clones were obtained following hygromycin B selection. Selective transporter function was determined and an evaluation of stable transporter-expressing cell lines was carried out according to published data (Abe et al., 1999; Cha et al., 2001; Chen et al., 2005; Gorboulev et al., 1997; Ho et al., 2000; Koepsell et al., 2007; König et al., 2000; Liang et al., 1995; Takeda et al., 2001; Tamai et al., 2001; Tanihara et al., 2007; Vavricka et al., 2002). Recombinant HEK293 cells expressing human OATP1B3 were purchased from DKFZ (Deutsches Krebsforschungszentrum, Heidelberg, Germany). HEK293 stably transfected with OATP1B1, OCT1, OCT2, OAT1, OAT3, or MATE1 were grown and maintained in DMEM supplemented with 10% FBS, 1% L-glutamine and 1% penicillin/streptomycin, and 100 ng/µL hygromycin B at 37°C with 5% CO_2. HEK293 cells stably transfected with OATP1B3 were grown and maintained in DMEM supplemented with 10% FBS, 1% L-glutamine and 1% penicilline/streptomycin and 800 ng/µL geneticin.

Cytotoxicity assay

The cytotoxicity of telaprevir was assessed by the *in vitro* toxicology assay kit, sulforhodamin B based (Sigma-Aldrich, Saint Louis, MO) as described previously by Skehan et al. (1990). The assay was performed under the same conditions as the incubation studies, with telaprevir at its highest concentration of 200 µM and an incubation time of 5 min.

Transporter inhibition assays

The transporter expressing HEK293 cells were seeded on BD poly-D-lysine 96-well microplates with a density of approximately $0.2 \cdot 10^6$ cells per well in DMEM supplemented with 10% FBS. OATP1B1 and OATP1B3 uptake studies were performed 72 h after seeding, whereas all other uptake studies were performed after 24 h. On the day of the study, the cultivation medium was replaced by the final incubation solution (buffer containing a probe substrate and telaprevir or a positive control inhibitor). Transporter substrates were [^{3}H]estradiol 17β-D-glucuronide (1 µM) for OATP1B1 and OATP1B3, [^{3}H]MPP$^+$

(0.0025 µM) for OCT1 and OCT2, [^{3}H]PAH (1µM) for OAT1, [^{3}H]estrone sulfate (1 µM) for OAT3, and [^{14}C]metformin (1 µM) for MATE1 uptake studies. Positive control inhibitors were a combination of atorvastatin and rifamycin (20 µM and 10 µM) for OATP1B1 and OATP1B3, decynium (10 µM) for OCT1, probenecid (100 µM) for OAT1 and OAT3, phenoxybenzamine (50 µM) for OCT2, and pyrimethamine (10 µM) for MATE1 uptake studies. For concentration-dependent inhibition studies, telaprevir was used in the following concentrations: 0.2 µM, 0.4 µM, 0.6 µM, 0.8µM, 1 µM, 2 µM, 4 µM, 6 µM, 8µM, 10 µM, 20 µM, 40 µM, 60 µM, 80 µM, 100 µM, 125 µM, 150 µM, 175 µM, and 200 µM. Organic solvent (DMSO) concentrations were limited to 1% of the total incubation volume (V/V). Uptake experiments were performed in HBSS supplemented with 12.5 mM HEPES (pH 7.4) for OAT1, OAT3, OCT1, and OCT2, or in HBSS supplemented with 12.5 mM HEPES (pH 7.0) for OATP1B1 and OATP1B3. MATE1 uptake was performed as described by Tanihara et al. (2007). For each incubation 200 µL of incubation solution were added per sample. Incubation times were 3 min (OATP1B1, OCT1, and OCT2) or 5 min (OATP1B3, OAT1, OAT2, and MATE1). After removal of the incubation solution, cells were washed twice with ice-cold PBS buffer and lysed in NaOH solution (0.2 N). Quantitation of radio-labeled test compounds was performed by scintillation counting. Radioactivity was determined in 5 mL Irgarsafe plus scintillation cocktail using Packard Tri-Carb 2700TR liquid scintillation counter. The protein contents of the solubilized cells were determined using the Bio-Rad Protein Assay kit (Bio-Rad Laboratories AG, Hercules, CA) according to the manufacturer's recommendations.

Data analysis

Cellular substrate uptake (pmol/min/mg protein) was given as the amount of radioactivity associated with the cells (dpm) divided by its concentration (dpm/pmol substrate) in the incubation medium and normalized to the incubation time (min) and the amount of protein (mg protein) inside the wells. Uptake data were converted into relative inhibition values given as % of control according to Eq.7.1:

$$\%\ of\ control = 100\% \frac{Uptake_{0\%} - Uptake_X}{Uptake_{0\%} - Uptake_{100\%}} \tag{7.1}$$

$Uptake_{0\%}$ refers to the cellular substrate uptake in the absence of an inhibitor or test compound, $Uptake_{100\%}$ states the substrate uptake in the presence of the positive control inhibitor, and $Uptake_X$ refers to substrate uptake in the presence of the test compound.
The IC_{50} values (inhibitor concentration causing 50% inhibition of the maximal drug effect) were calculated using sigmoidal Hill kinetics according to Eq. 7.2.

$$\%\ of\ control = \frac{\%_{max} \cdot I^n}{IC_{50}^n + I^n} \tag{7.2}$$

where n states the slope factor (Hill coefficient), I refers to the inhibitor concentration (μM), and $\%_{\max}$ is the maximal transporter inhibition. Eq.7.2 was fitted to the data to obtain estimates of the IC_{50} and $\%_{\max}$.

Statistics

Uptake experiments were performed in triplicate, where values are given as the mean of these replicates with error bars representing the standard deviation (SD). Statistical significance was calculated by unpaired Student's *t*-test. Differences were considered statistically significant when p was < 0.05. Parameter estimations were performed by data fitting with non linear least square method using SigmaPlot2008. The coefficients of determination, R^2, were calculated for each fit. Figures were created using MatlabR2009.

7.4 Results

All results presented in the following section were performed with telaprevir of high purity (99.2%). Identity of telaprevir was confirmed by mass spectroscopy according to Farnik et al. (2009). Direct infusion of the analyte confirmed the molecular mass and fragmentation pattern of telaprevir.
To rule out non-specific toxicity as the cause of observed inhibitory effects, we investigated whether telaprevir exhibited a cytotoxic potential at the concentrations used in this study. No cytotoxicity was observed in HEK293 cells over-expressing single drug transporters up to the highest concentration investigated (200 μM) (data not shown).

Inhibition of the renal transporters OAT1, OAT3, OCT2, and MATE1 by telaprevir

Cellular uptake of known renal transporter substrates was compared in the presence and absence of telaprevir. Functional expression of recombinant transporters was examined using transporter substrates in the presence and absence of specific inhibitors. The results were compared to incubations with telaprevir. As shown in Figure 7.1a, the uptake of 0.025 μM MPP^+ in OCT2 expressing cells was significantly reduced from 1.2 ± 0.1 pmol/min/mg protein to 0.6 ± 0.1 pmol/min/mg protein in the presence of 200 μM telaprevir. Co-application

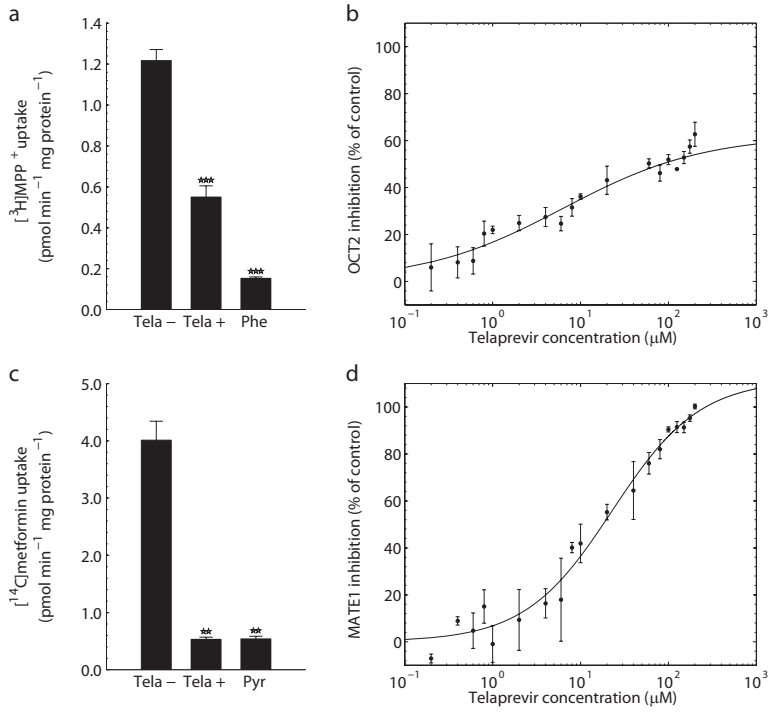

Figure 7.1: Inhibition of renal solute carriers by telaprevir. Inhibitory effect of telaprevir on the uptake of 0.025 μM [^{3}H]MPP$^+$ in OCT2 **(a,b)** and 1 μM [^{14}C]metformin in MATE1 **(c,d)** over-expressing HEK293 cells. Substrate uptake is shown in the absence (Tela-) and presence of 200 μM telaprevir (Tela+) or the reference inhibitors phenoxybenzamine (Phe; 50 μM) or pyrimethamine (Pyr; 10 μM), respectively **(a,c)**. Concentration-dependent inhibition of substrate uptake normalized to transporter inhibition by the reference inhibitors **(b,d)**. Shown are the average values of three independent incubations with the error bars representing the sample standard deviation. The stars indicate the significance level of the inhibitory effect derived from *t*-test comparing Tela+ as well as positive control against Tela- incubations(**$p < 0.01$, ***$p < 0.001$). The coefficient of determination, R^2, was calculated for each fit ($R^2 = 0.96$ (b), $R^2 = 0.98$ (d)).

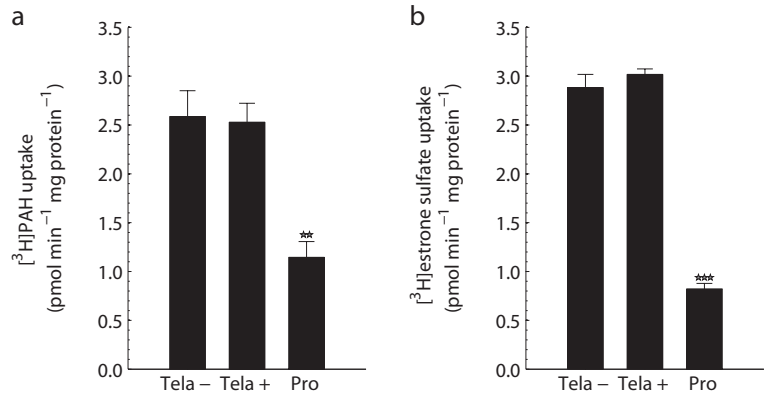

Figure 7.2: Interaction of telaprevir with renal organic anion transporters. Effect of telaprevir on the uptake of 1 µM [^{3}H]PAH in OAT1 **(a)** and 1 µM [^{3}H]estrone sulfate in OAT3 **(b)** over-expressing HEK293 cells. Substrate uptake is shown in the absence (Tela-) and presence of 60 µM telaprevir (Tela+) or 100 µM probenecid (Pro), respectively. Shown are the average values of three independent incubations with error bars representing the sample standard deviation.The stars indicate the significance level of the inhibitory effect derived from *t*-test comparing Tela+ as well as positive control against Tela- incubations(**p < 0.01, ***p < 0.001).

of 50 µM phenoxybenzamine (positive control) resulted in a reduction of substrate uptake to 0.2 ± 0.0 pmol/min/mg protein. Moreover, the uptake of 1 µM metformin was significantly reduced from 4.0 ± 0.3 pmol/min/mg protein to 0.5 ± 0.0 pmol/min/mg protein in MATE1 expressing cells (Fig. 7.1b). The inhibitory effect observed was in a similar range as the transporter inhibition caused by co-incubation with 10 µM pyrimethamine (0.5 ± 0.1 pmol/min/mg protein; positive control). In a subsequent step, the IC_{50} values were determined by co-application of the specific transporter substrate with increasing concentrations of telaprevir. As shown in Figure 7.1b and d telaprevir inhibited the uptake of reference substrates in a concentration-dependent manner with resulting IC_{50} values of 6.4 ± 3.5 µM and 23.0 ± 6.7 µM for OCT2 and MATE1, respectively. As shown in 7.2, no inhibitory effect on the uptake of 1 µM PAH and 1 µM estrone sulfate in OAT1 and OAT3 expressing cells was demonstrated in the presence of 60 µM telaprevir, whereas 100 µM of probenecid (positive control) significantly reduced the substrate uptake. Determined IC_{50} values as well as the maximal transporter inhibition ($\%_{max}$) are summarized in Table 7.1.

Inhibition of the hepatic transporters OATP1B1, OATP1B3, and OCT1 by telaprevir

Inhibitory effects of telaprevir on substrate uptake in cells expressing the hepatic uptake transporters OATP1B1, OATP1B3, and OCT1 are shown in Fig. 7.3. The uptake of 1 µM estradiol 17β-D-glucuronide, a typical substrate for OATPs (König et al., 2000; Tamai et al., 2001), in OATP1B1 and OATP1B3 expressing cells was significantly reduced from 4.8 ± 0.1 pmol/min/mg protein for OATP1B1 (FIg. 7.3a) and

1.0 ± 0.1 pmol/min/mg protein for OATP1B3 (Fig. 7.3c) to 0.4 ± 0.1 pmol/min/mg protein and 0.3 ± 0.0 pmol/min/mg protein, for OATP1B1 and OATP1B3, respectively. Moreover, inhibitory effects were comparable to inhibition by a combination of atorvastatin (20 µM) and rifamycin (10 µM), resulting in a reduction of estradiol 17β-D-glucuronide uptake to 0.5 ± 0.0 pmol/min/mg protein and 0.4 ± 0.1 pmol/min/mg protein for OATP1B1 and OATP1B3, respectively. Co-administration of estradiol 17β-D-glucuronide and telaprevir demonstrated a concentration-dependent inhibition, with resulting IC_{50} values of 2.2 ± 0.1 µM and 6.8 ± 0.9 µM for OATP1B1 and OATP1B3 (Fig.7.3b and d). Furthermore, the uptake of the OCT1 substrate MPP^+ (0.025 µM) was significantly reduced in the presence of 200 µM telaprevir from 1.3 ± 0.0 pmol/min/mg protein to 0.5 ± 0.0 pmol/min/mg protein. This effect was comparable to the inhibition of MPP^+ uptake in the presence of the reference inhibitor decynium (10 µM; 0.4 ± 0.0 pmol/min/mg protein) as shown in Figure 7.3e. Telaprevir inhibited MPP^+ uptake in OCT1 expressing cells in a concentration-dependent manner with an IC_{50} of 20.7 ± 7.7 µM (Fig. 7.3f). IC_{50} values as well as the maximal transporter inhibition ($\%_{max}$) compared to positive control are summarized in Table 7.1.

7.5 Discussion

Telaprevir was recently registered; therefore, data on clinically observed drug-drug interactions of telaprevir with metabolizing enzymes and transporters are still sparse. However, first clinical data have been published by Lee and Garg, indicating that telaprevir exhibits the potential to change the pharmacokinetics of co-administered drugs such as atorvastatin, amlodipine, cyclosporine, and tacrolimus (Lee et al., 2011). Telaprevir has a molecular formula of $C_{36}H_{53}N_7O_6$ with a molecular weight of 679.85 (Vertex, 2011). Telaprevir is optically active and possesses six chiral centers. It exhibits an acidic pKa of 11.8 and a basic pKa at 0.31 with 13 H bond acceptors and 4 H bond donors. Its physiochemical

Table 7.1: IC_{50} and maximal inhibition ($\%_{max}$) of telaprevir for different drug transporters.

localization	transporter	IC_{50}			$\%_{max}$		
		value (µM)	SD (µM)	*P*	value (%)	SD (%)	*P*
Kidney	OCT2	6.35	3.45	0.0856	62.29	6.91	<0.001
Kidney	MATE1	22.98	6.72	0.0033	111.76	9.95	<0.001
Liver	OATP1B1	2.15	0.13	<0.001	100.90	2.31	<0.001
Liver	OATP1B3	6.77	0.87	<0.001	105.39	3.88	<0.001
Liver	OCT1	20.67	7.74	< 0.0175	98.59	10.68	<0.001

Note: No inhibition of OAT1 and OAT3. Model parameter were estimated from nonlinear least square fit to the data, consisting of 17-19 datapoints with each datapoint corresponding to the mean value of three independent incubatins. Coefficient of determination, R^2, was > 0.96 for all fits. The *p*-values were calculated under asymptotic normality of the least squares fit estimates from *t*-test against the null hypothesis that the corresponding coefficient is equal to zero.

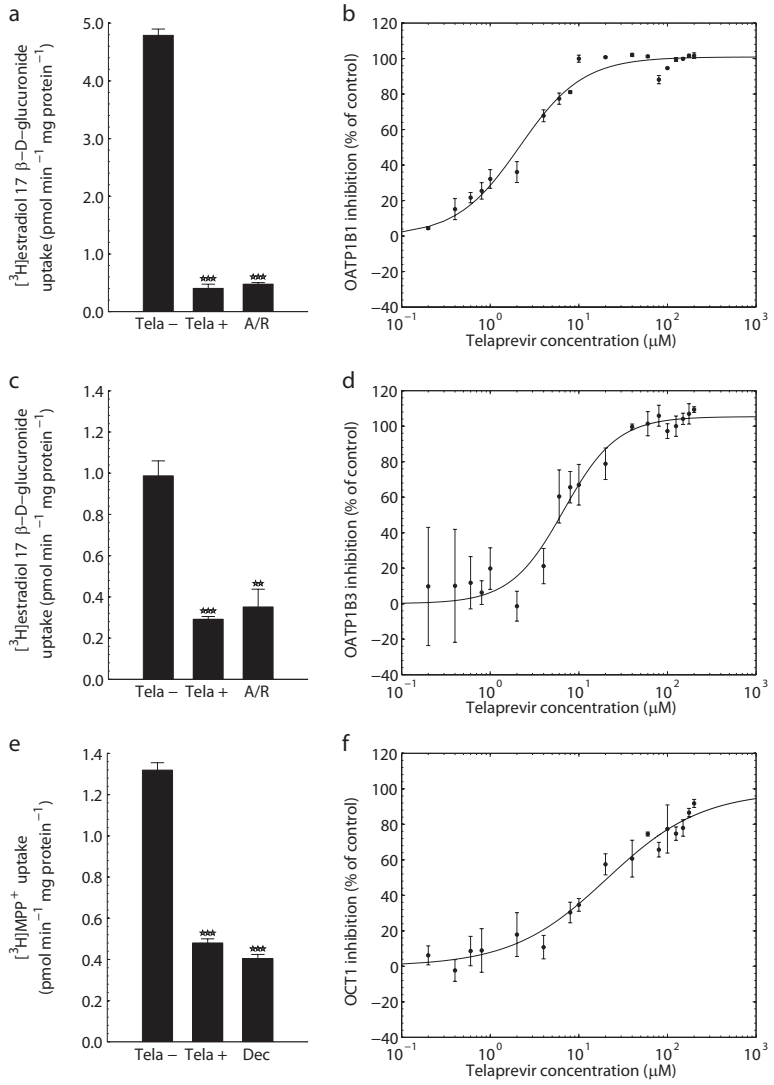

Figure 7.3: Inhibition of hepatic solute carriers by telaprevir. Inhibitory effect of telaprevir on the uptake of 1 μM [^{3}H]estradiol 17β-D-glucuronide (a-d) in OATP1B1 **(a,b)** and OATP1B3 **(c,d)** over-expressing cells, and 0.025 μM [^{3}H]MPP$^+$ in OCT1 **(e,f)** over-expressing HEK293 cells. Substrate uptake is shown in the absence (Tela-) and presence of 200 μM telaprevir (Tela+) or the reference inhibitors 20 μM atorvastatin co-applied with 10 μM rifamycin (A/R) or 10 μM decynium (Dec), respectively **(a,c,e)**. Concentration-dependent inhibition of substrate uptake normalized to transporter inhibition by the reference inhibitors **(b,d,f)**. Shown are the average values of three independent incubation with error bars representing the sample standard deviation.The stars indicate the significance level of the inhibitory effect derived from *t*-test comparing Tela+ as well as positive control against Tela- incubations(**p < 0.01, ***p < 0.001). The coefficient of determination, R^2, was calculated for each fit (R^2 = 0.98 (b), R^2 = 0.97 (d), R^2 = 0.98 (e)).

properties indicate that its charge is neutral at pH 7.4 (EMBL, 2012). Telaprevir has been described as a substrate as well as an inhibitor of CYP3A4 and P-gp (Vertex, 2011). To our knowledge, the interaction of telaprevir with drug transporters besides P-gp has not yet been investigated. In this study, the inhibitory potential of telaprevir on drug transporters located in kidney and liver was therefore characterized.

We examined the inhibitory effect of telaprevir on the transport of substrates of renal drug transporters OCT2, MATE1, OAT1, and OAT3. In the kidney, renal tubular secretion of several drugs such as cimetidine, metformin, and acyclovir is mediated by uptake through OCT2 into proximal tubular cells and subsequent excretion through MATEs (Nies et al., 2009). The IC_{50} value of telaprevir with respect to inhibition of renal solute carriers (OCT2 and MATE1) is in the µ- molar range. Because telaprevir concentrations in plasma have been described as 5.5 µM at steady state with a free concentration of 2.1 µM, there is a significant potential for telaprevir to inhibit transport of co-medications transported by OCT2 (Vertex, 2011). Clinical data on the effect of telaprevir on co-medications transported by OCT2 are currently not available, but it might be useful to monitor the effect of telaprevir on drugs excreted by OCT2 in clinical studies in the future.

Information on drug-drug interactions involving MATEs is currently sparse. First data suggest that clinically observed inhibition of tubular metformin secretion is not only caused by inhibition of OCT2-mediated tubular uptake, but also by inhibition of MATE1-mediated luminal secretion (Tsuda et al., 2009). However, telaprevir is extensively metabolized in the liver and after oral administration only 1% of the administered radioactive dose has been found in urine (Vertex, 2011). It can therefore be assumed that active excretion of unchanged telaprevir leading to high concentrations inside renal proximal tubular cells is unlikely. Inhibition of transporters located at the apical membrane, such as MATE1, can be predicted to be of minor clinical relevance.

The inhibitory effect of telaprevir on OAT1 and OAT3 seems to be negligible. Telaprevir exhibited no interaction with substrates transported by these transporters. Therefore, the likelihood of clinical DDI due to inhibition of renal OAT mediated drug transport is expected to be low.

Lee et al. conducted a clinical study in healthy volunteers in which they examined the effect of telaprevir on atorvastatin and amlodipine pharmacokinetics (Lee et al., 2011). The mean maximal concentration (C_{max}) and the area under the curve (AUC) of amlodipine were increased 1.3-fold and 2.8-fold, respectively, by co-administration of telaprevir. Telapreivr also exhibited a pronounced effect on atorvastatin pharmacokinetics, leading to an increase in C_{max} and AUC of 10.6-fold and 7.9-fold, respectively. The author attributed the observed effects mainly to CYP3A4 inhibition, because amlodipine and atorvastatin are substrates of this enzyme and telaprevir has been shown previously to be a susbtrate as well as an inhibitor of CYP3A4. However, they also speculated that telaprevir might exhibit an inhibitory effect on OATP1B1- mediated atorvastatin uptake. Our data showed a significant reduction of OATP1B1 and OATP1B3-mediated transport by co-administration of telaprevir, which exhibited an IC_{50} of approximately 2 µM for OATP1B1 and 7 µM for

OATP1B3. Thus, our data confirmed the assumption by Lee et al., that telaprevir is an inhibitor of OATP1B1.

In humans, telaprevir reaches a C_{max} at steady state of 5.2 µM with a free concentration of 2.1 µM when given as a 750 mg dose three times a day, indicating that *in vivo* inhibition of OATP1B1 and OATP1B3 is likely (Vertex, 2011). Hirano et al. introduced calculation of *R*-values, which represent the ratio of the uptake clearance in the absence of the inhibitor to that in its presence (Hirano et al., 2006). According to the FDA guideline on drug-drug interactions, *R*-values for OATPs should be estimated by using the total plasma concentrations C_{max} ($R = 1 + C_{max}/IC_{50}$)(FDA, 2012). Using this guideline, *R*-values can be estimated 3.75 for OATP1B3 and 1.75 for OATP1B3. Since the maximal concentration at the inlet of the liver is generally higher than in plasma, *R*-values calculated for concentrations at the inlet of the liver are expected to be even higher (Huang et al., 2010). To our knowledge, amlodipine has not been described as a substrate for OATPs, whereas atorvastatin is transported by OATP1B1 (Kameyama et al., 2005). The observed inhibition of OATP1B1 and OATP1B3 by telaprevir might explain the finding that telaprevir exhibited a greater effect on the C_{max} of atorvastatin compared to amlodipine (10.6-fold compared to 1.3-fold). This is in line with predictions by Camenisch et al. that inhibition of CYP3A4 alone leads to a maximal increase in the atorvastatin AUC of 3.6-fold, whereas additional inhibition of transporter increases the atorvastatin AUC in the range of 5- to -fold 28 (Camenisch and Umehara, 2012). Furthermore, we showed that telaprevir inhibited OCT1, with an IC_{50} of approximately 20.7 µM. Assuming a total concentration of 5.2 µM and a free concentration of 2.1 µM after oral administration of clinical relevant doses, the likelihood of an *in vivo* interaction of telaprevir with substrates of OCT1 such as metformin or HIV drugs cannot be ruled out entirely (Shu et al., 2008). Boceprevir a second member of the class of direct acting-antiviral agents has been described to increase kinetics of single dose pravastatin and has been found to inhibit OATP1B1 with an IC_{50} of 18 µM (Chu, 2011; Hilskotte et al., 2011). Comparison of telaprevir with other protease inhibitors used in HIV therapy such as ritonavir, saquinavir, lopinavir, inidnavir, and nelfinavir indicate that this class of compounds has besides its inhibitory potential on P-gp and BCRP also the potential to inhibit effectively transporters of the OATP family (Griffin et al., 2011; Gutmann et al., 1999). Ritonavir, saquinavir, lopinavir, and indinavir have been shown to effectively inhibit OATP1B1 and OATP1B3 with IC_{50}s in the range of 0.5-12.3 µM (Annaert et al., 2010). Pham et al. reported clinical data showing an increase in atorvastatin and rosuvastatin AUCs by co-administration of ritonavir and tipranivir which they attributed to inhibition of OATP1B1 (Pham et al., 2009). Additionally, some HIV protease inhibitors such as saquiniavir, indinavir, and nelifinavir have been found to inhibit transporters of the organic cation transporter family (Jung et al., 2008). Taken together, these data indicate that telaprevir exhibits a similar pattern for drug transporter inhibition as other protease inhibitors used in HIV therapy.

In conclusion, we demonstrated that telaprevir exhibited a potent inhibitory effect on drug transporters of the SLC family. In order to characterize these interactions it would be

of value to examine if telaprevir is also a substrate of these transporters. Up to date, no data about the intracellular uptake of telaprevir by drug transporters are available. Our data indicated that combinations of telaprevir with substrates of drug transporters such as OCT2, OATP1B1, and OATP1B3 should be carefully monitored. Further studies will be needed to extrapolate from our *in vitro* experiments to the *in vivo* situation in humans and to confirm potential drug interactions.

Acknowledgments

We thank Dr. Birk Poller for reviewing the manuscript and Mark Inglin for editorial assistance.

Chapter 8

Conclusion and Outlook

Within the scope of this work, *in vitro* based permeation studies were used to determine drug clearances and drug-drug interaction potentials in human. In chapter 4 we introduced a novel IVIVE method that allows the prediction of the human renal clearance based on filtration, secretion and reabsorption. We showed that our method can be applied to investigate the mechanism driving the human renal clearance and to assess the contribution of each process to the net renal excretion. In chapter 5 we predicted the quantitative OATP1B1,- and OATP1B3-mediated uptake of statins in hepatocytes, based on relative transporter expression (REF) and relative transporter activity (RAF) data. Our results demonstrated a direct relationship between transporter expression and activity. By that we showed that REF-scaling can be applied to extrapolate transporter activities determined in transporter-transfected cell lines into hepatocyte values. In chapter 6 we applied the mechanistic extended clearance concept to predict the drug-drug interaction potential of statins based on *in vitro* studies. On one hand, we confirmed the applicability of the mechanistic clearance concept to predict the human hepatic clearance based on IVIVE and on the other hand we showed that the ECCCS provides a powerful tool to anticipate the DDI potential of statins. Finally, in chapter 7, we assessed the inhibitory potential of telaprevir, a new marketed antiviral agent, on major drug transporters of the SLC family. We showed that telaprevir significantly inhibited the uptake of transporter-specific reference compounds of major renal and hepatic drug transporters. In the following the significance of each study is illustrated in the context of drug development.

Renal clearance prediction

Renal clearance is recognized as major elimination pathway of drugs from the body. Therefore, the assessment of the contribution of the net renal clearance to the total body clearance is of interest in preclinical drug development. However, to date *in vitro*-based methods that would allow the early assessment of human renal drug clearances are lacking. Reported methods either require a multitude of *in vitro* input parameters, or are restricted to compounds that do not undergo reabsorption. In contrast, our novel method allows the prediction of the renal clearance of basic and neutral NMEs simply by measuring

the bidirectional drug transport in LLC-PK_1 cells. Furthermore, the use of a cell line as underlying *in vitro* system accounts for a broad application of our model since it is not restricted to the availability of primary cells. However, the ideal *in vitro* system would be a human cell line that is feasible for drug transmembrane transport studies and that contains a functional organic anion and cation transport system. Currently lacking, in the future such a cell line might become available and thus our model could be improved to predict the net renal clearance for any NME, including anionic compounds.
Besides the prediction of the net human renal clearance our model was shown to allow insights into the mechanisms driving renal drug excretion. By that, we demonstrated that the contribution of filtration, secretion, and reabsorption to the net renal clearance correlated with the compounds assignments to the BDDCS. Consequently, estimates about the involvement of these processes to the net renal elimination of drugs can be made if their BDDCS assignments are known.
Furthermore, since our novel IVIVE method allows a mechanistic assessment of the underlying renal clearance pathways, the impact of pathway inhibition on the net renal clearance can be investigated. Thus, our model can provide a valuable *in vitro* tool to assess the renal DDI potential of NMEs in preclinical drug development.

Transporter expression- activity relationship

First investigations on the quantitative relationship between transporter expression and activity were performed with the help of western blot analysis. However, this approach is limited to the availability of transporter-specific antibodies. More recently, QTAP methods have been demonstrated to be a valuable tool to determine absolute transporter abundances in tissue and cell samples. First attempts have been made to use transporter protein expression levels determined by QTAP to predict the transporter activities. However, to date the validation of QTAP-based REF-scaling with an independent method such as RAF-scaling was still lacking. Our study is therefore expected to provide a proof of concept for the application of REF-based scaling. Thus, we anticipate that REF-scaling is likely applicable to extrapolate transporter activities from recombinant cell systems to any tissue, given the respective protein abundance data were known. REF-based scaling would therefore enable the characterization of active drug transport even in tissues for which currently no *in vitro* systems are available.
We further demonstrated that REF-scaling can be used to assess the absolute contribution of the OATP1B1 and OATP1B3 mediated uptake of statins into human cryopreserved hepatocytes. To complete the characterization of the active hepatic uptake of cerivastatin, fluvastatin, pitavastatin, and lovastatin, REF-scaling could be further applied to assess the involvement of other hepatic transporters including OATP2B1 and NTCP. Once the uptake profiles are assessed, the transporter contributions could be used to assess the impact of specific transporter inhibition on drug exposure using physiological-based or static pharmacokinetic modeling. This would help to further improve predictions of the DDI potential of statins or any compound where this method was applied to.

QTAP analysis demonstrated to be a powerful tool to determine the transporter protein abundances in cryopreserved hepatocytes and cell lines. In the frame of this study only OATP1B1 and OATP1B3 abundances were investigated. However, QTAP enables the absolute quantification of any transporter in any *in vitro* system of interest. Given the demonstrated direct translation of transporter expression into activity, knowledge about transporter expression levels would be very valuable to characterize *in vitro* systems regarding their transporter abundances. For example, HEK293, LLC-PK_1, and MDCK cells are widely used host cell lines to generate transporter-transfected *in vitro* systems. However, they also express endogenous drug transporters which could impact the transporter uptake or efflux. Absolute quantification of endogenous drug transporter could therefore help to asses their impact on drug permeation studies.

Prediction of the drug-drug interaction potential: the victim perspective

Commonly, clinical DDI studies are performed in the late drug development phase. Yet, the assessment of the impact of co-medication on the exposure of a NMEs is of interest in early drug development. The application of the extended clearance concept to anticipate DDI can be used in preclinical drug development since the hepatic clearance mechanism can be assessed by IVIVE. We therefore expect this bottom-up approach to provide a powerful tool for a first risk assessment of NMEs.

Our study demonstrated that the application of the extended clearance concept provides a valuable tool to anticipate the DDI potential of statins. By that, the assignments of statins to the ECCCS well projected their major DDI potential. Since statins are widely prescribed, the likelihood for statin patients to receive co-medication is high. Our DDI assessment could therefore be valuable in order to select a statin that is not affected by the patients co-medication. In future, ECCCS assignments of any compound could therefore be used to contribute to personalized medical treatment.

Prediction of the drug-transporter interaction potential: the perpetrator perspective

Above we discussed the impact of co-medication on NMEs as potential victim drugs. Yet, it is crucial to characterize NMEs with respect to their perpetrator potential. Since drug transporters play a pivotal role in disposition and drug clearance the assessment of the inhibitory potential of NMEs on transporters is of importance in drug development. We demonstrated in our study that telaprevir is anticipated to exhibit clinically relevant inhibition of OATP1B1, OATP1B3, and OCT2 mediated transport. In order to anticipate the interaction potential of telaprevir with any victim drug, our generated IC_{50} values can be applied to perform static DDI assessments.

Furthermore, in clinics, co-medication with telaprevir and atorvastatin increased systemic

exposure of atorvastatin by over seven-fold. Our study demonstrated that the inhibition of OATP1B1 and OATP1B3 likely contributes to the observed effects. Thus our study contributed to the mechanistic understanding of clinically observed DDIs with telaprevir.

Summary

With the help of this work the safety profiles of NMEs can now be assessed in preclinical drug development based on *in vitro* methods. Thus, in a first step the renal and hepatic clearances can be determined based on the IVIVE methods. Subsequently, the mechanistic extended clearance concept can be applied to assess the DDI potential of NMEs. Assuming, that hepatic drug uptake is a major DDI risk of the NME, the contribution of specific drug transporters to the DDI potential could be further investigated using REF-scaling. Finally, NMEs can be characterized in terms of their inhibitory potential on renal and hepatic drug transporters to assess their risk as clinical perpetrators.

It is therefore expected, that the establishment, validation, and application of novel *in vitro* based methods, described in this work, will add significant value in the early assessment of the PK profile of NMEs.

References

Abe, K., Bridges, A., and Brouwer, K. (2009). Use of sandwich-cultured human hepatocytes to predict biliary clearance of angiotensin II receptor blockers and HMG-CoA reductase inhibitors. *Drug Metab Dispos*, 37(3):447–452.

Abe, T., Kakyo, M., Takui, T., Nakagomi, R., Nishio, T., Nakai, D., Nomura, H., Unno, M., Suzuki, M., Naitoh, T., Matsuno, S., and Yawo, H. (1999). Identification of a novel gene family encoding human liver-specific organic anion transporter LST-1. *J Biol Chem*, 274(24):17159–17163.

Ahlin, G., Hilgendor, C., Karlsson, J., Szigyarto, C., Uhlen, M., and Artusson, P. (2009). Endogenous gene and protein expression of drug-transporting proteins in cell lines routinely used in drug discovery programs. *Drug Metab Dispos*, 37(12):2275–2283.

Amidon, G. L., Lennernas, H., Shah, V., and Crison, J. (1995). A theoretical basis for a biopharmaceutics drug classification: the correlation of in vitro drug product dissolution and in vivo bioavailability. *Pharm. Res.*, 33(3-4):413–420.

Annaert, P., Ye, Z., Stieger, B., and Augustijns, P. (2010). Interaction of HIV protease inhibitors with OATP1B1, 1B3, and 2B1. *Xenobiotica*, 40:163–76.

Asselah, T. and Marcellin, P. (2011). New direct-acting antivirals: combination for the treatment of chronic hepatitis C. *Liver Int*, 31(Suppl. 1):38–77.

Backman, J., Kyrklund, C., Kivistoe, K., Wangk, J., and Neuvonen, P. (2000). Plasma concentration of active simvastatin acid are increased by gemfibrozil. *Clin Pharmacol Ther*, 68(2):122–9.

Balogh, L., Kimoto, E., Chupka, J., Zhang, H., and Lai, Y. (2012). Membrane protein quantification by peptide-based mass spectrometry approaches: Studies on the organic anion-transporting polypeptide family. *J Proteomics Bioinform*, S4.

Barton, H., Lai, Y., Goosen, T., Jones, H., El-Kattan, A., Gosset, J., Lin, J., and Varma, M. (2013). Model-based approaches to predict drug-drug interactions associated with hepatic uptake transporters: preclinical, clinical and beyhond. *Expert Opin Drug Metab Toxicol*, 9(4):459–472.

Benet, L., Amidon, G., Barends, D., Lennernaes, H., Polli, J., Shah, V., Stavchansky, S., and Yu, L. (2008). The use of BDDCS in classifying the permeability of marketed drugs. *Pharm Res.*, 25(3):483–8.

Benet, L. Z. (2013). The Role of BCS (Biopharmaceutics Classification System) and BDDCS (Biopharmaceutics Drug Disposition Classification System) in Drug Development. 102(1):34–42.

Benet, L. Z., Broccatelli, F., and Oprea, T. I. (2011). BDDCS applied to over 900 drugs. *The AAPS journal*, 13(4):519–47.

Bi, Y., Kimoto, E., Sevidal, S., Jones, H., Barton, H., Kemphsall, S., Whalen, K., Zhang, H., Ji, C., Fenner, K., El-Kattan, A., and Lai, Y. (2012). In vitro evaluation of hepatic transporter-mediated clinical drug-drug interactions: hepatocyte model optimization and retrospective investigation. *Drug Metab Dispos*, 40(6):1085–1092.

Bi, Y., Qiu, X., Rotter, C., Kimoto, E., Piotroski, M., Varma, M., Ei-Kattan, A., and Lai, Y. (2013). Quantitative assessment of the contribution of sodium-dependent taurocholate co-transporting polypeptide (NTCP) to the heptatic uptake of rosuvastatin, pitavastatin and fluvastatin. *Biopharm Drug Dispos*, 34(8):452–461.

Boulenc, X. and Barberan, O. (2011). Metabolic-based drug-drug interactions prediction, recent approaches for risk assessment along drug development. *Drug Metabol Drug Interact.*, 26(4):147–68.

Bow, D., Perry, J., DS, M., Pritchard, J., and Brouwer, K. (2008). Localization of P-gp (Absb1) and Mrp2 (Abcc2) in freshly isolated rat hepatocytes. *Drug Metab Dispos*, 36(1):198–202.

Brandsch, M. (2009). Transport of drugs by proton-coupled peptide transporters : pearls and pitfalls. *Expert Opin Drug Metab Toxicol*, 5(8):887–906.

Brown, C. D. A., Sayer, R., Windass, A. S., Haslam, I. S., Broe, M. E. D., Haese, P. C. D., and Verhulst, A. (2008). Characterisation of human tubular cell monolayers as a model of proximal tubular xenobiotic handling. *Toxicology and Applied Pharmacology*, 233(3):428–438.

Brunton, L., Chabner, B. A., and Knollman, B. (2011). Pharmacokinetics: The dynamics of drug absorption, distribution, metabolism, and elimination. In Brunton, L. L., editor, *Goodman & Gilman's The Pharmacological Basis of Therapeutics*, chapter 2. Mc Graw Hill Medical, 12 edition.

Camenisch, G. and Umehara, K.-i. (2012). Predicting human hepatic clearance from in vitro drug metabolism and transport data: a scientific and pharmaceutical perspective for assessing drug-drug interactions. *Biopharm Drug Dispos*, 33(4):179–94.

Carlile, D., Zomorodi, K., and Houston, J. (1997). Scaling factors to relate drug metabolic clearance in hepatic microsomes, isolated hepatocytes, and the intact liver: studies with induced livers involving diazepam. *Drug Metab Dispos*, 25:903–911.

Cha, S., Sekine, T., Fukushima, J., Kanai, Y., Kobayashi, Y., Goya, T., and Endou, H. (2001). Identification and characterization of human organic anion transporter 3 expressing predominantly in the kidney. *Mol Pharmacol*, 59(5):1277–1286.

Chaturvedi, P., Decker, C., and Odinecs, A. (2001). Prediction of pharmacokinetic properties using experimental approaches during early drug discovery. *Curr Opin Chem Biol*, 25(4):452–463.

Chen, C., Mireles, R., Campbell, S., Lin, J., Mills, J., Xu, J., and Smolarek, T. (2005). Differential interaction of 3-hydroxy-3-methylglutaryl-coa reductase inhibitors with ABCB1, ABCC2, and OATP1. *Drug Metab Dispos*, 33(4):537–546.

Chiba, M., Ishii, Y., and Sugiyama, Y. (2009). Prediction of hepatic clearance in human from in vitro data for successful drug development. *The AAPS journal*, 11(2):262–76.

Christoph, F. (2008). The role of hepatic transporters in drug elimination. *Expert Opin. Drug Metab. Toxicol.*, 4(4):363–379.

Chu, X. (2011). Drug interaction potential of boceprevir, as an inhibitor and inducer of drug metabolizing enzymes and transporters (abstract). *The liver meeting: 62nd AASLD annual meeting*.

Chu, X., Korzekwa, K., Elsby, R., Fenner, K., Galetin, A., Lai, Y., Matsson, P., Moss, A., Nagar, S., Rosania, G. R., Bai, J. P. F., Polli, J. W., Sugiyama, Y., Brouwer, K. L., and Consortium, I. T. (2013). Intracellular drug concentrations and transporters: measurement, modeling, and implications for the liver. *Clin Pharmacol Ther.*, 94(1):126–41.

Cummins, C., Jacobsen, W., and Benet, L. (2002). Unmasking the dynamic interplay between intestinal P-glycoprotein and CYP3A4. *J Pharmacol Exp Ther*, 300(3):1036–45.

De Bruyn, T., Ye, T.-W., Peeters, A., Sahi, J., Baes, M., Augustijns, P. F., and Annaert, P. P. (2011). Determination of OATP-, NTCP,- and OCT- mediated substrate activities in individual and pooled batches of cryopreserved human hepatocytes. *Eur J Pharm Sci*, 43(4):297–307.

Dewoskin, R. and Thompson, C. (2008). Renal clearance parameters for PBPK model analysis of early lifestage differences in the disposition of environmental toxicants. *Regul Toxicol Pharmacol*, 51(1):66–86.

Doyle, L. and Yang, W. (1998). A multidrug resistance transporter

from human MCF-7 breast cancer cells. *Proc. Natl. Acad. Scie. USA*, 95(Dec):15665–15670.

Dunn, J., Tompkin, R., and Yarmush, M. (1991). Long-term in vitro function of adult hepatocytes in a collagen sandwich configuration. *Biotehcnol Prog*, 7(3):237–45.

Dunn, J., Yarmush, M., Koebe, H., and Tompkins, R. (1989). Hepatocyte function and extracellular matrix geometry: long-term culture in a sandwich configuration. *FASEB J*, 3(2):174–177.

Duthaler, U., Keiser, J., and Huwyler, J. (2011). Development and validation of a liquid chromatography and ion spray tandem mass spectrometry method for the quantification of artesunate, artemether and their major metabolites dihydroartemisinin and dihydroartemisinin-glucuronide in sheep plasma. *J Mass Spectrom.*, 46(2):2172–181.

Eagling, V., Back, D., and Barry, M. (1997). Differential inhibition of cytochrome P450 isoforms by the protease inhibitors, ritonavir, saquinavir and indinavir. *British journal of clinical pharmacology*, 44:190–4.

Einolf, H. (2007). Comparison of different approaches to predict metabolic drug-drug interactions. *Xenobiotica*, 37(10-11):1257–1294.

Ekaratanawong, S., Anzai, N., Jutabha, P., Miyazaki, H., and Noshiro, R. (2004). Human Organic Anion Transporter 4 Is a Renal Apical Organic Anion / Dicarboxylate Exchanger in the Proximal Tubules. *J Pharmacol Sci*, 94:297–304.

El-Sheigk, A., von den Heuvel, J., Koenderink, J., and Russel, F. (2007). Interaction of nonsteroidal anti-inflammatory drugs with multidrug resistance protein (MRP)2/ABCC2- and MRP4/ABCC4-mediated methotrexate transport. *J Pharmacol Exp Ther.*, 320(1):229–235.

El-Sheikh, A., Greupnik, R., Wortelboer, H., Heuvel, J., Schreus, M., Koenderink, J., Masereeuw, R., and Russel, F. (2013). Interaction of immunosuppressive drugs with human organic anion transporter (OAT)1 and OAT3, and multidrug resistance-associated protein (MRP)2 and MRP4. *Transl Res.*, 162(6):398–409.

Elsby, R., Hilgendorf, C., and Fenner, K. (2012). Understanding the critical disposition pathways of statins to assess drug-drug interaction risk during drug development: it's not just about OATP1B1. *Clin Pharmacol Ther.*, 92(5):584–98.

EMBL (2012). Coumpound report, compound id chembl231813, telaprevir. *www.ebi.ac.uk*.

Everett, D., Chando, T., Didonato, G., Singhvi, S., Pan, H., and Weinstein, S. (1991). Biotransformation of pravastatin sodium in humans. *Durg Metab Dispos*, 19(4):740–8.

Fagerholm, U. (2007). Prediction of human pharmacokinetics – renal metabolic and excretion clearance. *J Pharm Pharmacol.*, 59(11):1463–71.

Farnik, H., El-Duweik, J., Welsch, C., Sarrazin, C., Lötsch, J., Zeuzem, S., Geisslinger, G., and Schmidt, H. (2009). Highly sensitive determination of HCV protease inhibitors boceprevir (SCH 503034) and telaprevir (VX 950) in human plasma by LC-MS/MS. *J Chromatogr B Analyt Technol Biomed Life Sci.*, 877(31):4001–4006.

FDA (2005). Guidance for industry: Waiver of in vivo bioavailability and bioequivalence studies for immediate-release solid oral dosage forms based on a biopharmaceutics classification system.

FDA (2012). Drug interaction studies- study design, data analysis, implications for dosing, and labeling recommendations.

FDA (2014). drugs(at)fda database. *www.accessdata.fda.gov*.

Feng, B., LaPerle, J. L., Chang, G., and Varma, M. V. S. (2010). Renal clearance in drug discovery and development: molecular descriptors, drug transporters and disease state. *Expert opinion on drug metabolism & toxicology*, 6(8):939–52.

Fletcher, J., Haber, M., Henderson, M., and Norris, M. (2010). ABC transporters in cancer : more than just drug efflux pumps. *Nature Reviews Cancer*, 10(2):147–156.

Frezard, F. and Garner-Suillerot, A. (1998). Permeability of lipid bilayer to anthracycline derivatives. role of the bilayer composition and of the temperature. *Biochem Biophys Acta*, 1389(1):13–22.

Fricker, G., Drewe, J., Huwyler, J., Gutmann, H., and Beglinger, C. (1996). Relevance of p-glycoprotein for the enteral absorption of cyclosporin A: in vitro- in vivo correlation. *Br J Pharmacol*, 118(7):1841–7.

Fujino, H., Yamada, I., Shimada, S., Yoneda, M., and Kojima, J. (2003). Metabolic fate of pitavastatin, a new inhibitor of HMG-CoA reductase: human UDP-glucuronosyltransferase enzymes involved in lactonization. *Xenobiotica*, 33(1):27–41.

Funk, R. and Krise, J. (2012). Cationic amphiphhilic drugs cause a marked expansion of apparent lysosomal volume: implications for an intracellular distribution-based drug interaction. *Mol Pharm.*, 9(5):1384–95.

Garg, V., Heeswijk, R., Lee, J., Alves, K., Nadkarni, P., and Luo, X. (2011). Effect of telaprevir on the pharmacokinetics of cyclosporine and tacrolimus. *Hepatology*, 54(1):20–7.

Gerloff, T., Stieger, B., Madon, J., Landmann, L., Roth, J., Hofmann, A. F., Peter, J., Hagenbuch, B., and Meier, P. J. (1998). Membranes and Bioenergeticcs : The Sister of P-glycoprotein Represents the Canalicular Bile Salt Export Pump of Mammalian Liver. *J. Biol. Chem.*, 273:10046–10050.

Gorboulev, V., Ulzheimer, J., Akhoundova, A., Ulzheimer-Teuber, I., Karbach, U., Quester, S., Baumann, C., Lang, F ad Bush, A., and Loepsell, H. (1997). Cloning and characterization of two human polyspecific organic cation transporters. *DNA Cell Biol*, 16(7):871–881.

Gowder, S. and McMartin, K. E. (2010). Development of a primary culture system of rat kidney proximal tubule cells for transport studies. *Jour. of Epithel. Biol. Pharmacol.*, 3:15–19.

Griffin, L., Annaert, P., and Brouwer, K. (2011). Influence of drug transport proteins on the pharmacokinetics and drug interactions of HIV protease inhibitors. *J Pharm Sci*, 100:3636–54.

Groothuis, G., Hulstaert, C., and Hardonk, M. (1981). Plasma membrane specialization and intracellular polarity of freshly isloated rat hepatocytes. *Eur J Cell Biol*, 26(1):43–51.

Grube, M., Kock, K., Oswald, S., Draber, K., Meissner, K., Eckel, L., Böhm, M., Felix, S., Vogelgesang, S., Jedlitschky, G., Siegmund, W., Warzok, R., and Kroemer, H. (2006). Organic anion transporting polypeptide 2B1 is a high-affinity transporter for atorvastatin and is expressed in the human heart. *Clin Pharmacol Ther*, 80(6):607–20.

Gutmann, H., Fricker, G., Drewe, J., Toeroek, M., and Miller, D. (1999). Interactions of HIV protease inhibitors with ATP-dependent drug export proteins. *Mol Pharmacol*, 56:383–9.

Habu, Y., Yano, I., Okuda, M., Hashimoto, Y., and Inui, K. (2000). Kinetic analysis of p-aminohippurate transport in the OK kidney epithelial cell line. *Pharm Res*, 17(9):1155–1157.

Hagenbuch, B. and Gui, C. (2008). Xenobiotic transporters of the human organic anion transporting polypeptides (OATP) family. *Xenobiotica*, 38(7-8):778–801.

Hagenbuch, B. and Meier, P. (2004). Organic anion transporting polypeptides of the OATP/SLC21 family: phylogenetic classification as OATP/SLCO superfamily, new nomenclature and molecular/functional properties. *Pflugers Arch*, 447(5):653–665.

Hagos, Y., Stein, D., Ugele, B., Burckhardt, G., and Bahn, A. (2007). Human renal organic anion transporter 4 operates as an asymmetric urate transporter. *Journal of the American Society of Nephrology : JASN*, 18(2):430–9.

Hilgendorf, C., Ahlin, G., Artursson, P., Ungell, A., and Karlsson, J. (2007). Expression of thirty-six drug transporter genes in human intestine, liver, kidney, and organotypic cell lines. *Drug Metab Dispos*, 35(8):1333–1340.

Hillgren, K. M., Keppler, D., Zur, A. A., Giacomini, K. M., Stieger, B., Cass, C. E., and Zhang, L. (2013). Emerging Transporters of Clinical Importance : An Update From the International Transporter Consortium. *Clin Pharmacol Ther.*, 94(1).

Hilskotte, E., Gupta, S., Xuan, F., van Zutven, M., O'Mara, E., and Galitz, L. (2011). Pharmacokinetic evaluation of the interaction between the HCV protease inhibitor boceprevir and the HMG-CoA reductase inhibitors atorvastatin and pravastatin (abstract). *HEP DART*.

Hirano, M., Maeda, K., Hayashi, H., and Kusuhara, H. (2005). Bile salt export pump (BSEP/ABCB11) can transport a non-bile acid substrate, pravastatin. *J Pharmacol Exp Ther.*, 314(2):876–882.

Hirano, M., Maeda, K., Shitara, Y., and Sugiyama, Y. (2004). Contribution of OATP2 (OATP1B1) and OATP8 (OATP1B3) to the hepatic uptake of pitavastatin in humans. *J Pharmacol Exp Ther*, 311(1):139–146.

Hirano, M., Maeda, K., Shitara, Y., and Sugiyama, Y. (2006). Drug-drug interaction between pitavastatin and various drugs via OATP1B1. *Drug Metab Dispos*, 34:1229–36.

Ho, E., Lin, D., Mendel, D., and Cihlar, T. (2000). Cytotoxicity of antiviral nucleotides adefovir and cidofovir is induced by the expression of human renal organic anion transporter 1. *J AM Soc Nephrol*, 11(3):383–393.

Ho, R., Tirona, R., Leake, B., Glaeser, H., Lee, W., Lemke, C. J., Wang, Y., and Kim, R. (2006). Drug and bile acid transporters in rosuvastatin hepatic uptake: function, expression, and pharmacogenetics. *Gastroenterology*, 130(6):1793–806.

Hoffmaster, K., Turncliff, R., LeCluyse, E., Kim, R., Meier, P., and Brouwer, K. (2004). P-glycoprotein expression, localization, and function in sandwich-cultured primary rat and human hepatocytes: relevance to the heptobiliary disposition of a model opiod peptide. *Pharm Res*, 21(7):1294–1302.

Hori, R., Okamura, M., Takayama, a., Hirozane, K., and Takano, M. (1993). Transport of organic anion in the OK kidney epithelial cell line. *Am J Physiol*, 264(6 Pt 2):F975–80.

Hosoyamada, M., Sekine, T., Kanai, Y., and Endou, H. (1999). Molecular cloning and functional expression of a multispecific organic anion transporter from human kidney. *Am J Physiol.*, 276(1 Pt 2):F122–8.

Houston, J. and Carlili, D. (1997). Prediction of hepatc clearance from microsomes, hepatocytes, and liver slices. *Drug Metab Rev*, 47:1469–1479.

Huang, S., Zhang, I., and Giacomini, K. (2010). The International Transporter Consortium: a collaborative group of scientists from academia, industry, and the FDA. *Clin Pharmacol Ther*, 87:32–6.

ITC (2010). The international transporter consortium: Membrane tansporters in drug development. *Nat Rev Drug Discov.*, 9(3):215–236.

Ito, K. and Houston, J. (2004). Comparison of the use of liver models for predicting drug clearance using in vitro kinetic data from hepatic microsomes and isolated hepatocytes. *Pharm Res*, 21(5):785–792.

Jamei, M., Bajot, F., Neuhoff, S., Barter, Z., Yang, J., Rostami-Hodjegan, a., and Rowland-Yeo, K. (2014). A mechanistic framework for in vitro-in vivo extrapolation of liver membrane transporters: prediction of drug-drug interaction between rosuvastatin and cyclosporine. *Clin Pharmacokinet*, 53(1):73–87.

Jin, H. and Di, L. (2008). Permeability–in vitro assays for assessing drug transporter activity. *Current drug metabolism*, 9(9):911–20.

Jones, H., Barton, H., Lai, Y., Bi, Y., Kimoto, E amd Kempshall, S., Tate, S., El-Kattan, A., Houston, J., Galetin, A., and Fenner, K. (2012). Mechanistic pharmacokinetic modeling for the prediction of transporter-mediated disposition in humans from sandwich culture human hepatocyte data. *Drug Metab Dispos*, 40(5):1007–1017.

Juliono, R. and Ling, V. (1976). A surface glycoprotein modulating drug permeability in Chinese hamster ovary cell mutants. *Biochem Biophys Acta*, 455(1):152–62.

Jung, N., Lehmann, C., Rubbert, A., Knispel, M., Hartmann, P., Lunzen, J., Stellbrink, H., Faetkenheuer, G., and Taubert, D. (2008). Relevance of the organic cation transporters 1 and 2 for antiretroviral drug therapy in human immunodeficiency virus infection. *Drug Metab Dispos*, 36(8):1616–1623.

Kalliokoski, A. and Niemi, M. (2009). Impact of OATP transporters on pharmacokinetics. *Br J Pharmacol*, 158(3):693–705.

Kameyama, Y., Yamashita, K., Kobayashi, K., Hosokawa, M., and Chiba, K. (2005). Functional characterization of SLCO1B1*15+C1007G, by using transient systems of HeLa and HEK293 cells. *Pharmacogenet Genomics*, 15:513–22.

Kamiie, J., Ohtsuki, S., Iwase, R., Ohmine, K., Katsukura, Y., Yanai, K., Sekine, Y., Uchida, Y., Ito, S., and Terasaki, T. (2008). Quantitative atlas of membrane transporter proteins: development and application of a highly sensitive simultaneous LC/MS/MS method combined with novel in –silico peptide selection criteria. *Pharm Res*, 25(6):1496–1483.

Karlgren, M., Vildhede, A., Norinder, U., Wisniewski, J., Kimoto, E., Lai, Y., Haglund, U., and Artursson, P. (2012). Classification of inhibitors of hepatic organic anion tansporting polypeptides (OATPs): influence of protein expression on drug-drug interactions. *J Med Chem*, 55(10):4740–4763.

Kazmi, F., Hensley, T., Pope, C., Funk, R. S., Loewen, G. J., Buckley, D. B., and Parkinson, A. (2013). Lysosomal sequestration (trapping) of lipophilic amine (cationic amphiphilic) drugs in immortalized human hepatocytes (Fa2N-4 Cells). *DMD*, 41:897–905.

Keskitalo, J., Zolk, O., Fromm, M., Kurkinen, K., Neuvonen, P., and Niemi, M. (2009). ABCG2 polymorphism markedly affects the pharmacokinetics of atorvastatin and rosuvastatin. *Clin Pharmacol Ther*, 86(2):197–203.

Khojasteh, S. C., Wong, H., and Hop, C. E. (2011a). ADME properties and their dependence on physiochemical properties. In *Drug Metabolism and Pharmacokinetics Quick Guide*, chapter 9. Springer Science+Business Media.

Khojasteh, S. C., Wong, H., and Hop, C. E. (2011b). Prediction of human pharmacokinetics. In *Drug Metabolism and Pharmacokinetics Quick Guide*, chapter 7. Springer Science+Business Media.

Kimoto, E., Yoshida, K., Balogh, L., Bi, Y., Maeda, K., El-Kattan, A., Sugiyama, Y., and Lai, Y. (2012). Characterization of organic anion transporting polypeptide (OATP) expressin and its fucntional contribution to the uptake of substrates in human hepatocytes. *Mol Pharm*, 9(12):3535–3542.

Kirchheiner, J., Kudlicz, D., Meisel, C., Bauer, S., Meineke, I., Roots, I., and Brockmoller, J. (2003). Influence of CYP2C9 polymorphisms on the pharmacokinetics and cholesterol-lowering activity of (-)-3S,5R-fluvastatin and (+)-3R,5S-fluvastatin in healthy volunteers. *Clinical pharmacology and therapeutics*, 74:186–94.

Kiser, J., Burton, J., Anderson, P., and Eversion, G. (2012). Review and management of drug interactions with boceprevir and telaprevir. *Hepatology*, 55(5):1620–1628.

Kitamura, S., Maeda, K., Wang, Y., and Sugiyama, Y. (2008). Involvement of multiple transporters in the hepatobiliary transport of rosuvastatin. *Drug Metabl Dispos*, 36(10):2014–2023.

Klaassen, C. D. and Aleksunes, L. M. (2010). Xenobiotic , Bile Acid , and Cholesterol Transporters: function and regulation. *Pharmacol Rev.*, 62(1):1–96.

Knauer, M., Urquhar, B., Meyer zu Schwabedissen, H., Schwarz, U., Lemke, C., Leake, B., Kim, R., and Tirona, R. (2010). Human skeletal muscle drug transporters determine local exposure and toxicity of statins. *Circ Res.*, 106(2):297–306.

Koepsell, H., Lips, K., and Volk, C. (2007). Polyspecific organic cation transporters: structure, function, physiological roles, and biopharmaceutical implications. *Pharm Res*, 24(7):1227–1251.

König, J., Cui, Y., Nies, a. T., and Keppler, D. (2000). Localization and genomic organization of a new hepatocellular organic anion transporting polypeptide. *The Journal of biological chemistry*, 275(30):23161–8.

König, J., Müller, F., and Fromm, M. F. (2013). Transporters and drug-drug interactions: important determinants of drug disposition and effects. *Pharmacological reviews*, 65(3):944–66.

König, J., Seithel, A., Gradhand, U., and Fromm, M. (2006). Pharmacogenomics of human OATP transporters. *Naunyn Schmiedebergs Arch Pharmacol.*, 372(6):432–443.

Kuntz, E. and Kuntz, H.-D. (2006). Morphology of the liver. In *Hepatology. Principles and Practice.*, chapter 2. Springer Medizin Verlag, 2 edition.

Kunze, A., Huwyler, J., Camenisch, G., and Gutmann, H. (2012). Interaction of the antiviral drug telaprevir with renal and hepatic drug transporters. *Biochem Pharmacol*, 84(8):1096–1102.

Kunze, A., Huwyler, J., Camenisch, G., and Poller, B. (2014a). Prediction of organic anion-transporting polypeptide 1B1- and 1B3-mediated hepatic uptake of statins based on transporter protein expression and activity data. *Drug Metab Dispos.*, 42(9):1514–21.

Kunze, A., Huwyler, J., Poller, B., Gutmann, H., and Camenisch, G. (2014b). In vitro – in vivo extrapolation method to predict human renal clearance of drugs. *J Pharm Sci.*, 103(3):994–1001.

Kusuhara, H. and Sugiyama, Y. (2009). In vitro-in vivo extrapolation of transporter-mediated clearance in the liver and kidney. *Drug Metab Pharmacokinet*, 24(1):37–52.

Kuteykin-Teplyakov, K., Luna-Tortós, C., Ambroziak, K., and Löscher, W. (2010). Differences in the expression of endogenous efflux transporters in MDR1-transfected versus wildtype cell lines affect P-glycoprotein mediated drug transport. *Br J Pharmacol*, 160(6):1453–63.

Kyrklund, C., Backman, J., Kivistoe, K., M, N., Laitila, J., and Neuvonen, P. (2001). Plasma concentrations of active lovastatin acid are markedly increased by gemfibrozil but not by bezafibrate. *Clin Pharmacol Ther*, 69(5):340–5.

Lash, L., Putt, D., and Cai, H. (2006). Membrane transport function in primary cultures of human proximal tubuluar cells. *Toxicology*, 228(2-3):200–218.

Lau, Y., Okochi, H., Huang, Y., and Benet, L. (2006). Multiple transporters affect the disposition of atorvastatin and its two active hydroxi metabolites: application of in vitro and ex situ systems. *J Pharmacol Ther*, 316(2):762–71.

Lavanchy, D. (2009). The global burden of hepatitis C. *Liver Int*, 29(Suppl. 1):74–81.

Lave, T., Chapman, K., Goldsmith, P., and Rowland, M. (2009). Human clearance prediciton: shifting the paradigm. *Expert Opin Drug Metab Toxicol*, 5(9):1039–48.

Lee, J., Heeswijk, R., Alves, K., Smith, F., and Garg, V. (2011). Effect of the hepatitits C virus protease inhibitor telaprevir on pharmacokinetics of amlodipine and atorvastatin. *Antimicrob Agents Chemother.*, 55(10):4569–74.

Lee, M. L., Jigorel, E., Glaise, D., Gripon, P., Guguen-Guilouzo, and Fardel, O. (2006). Functional expression of sinusoidal and canalicular hepatic drug transporters in the differentiated human hepatoma HepRG cell line. *Eur J Pharm Sci*, 28:109–117.

Li, J., Volpe, D. A., Wang, Y., Zhang, W., Bode, C., Owen, A., and Hidalgo, I. J. (2011). Use of Transporter Knockdown Caco-2 Cells to Investigate the In Vitro Efflux of Statin Drugs. *Drug Metab Dispos*, 39(7):1196–1202.

Li, M., Anderson, G. D., and Wang, J. (2006). Drug-drug interactions involving membrane transporters in the human kidney. *Expert Opin Drug Metab Toxicol.*, 2(4):505–32.

Liang, M., Ramsey, C. R., and Knox, F. G. (1999). The paracellular permeability of opossum kidney cells, a proximal tubule cell line. *Kidney international*, 56(6):2304–8.

Liang, R., Fei, Y., Prasad, P., Ramamoorthy, S., Han, H., Yang-Feng, T., Hediger, M., Ganapathy, V., and Leibach, F. (1995). Human intestinal H+/peptide cotransporter. Cloning, functional expression, and chromosomal localization. *J Biol Chem*, 270(12):6456–6463.

Liddle, C. and Stedman, C. A. (2007). Hepatic metabolism of drugs. In Rodes, J., Benhamou, J.-P., Blei, A. T., Reichen, J., and Rizzetto, M., editors, *Textbook of Hepatology. From Basic Science to Clinical Practice*, chapter 2.3.15. Blackwell Publsihing Ltd, 3 edition.

Liegler, D., Henderson, E., Hahn, M., and Oliverio, V. (1969). The effect of organic acids on renal clearance of methotrexate in man. *Clin Pharmacol Ther.*, 10(6):849–857.

Liu, Y., She, M., Wu, Z., and Dai, R. (2011). The inhibition study of human UDP-glucuronosyltransferases with cytochrome P450 selective substrates and inhibitors. *J Enzyme Inhib Med Chem*, 26(3):386–93.

Lohr, J. W., Willsky, G. R., and Acara, M. A. (1998). Renal drug metabolism. *Pharmacol Rev.*, 50(1):107–41.

Lote, C. J. (2012). Essential anatomy of the kidney. In *Principles of Renal Physiology*, chapter 2, pages 21–32. Springer Science+Business Media, 5 edition.

Lu, C., Li, P., Gallegos, R., Uttamsingh, V., Xia, C., Miwa, G., Balani, S., and Gan, L. (2006). Comparison of intrinsic clearance in liver microsomes and heatocytes from rats and humans: Evaluation of free fraction and uptake in hepatocytes. *Drug Metab Dispos*, 34:1600–1605.

Lundquist, P., Lööf, J., Sohlenius-Sternbeck, A.-K., Floby, E., Johansson, J., Bylund, J., Hoogstraate, J., Afzelius, L., and Andersson, T. B. (2014). The Impact of Solute Carrier (SLC) Drug Uptake Transporter Loss in Human and Rat Cryopreserved Hepatocytes on Clearance Predictions. *Drug metabolism and disposition*, 42(3):469–80.

Luttringer, O., Theil, F., Lave, T., Wernli-Kuratli, K., Guentert, T., and De Saizieu, A. (2002). Biochemical influence of isolation procedure, extracellular matrix and dexmethasone on the regulation of membrane transporters gene expression in rat hepatocytes. *Drug Metab Dispos*, 64(11):1637–1650.

Malarkey, D. E., Johnson, K., Ryan, L., Boorman, G., and Maronpot, R. R. (2005). New insights into functional aspects of liver morphology. *Toxicol Pathol.*, 33(1):27–34.

Martin, P., Warwick, M., Dane, A., Hill, S., Giles, P., Phillips, P., and Lenz, E. (2003a). Metabolism, excretion, and pharmacokinetics of rosuvastatin in healthy adult male volunteers. *Clin Ther.*, 25(11):2822–35.

Martin, P. D., Warwick, M., Dane, A., Brindley, C., and Short, T. (2003b). Absolute oral bioavailability of rosuvastatin in healthy white adult male volunteers. *Clinical therapeutics*, 25(10):2553–63.

Masago, M., Takaai, M., Sakata, J., Horie, A., Ito, T., Ishida, K., Taguchi, M., and Hashimoto, Y. (2010). Membrane transport mechanisms of quinidine and procainamide in renal LLC-PK1 and intestinal LS180 cells. *Biological & pharmaceutical bulletin*, 33(8):1407–12.

Masereeuw, R. and Russel, F. G. M. (2001). Mechanisms and clinical implications of renal drug excretion. *Drug Metab Rev.*, 33(3-4):299–351.

Masters, J. (2000). Human cancer cell lines: fact and fantasy. *Nat Rev Mol Cell Biol*, 1(3):233–236.

Mateus, A., Matsson, P., and Artursson, P. (2013). Rapid measurement of intracellular unbound drug concentrations. *Mol Pharm*, 10(6):2467–78.

Matsushima, S., Maeda, K., Ishiguro, N., Igarashi, T., and Sugiyama, Y. (2008). Investigation of the inhibitory effects of various drugs on the hepatic uptake of fexofenadine in humans. *Drug Metab Dispos*, 36(4):663–669.

Maurice, M., Rogier, E., Cassio, D., and Feldmann, G. (1988). Formation of plasma membrane domains in rat hepatocytes and heptoma cell lines in culture. *J Cell Sci*, 90(Pt 1):79–92.

Morrissey, K. M., Stocker, S. L., Wittwer, M. B., Xu, L., and Giacomini, K. M. (2013). Renal transporters in drug development. *Annual review of pharmacology and toxicology*, 53:503–29.

Nakagomi-Hagihara, R., Nakai, D., and Tokui, T. (2007). Inhibition of human organic anion transporter 3 mediated pravastatin transport by gemfibrozil and the metabolites in humans. *Xenobiotica*, 37(4):416–26.

Nakamura, T., Yonezawa, A., Hashimoto, S., Katsura, T., and Inui, K. (2010). Disruption of multidrug and toxin extrusion MATE1 potentiates cisplatin-induced nephrotoxicity. *Biochem Pharmacol*, 80(11):1762–1767.

Neuhoff, S., Gaohua, L., Burt, H., Jamei, M., Li, L., Tucker, G. T., and Rostami-hodjegan, A. (2013). Transporters in drug development. In Sugiyama, Y. and Steffansen, B., editors, *Rang and Dale's Pharmacology*, chapter 7, pages 155–177. Springer Scoemce+ Business, New York, NY.

Neuvonen, P., Niemi, M., and Backman, J. (2006). Drug interactions with lipid-lowering drugs: mechanism and clinical relevance. *Clin Pharmacol Ther*, 80(6):565–581.

Niemi, M., Arnold, K., Backman, J., Pasanen, M., Godtel-

Armbrust, U., Wojnowski, L., Zanger, U., Neuvonen, P., Eichelbaum, M., KT, K., and Lang, K. (2006). Association of genetic polymorphism in ABCC2 with hepatic multidrug resistance-associated protein 2 expression and pravastatin pharmacokinetics. *Pharmacogenetics and genomics*, 16:801–8.

Nies, A., Koepsell, H., Witner, S., Burk, O., Klein, K., and Kerb, R. (2009). Expression of organic cation transporters OCT1 (SLC22A1) and OCT3 (SLC22A3) is affected by genetic factors and cholestasis in human liver. *Hepatology*, 50:1227–40.

Nies, A., Niemi, M., Burk, O., Winter, S., Zanger, U., Stieger, B., Schwaab, M., and Scheffeler, E. (2013). Genetics is a major determinant of expression of the human hepatic uptake transporter OATP1B1, but not of OATP1B3 and OATP2B1. *Genome Med.*, 5(1).

Nies, A. T., Koepsell, H., Damme, K., and Schwab, M. (2011). Organic cation transporters (octs , mates), in vitro and in vivo evidence for the importance in drug therapy. In Fromm, M. F. and Kim, R. B., editors, *Drug Transporters: Handbook of Experimental Pharmacology*. Springer.

Nigam, S., Bush, K., and Bhatnagar, V. (2007). Drug and toxicant handling by the OAT organic anion transporters in the kidney and other tissues. *Nat Clin Pract Nephrol*, 3(8):443–448.

Noe, J., Portmann, R., Brun, M., and Funk, C. (2007). Substrate-dependent drug-drug interactions between gefibrozil, fluvastatin and other organic anion-transporting peptide (OATP) substrates on OATP1B1, OATP2B1, and OATP1B3. *Drug Metab Dispos*, 35(8):1308–1314.

Obach, R. (1999). Prediction of human clearance of twenty-nine drugs from hepatic microsomal intrinsic clearance data: An examination of in vitro half-life approach and nonspecific binding to microsomes. *Drug Metab Dispos*, 27(11):1350–1359.

Obach, R. S., Baxter, J. G., Liston, T. E., Silber, B. M., Jones, B. C., MacIntyre, F., Rance, D. J., and Wastall, P. (1997). The prediction of human pharmacokinetic parameters from preclinical and in vitro metabolism data. *J Pharmacol Exp Therapeut*, 283(1):46–58.

Ohtsuki, S., Schaefer, O., Kawakami, H., Inoue, T., Liehner, S., Saito, A., Ishiquro, N., Kishimoto, W., Ludwig-Schwellinger, E., Ebner, T., and Terasaki, T. (2012). Simultaneous absolute protein quantification of transporters, cytochromes P450, and UDP-glucuronosyltransfereases as a novel approach for the characterization of individual human liver: comparision with mRNA levels and activities. *Drug Metabl Dispos*, 40(1):83–92.

Ohtsuki, S., Uchida, Y., Kubo, Y., and Terasaki, T. (2011). Quantitative Targeted Absolute Proteomics-Based ADME Research as a New Path to Drug Discovery and Development : Methodology , Advantages , Strategy , and Prospects. 100(9):3547–3559.

Okudaira, N. and Sugiyama, Y. (1996). Use of an isolated perfused kidney to assess renal clearance of drugs: Information obtained in steady-state and non-steady-state experimental systems. *Pharm Biotechnol*, 8:211–238.

Otsuka, M., Matsumoto, T., Morimoto, R., Arioka, S., Omote, H., and Moriyama, Y. (2005). A human transporter protein that mediates the final. *Proc Natl Acad Sci USA*, 102(50).

Pang, K. and Rowland, M. (1977). Hepatic clearance of drugs. i. theoretical considerations of a "well-stirred" model and a "parallel tube" model. influence of hepatic blood flow, plasma and blood cell binding, and the hepatocellular enzymatic activity on hepatic drug clearance. *Journal of Pharmacokinetics and Biopharmaceutics*, 5(6):625–653.

Pasanen, M., Fredrikson, H., Neuvonen, P., and Niemi, M. (2007). Different effects of SLCO1B1 polymorphism on the pharmacokinetics of atorvastatin and rosuvastatin. *Clinical pharmacology and therapeutics*, 82:726–33.

Petzinger, J. G. T. W. E. (2006). The solute carrier family SLC10 : more than a family of bile acid transporters regarding function and phylogenetic relationships. *Naunyn Schmiedbergs Arch Pharmacol.*, 372(6):413–431.

Pham, P., Porte, C., LÃl'ee, L., Van, H., Sabo, J., and Elgadi, M. (2009). Differential effects of tipranavir plus ritonavir on atorvastatin or rosuvastatin pharmcacokinetics in healthy volunteers. *Antimicrob Agents Chemother*, 53:4385–92.

Prueksaritantont, T., Subramanian, R., Fang, X an d Ma, B., Qiu, Y., Lin, J., Pearson, P., and Baillie, T. (2002a). Glucuronidation of statins in animals and humans: novel mechanism of statin lactonization. *Drug Metab Dispos*, 30(5):505–12.

Prueksaritantont, T., Tang, C., Qiu, Y., Mu, L., Subramanian, R., and Lin, J. (2002b). Effects of fibrates on metabolism of statins in human hepatocytes. *Drug Metab Dispos*, 30(11):1280–7.

Prueksaritantont, T., Zhao, J., Ma, B., Roadcap, B., Tang, C., Qiu, Y., Liu, L., Lin, J., Pearson, P., and Baillie, T. (2002c). Mechanistic studies on metabolic interactions between gemfibrozil and statins. *J Pharmacol Exp Ther*, 301(1):1042–51.

Rane, A., Wilinson, G., and Shand, D. (1977). Quantitative prediction of in vivo drug clearance and drug interactions from in vitro data on metabolism together with binding and transport. *J Pharmacol Exp Ther*, 200:420–424.

Rang, H. P., Dale, M. M., Ritter, J. M., Flower, R. J., and G, H. (2012). Drug asborption and distribution. In Hyde, M. and A, M., editors, *Rang and Dale's Pharmacology*, chapter 8. Elsevier, 4 edition.

Riedmaier, A. E., Nies, A. T., Schaeffeler, E., and Schwab, M. (2012). Organic Anion Transporters and Their Implications in Pharmacotherapy. *Pharmacol Rev.*, 64(3):421–449.

Roth, M., Obaidat, A., and Hagenbuch, B. (2012). OATPs, OATs and OCTs: the organic anion and cation transporters of the SLCO and SLC22A gene superfamilies. *Br J Pharmacol*, 165(5):1260–87.

Rowland, M. and Tozer, T. N. (2011a). Elimination. In Troy, D. B., editor, *Clinical Pharmacokinetics and Pharmacodynamics: Concepts and Applications*, chapter 5. Lippincott Williams & Wilkins, 4 edition.

Rowland, M. and Tozer, T. N. (2011b). kinetics following an intravenous bolus dose. In Troy, D. B., editor, *Clinical Pharmacokinetics and Pharmacodynamics: Concepts and Applications*, chapter 4. Lippincott Williams & Wilkins, 1 edition.

Rowland, M. and Tozer, T. N. (2011c). Membranes and distribution. In Troy, D. B., editor, *Clinical Pharmacokinetics and Pharmacodynamics: Concepts and Applications*, chapter 4. Lippincott Williams & Wilkins, 4 edition.

Russel, F. G. M. (2010). Transporters : Importance in Drug Absorption , Distribution , and Removal. In Pang, K. S., Rodrigues, A. D., and Peter, R. M., editors, *Enzyme- and Transporter-Based Drug-Drug Interactions: Progress and Future Challenges*, chapter 2, pages 27–50. American Association of Pharmaceutical Scientists.

Sair (2014). Sair and Lab and Bioinformatics and group. Transporter Classification Database. *www.tcdb.org*.

Saito, H., Yamamoto, M., Inui, K., and Hori, R. (1992). Transcellular transport of organic cation across monolayers of kidney epithelial cell line LLC-PK. *Am J Physiol*, 262(1 Pt 1):C59–C66.

Sakamoto, A., Matsumaru, T., Ishiquro, N., Schaefer, O., Ohtsuki, S., Inoue, T., Kawakami, H., and Terasaki, T. (2011). Reliability and robustness of simultaneous absolute quantification of drug transporters, cytochrome P450 enzymes, and Udp-glucuronosyltransferases in human liver tissue by multiplexed MRM/selected reaction monitoring mode tandem mass spectrometry with nano-liquid chromatography. *J Pharm Sci*, 100(9):4037–4043.

Sasaki, M., Suzuki, H., Ito, K., Abe, T., and Sugiyama, Y. (2002). Transcellular transport of organic anions across a double-transfected Madin-Darby canine kidney II cell monolayer expressing both human organic anion-transporting polypeptide (OATP2/SLC21A6) and Multidrug resistance-associated protein 2 (MRP2/ABCC2). *J Biol Chem*, 277(8):6497–503.

Schaefer, O., Ohtsuki, S., Kawakami, H., Inoue, T., Liehner, S., Saito, A., Sakamoto, A., Ishiguro, N., Matsmaru, T., Terasaki, T., and Ebner, T. (2012). Asbolute qunatification and differ-

ential expression of drug transporters, cytochrome P450 enzymes, and UDP-glucuronosyltranferases in cultured primary human hepatocytes. *Drug Metab Dispos*, 40(1):93–103.

Schlatter, P., Gutmann, H., and Drewe, J. (2006). Primary porcine proximal tubular cells as a model for transepithelial drug transport in human kidney. *European journal of pharmaceutical sciences : official journal of the European Federation for Pharmaceutical Sciences*, 28(1-2):141–54.

Schlessinger A, Yee, S. S. A. and KM, G. (2013). SLC calssification: an update. *Clin Pharmacol Ther.*, 94(1):19–23.

Scripture, C. D. and Pieper, J. a. (2001). Clinical pharmacokinetics of fluvastatin. *Clin Pharmacokinet*, 40(4):263–81.

Sekine, T., Cha, S. H., Tsuda, M., Apiwattanakul, N., Nakajima, N., Kanai, Y., and Y, H. E. (1998). Identification of multispecific organic anion transporter 2 expressed predominantly in the liver. 429(2):179–182.

Sharma, P., Butters, C., Smith, V., Elsby, R., and Surry, D. (2012). Prediction of the in vivo OATP1B1-mediated drug-drug interaction potential of an investigational drug against a range of statins. *Eur J Pharm Sci.*, 30(47):244–55.

Shepard, C., Finelli, L., and Alter, M. (2005). Global epidemiology of hepatitis C virus infection. *Lancet Infect Dis*, 5(9):558–67.

Shimizu, M., Fuse, K., Okudaira, K., Nishigaki, R., Maeda, K., Kusuhara, H., and Sugiyama, Y. (2005). Contribution of OATP (organic anion-transporting polypeptide) family transporters to the hepatic uptake of fexofenadine in humans. *Drug Metabl Dispos*, 33(10):1477–1481.

Shitara, Y., Hirano, M., Sato, H., and Sugiyama, Y. (2004). Gemfibrozil and its clucuronide inhibit the organic anion transporting polypeptide 2 (OATP2/OATP1B1:SLC21A6)-mediated hepatic uptake and CYP2C8-mediated metabolism of cerivastatin: analysis of the mechanism of the clinically relevant drug-drug interaction between cerivastatin and gemfibrozil. *J Pharmacol Exp Ther*, 311(1):228–236.

Shitara, Y., Horie, T., and Sugiyama, Y. (2006). Transporters as a determinant of drug clearance and tissue distribution. *European journal of pharmaceutical sciences : official journal of the European Federation for Pharmaceutical Sciences*, 27(5):425–46.

Shitara, Y., Li, A., Kato, Y., Lu, C., Ito, K., Itoh, T., and Sugiyama, Y. (2003). Function of utpake transporters for taurocholate and estradiol 17-D-glucuronide in cryopreserved human hepatocytes. *Drug Metab Pharmacokin.*, 18(1):33–41.

Shitara, Y., Maeda, K., Ikejiri, K., Yoshida, K., Horie, T., and Sugiyama, Y. (2013). Clinical significance of organic anion transporting polypeptides (OATPs) in drug disposition : their roles in hepatic clearance and intestinal absorption. *Biopharm Drug Dispos*, 78:45–78.

Shitara, Y., Sato, H., and Sugiyama, Y. (2005). Evaluation of drug-drug interaction in the hepatobiliary and renal transport of drugs. *Annu Rev Pharmacol Toxicol*, 45:689–723.

Shitara, Y. and Sugiyama, Y. (2006). Pharmacokinetic and pharmacodynamic alterations of 3-hydroxy-3-methylglutaryl coenzyme A (HMG-CoA) reductase inhibitors: drug-drug interactions and interindividual differences in transporter and metabolic enzyme functions. *Pharmacol Ther.*, 112(1):71–105.

Shu, Y., Brown, C., Castro, R., Shi, R., Lin, E., Owen, R., Sheardown, S., Yue, L., Burchard, E., Brett, C., and Giacomini, K. (2008). Effect of genetic variation in the organic cation transporter 1, on metformin pharmacokinetics. *Clin Pharmacol Ther.*, 83(2):273–280.

Silbernagel, S. and Despopoulos, A. (2009). Fundamentals and cell physiology. In *Color Atlas of Physiology*, chapter 1. Thieme, 6 edition.

Skehan, P., Storeng, R., Scudiero, D., Monks, A., McMahon, J., and Vistica, D. (1990). New colorimetric cytotoxicity assay for anticancer-drug screening. *J Natl Cancer Inst*, 82:1107–1112.

Smith, D. E., Clémençon, B., and Hediger, M. A. (2013). Proton-coupled oligopeptide transporter family SLC15 : Physiological , pharmacological and pathological implications. *Mol Aspects Med.*, 34(2-3):323–336.

Staffa, J., Chang, J., and Green, L. (2002). Cerivastatin and reports of fatal rhabdomyolysis. *N Engl J Med*, 346(7):539–540.

Steen, H. and Mann, M. (2004). The ABC's (and XYZ's) of peptide sequencing. *Nat Rev Mol Cell Biol*, 5(9):699–711.

Sun, W., Wu, R. R., Poelje, P. D. V., and Erion, M. D. (2001). Isolation of a Family of Organic Anion Transporters from Human Liver and Kidney. *Biochem Biophys Res Commun.*, 283(2):417–422.

Swift, B., Pfeifer, N., and K, B. (2010). Sandwich-cultured hepatocytes: an in vitro model to evaluate hepatobiliary transporter-based drug interactions and hepatotoxicity. *Drug Metab Rev*, 42(3):446–71.

Takaai, M., Suzuki, H., Ishida, K., Tahara, K., and Hashimoto, Y. (2007). Pharmacokinetic analysis of transcellular transport of levofloxacin across LLC-PK1 and Caco-2 cell monolayers. *Biol Pharm Bull*, 30(11):2167–72.

Takada, T., Suzuki, H., and Sugiyama, Y. (2005). Characterization of Polarized Expression of Point- or Deletion-Mutated Human BCRP/ABCG2 in LLC-PK1 Cells. *Pharmaceutical Research*, 22(3):458–464.

Takano, M., Hirozane, K., Okamura, M., Takayama, A., Nagai, J., and Hori, R. (1994). p-Aminohippurate transport in apical and basolateral membranes of the OK kidney epithelial cells. *J Pharmacol Exp Ther*, 269(3):970–975.

Takeda, M., Narkawa, S., Hosoyamada, M., Cha, S., Sekine, T., and Endou, H. (2001). Characterization of organic anion transport inhibitors using cells stably expressing human organic anion transporters. *Eur J Pharmacol*, 419:113–120.

Tamai, I., Nozawa, T., Koshida, M., Nezu, J., Sai, Y., and Tsuij, A. (2001). Functional characterization of human organic anion transporting polypeptide B (OATP-B) in comparision with liver-specific OATP-C. *Pharm Res*, 18:1262–1269.

Tanihara, Y., Masuda, S., Sato, T., Katsura, T., Ogawa, O., and Inui, K. (2007). Substrate specificity of MATE1 and MATE2-K, human multidrug and toxin extrusions/H(+)-organic cation antiporters. *Biochem Pharmacol*, 74:359–371.

Tavelin, S., Grasjoe, J., Taipalensuu, J., Ocklund, G., and Artursso, P. (2002). Applications of epithelial cell culture in studies of drug transport. In Wise, C., editor, *Epithelial Cell Culture Protocols*, volume 138, chapter 21. Springer.

Terada, T. and Inui, K.-i. (2007). Gene expression and regulation of drug transporters in the intestine and kidney. *Biochem Pharmacol*, 73(3):440–449.

Thyss, A., Milano, G., Kubar, J., Namer, M., and Schneider, M. (1986). Clinical and pharmacokinetic evidence of a life-treatening interaction between methotrexate and ketoprofen. *Lancet*, 1(8475):256–258.

Tsuda, M., Terada, T., Ueba, M., Sato, T., Masuda, S., and Katsura, T. (2009). Involvement of human multidrug and toxin extrusion 1 in the drug interaction between cimetidine and metformin in renal epithelial cells. *J Pharacol Exp Ther*, 329:185–91.

Uchida, Y., Ohtsuki, S., Katsukura, Y., Ikeda, C., Suzuki, T., Kamiie, J., and Terasaki, T. (2011). Quantitative targeted absolute proteomics of human blood-brain barrier transporters and receptors. *J Neurochem*, 117(2):333–345.

Ueo, H., Motohashi, H., Katsura, T., and Inui, K. (2005). Human organic anion transporter hOAT3 is a potent transporter of cephalosporin antibiotics, in comparison with hOAT1. *Biochem Pharmacol*, 70(7):1104–1113.

Umehara, K.-i. and Camenisch, G. (2012). Novel In Vitro-In Vivo Extrapolation (IVIVE) Method to Predict Hepatic Organ Clearance in Rat. *Pharm Res*, 29(2):603–617.

Urakami, Y. U., Imura, N. K., Kuda, M. O., Asuda, S. M., Atsura, T. K., and Nui, K.-i. I. (2005). Transcellular transport of creatinine in renal tubular eqithelial cell line LLC-PK1. *Drug Metab Pharmacokinet*, 20:200–205.

Uwai, Y., Saito, H., and Inui, K. (2000). Interaction between methotrexate and nonsteroidal anti-inflammatory drugs in organic anion transporter. *Eur J Pharmacol*, 409(1):31–36.

Uwai, Y., Taniguchi, R., Motohashi, H., Saito, H., Okuda, M., and Inui, K. (2004). Methotrexate-loxoprofen interaction: involvement of human organic anion transporters hOAT1 and hOAT3. *Drug Metab Pharmacokinet.*, 19(5):369–374.

Varma, M. V. S., Feng, B., Obach, R. S., Troutman, M. D., Chupka, J., Miller, H. R., and El-Kattan, A. (2009). Physicochemical determinants of human renal clearance. *Journal of medicinal chemistry*, 52(15):4844–52.

Vavricka, S., Van, M., Ha, H., Meier, P., and Fattinger, K. (2002). Interactions of rifamycin SV and rifampicin with organic anion uptake systems of human liver. *Hepatology*, 36:164–172.

Verhulst, A., Sayer, R., DeBroe, M., DHaese, P., and Brown, C. (2008). Human proximal tubular epithelium actively secretes but does not retain rosuvastatin. *Molecular pharmacology*, 74:1084–91.

Vertex (2011). Vertex Pharmaceuticals Inc. Incivek (telarevir). Product Monograph, Cambridge, MA.

Vildhede, A., Karlgren, M., Svedberg, E., Wisniewski, J., Lai, Y., Noren, A., and Artursson, P. (2014). Hepatic uptake of atorvastatin: influence of variability in transporter expression on uptake clearance and drug-drug interactions. *Drug Metab Dispos*, 42(7):1210–8.

Watanabe, T., Kusuhara, H., Debori, Y., Maeda, K., Kondo, T., Nakayama, H., Horita, S., Oglivie, B., Parkinson, A., Hu, Z., and Sugiyama, Y. (2011). Prediction of the overall renal tubular secretion and hepatic clearance of anionic drugs and renal drug-drug interaction involving organic anion transporter 3 in humans by in vitro uptake experiments. *Drug Metab Dispos*, 39(6):1031–1038.

Watanabe, T., Kusuhara, H., Maeda, K., Kanamaru, H., Saito, Y., Hu, Z., and Sugiyama, Y. (2010). Investigation of the rate-determining process in the hepatic elimination of HMG-CoA reductase inhibitors in rats and humans. *Drug Metab Dispos*, 38(2):215–22.

Webborn, P., Parker, A., Denton, R., and Riley, R. (2007). In vitro-in vivo extrapolation of hepatic clearance invovling active uptake: theoretical and experimental aspects. *Xenobiotica*, 37(11):1090–1109.

Williams, A. J., Hyland, R., Jones, B. C., Smith, D. A., Hurst, S., Goosen, T. C., Peterkin, V., Koup, J. R., and Ball, S. E. (2004). Durg-Drug Interactions for UDP-gucuronosyltransferase substrates: a pharmacokinetic explanation for typically observed low exposure (AUC_i/AUC) ratios. . *DMD*, 32(11):1201–1208.

Williamson, B., Soars, A., Owen, A., White, P., Riley, R., and Soars, M. (2013). Dissecting the relative contribution of OATP1B1-mediated uptake of xenobiotics into human hepatocytes using siRNA. *Xenobiotica*, 43(10):920–31.

Windass, A., Lowes, S., Wang, Y., and Brown, C. (2007). The contribution of organic anion transporters OAT1 and OAT3 to the renal uptake of rosuvastatin. 322:1221–1227.

Wu, C.-Y. and Benet, L. (2005). Predicting drug disposition via application of BCS: Transport/absorption/elimination interplay and development of a biopharmaceutics drug disposition classification system. *Pharm Res.*, 22(1):11–23.

Wu, X., Whitfield, L., and Stewart, B. (2000). Atorvastatin transport in the Caco-2 cell model: contributions of P-glycoprotein and the proton-monocarboxylic acid co-transporter. *Pharm res*, 17(2):2009–15.

Xia, C., Milton, M., and Gan, L. (2007). Evaluation of drug-transporter interactions using in vitro and in vivo models. *Curr Drug Metab*, 8(4):341–363.

Yabe, Y., Galetin, A., and Houston, B. J. (2011). Kinetic characterization of rat hepatic uptake of 16 actively transported drugs. *Drug Metab Dispos*, 39(10):1808–1814.

Yoshida, K., Maeda, K., and Sugiyama, Y. (2012). Transporter-mediated drug-drug interactions involving OATP substrates: predictions based on in vitro inhibition studies. *Clin Pharmacol Ther.*, 91(6):1053–64.